PONTIFÍCIA UNIVERSIDADE CATÓLICA DO PARANÁ
ESCOLA POLITÉCNICA
PROGRAMA DE PÓS-GRADUAÇÃO EM ENGENHARIA MECÂNICA

RICARDO JOSÉ BERTIN

A numerical investigation of internal failure pressure of pipelines containing a single and double pit corrosion defect, considering plasticity

CURITIBA
2015

RICARDO JOSÉ BERTIN

A numerical investigation of internal failure pressure of pipelines containing a single and double pit corrosion defect, considering plasticity

Thesis presented to the Programa de Pós-Graduação em Engenharia Mecânica, área de concentração: Mecânica dos Sólidos Computacional, Escola Politécnica, Pontifícia Universidade Católica do Paraná, in partial fulfillment of the requirements for the degree of Doctor in Mechanical Engineering

Orientador: Prof. Dr. João Elias Abdalla Filho

CURITIBA

2015

FOLHA DE APROVAÇÃO

A ser incluída posteriormente

(folha incluída neste momento para efeito de paginação)

To Jacqueline, Rafael and Patrícia, my eternal love.

ACKNOWLEDGEMENTS

I would like to express my deepest gratitude to Prof. Dr. João Elias Abdalla Filho for his paramount contribution to this work, understanding, patience, secure guidance, and exchange of ideas about several topics, most of them pertaining to this work.

My deepest gratitude goes also to Prof. Dr. Roberto Dalledone Machado, for his invaluable contributions in more than one occasion.

I am most grateful to all professors of the PPGEM, in special: Prof. Dr. Fred Lacerda Amorim, Prof. Dr. Nathan Mendes, Prof. Dr. Key Fonseca de Lima, Prof. Dr. Luís Mauro Moura, Prof. Dr. Ricardo Diego Torres and Prof. Dr. Viviana Cocco Mariani. Many thanks should be also given to Mrs. Jane Marques da Rocha, secretary of PPGEM, for her constant good humor, dedication, helpful and kind smile and good coffee.

I would like to thank my fellow colleagues of PPGEM, special mention to Maria José Cantillo Molina, Florentino Augusto Fagundes, Hsu Yang Shang and César Augusto Neitzke.

I would also like to thank my colleagues, professors and coworkers, of PUCPR for their support and friendship. Since to nominate each and every one of them would be impossible for my unreliable memory, I beg them to please fill properly and individually acknowledge. Thanks should also be given to my undergraduate students, from whom I continuously learn, for their understanding.

I would like to also express my gratitude to my parents, Mílvio and Ione, my parents-in-law, Dultevir and Ana Helena, my two sisters, Lilian and Celina, my four brothers and sisters-in-law, Alberto, José, Andrea and Alexandre, my five nephews and nieces, Daniel, André, Maria Pia, Teo and Alexandre and several relatives, specially including my deceased grandmother Urbana, for their faith in me. Your support, your friendship, your encouragement, your prayers and your smile were determinant to achieve this humble dream of mine.

Last, but not least, my uttermost gratitude to my beloved wife Jacqueline, my son Rafael and my daughter Patricia. Your unconditional love, continuous support and eternal patience were fundamental to this accomplishment.

Finally my sincere thanks to those not expressly mentioned, but to whom I will be forever in debt.

Ut tension sic vis

Hooke, 1678

ABSTRACT

BERTIN, R.J. **A numerical investigation of internal failure pressure of pipelines containing a single and double pit corrosion defect, considering plasticity**. 2015. 165p. Thesis (Doctoral) – Programa de Pós-Graduação em Engenharia Mecânica, Escola Politécnica, Pontifícia Universidade Católica do Paraná, Curitiba, 2015.

Defects in engineering structures can be classified into five different types: fabrication defects, construction, operation, environmental and combined defects. Corrosion as a type of defect is somehow related to all five previous defects. For metals, corrosion is a destructive and non intentional attack that compromises their structural function. The attack normally initiates on the surface of the material and, progressing to its interior, reduces the wall thickness and alters locally the mechanical properties of that material. Areas of corrosion on metal surface often progress from a single pit corrosion, a small hole difficult to detect at early stage. The objective of this work is to propose a formulation to calculate the internal failure pressure in oil or gas pipelines with a single pit corrosion defect that allows defect to progress. Three API-5L-X60 steel pipes of diameters 300, 400 and 500 mm with a single pit on their external surface, modeled as a semi ellipsoid with constant diameter of 1.0 mm and various depths, from 0.1 to 4.0 mm, are simulated with internal pressures from 5.0 to 25.0 MPa, in 5.0 MPa increments. Also a 300 mm diameter pipe, subjected to internal pressure of 25 MPa, with two longitudinally aligned pit corrosion defects are simulated. Plasticity is taken into account as the material is modeled as multilinear isotropic hardening. After an extensive parametric study, a formulation to calculate failure pressure is derived as a function of the pipe diameter, wall thickness, and the pit aspect ratio. It is concluded that maximum stress inside the pit corrosion increases with increase in pipe diameter and pit aspect ratio. The nature of stress concentrator of the pit, even for shallow ones, is corroborated, as well as the direct relation between the pit corrosion aspect ratio and stress concentration factor - SCF.

Keywords: pit corrosion, pit-to-crack transition, failure pressure, finite element analysis, oil and gas pipeline

RESUMO

BERTIN, R.J. **A numerical investigation of internal failure pressure of pipelines containing a single and double pit corrosion defect, considering plasticity**. 2015. 165f. Tese (Doutorado) – Programa de Pós-Graduação em Engenharia Mecânica, Escola Politécnica, Pontifícia Universidade Católica do Paraná, Curitiba, 2015.

Defeitos em estruturas de engenharia podem ser classificados em cinco tipos diferentes: defeitos de fabricação, de construção, de operação, ambientais e defeitos combinados. A Corrosão, como um defeito, de alguma forma está relacionada a todos os cinco tipos de defeitos relacionados. Nos metais, a corrosão é um ataque não intencional e destrutivo que compromete sua função estrutural. Em dutos metálicos, o ataque normalmente inicia na superfície do material e, progredindo para o seu interior, reduz a espessura da parede e altera as propriedades mecânicas do referido material. Áreas de corrosão na superfície de metal, muitas vezes evoluem de um único pite de corrosão, um pequeno buraco de difícil detecção em estágio inicial. O objetivo deste trabalho é o de propor uma formulação para calcular a pressão interna de falha em dutos de petróleo ou gás com um único pite de corrosão que permite ao defeito progredir. Três dutos de aço API-5L-X60 com diâmetros de 300, 400 e 500 mm e um único pite na superfície externa, modelado como um semi elipsoide com diâmetro constante de 1,0 mm e profundidade variando entre 0,1 e 4,0 mm, são simulados com pressões externas de 5,0 a 25,0 MPa em incrementos de 5,0 MPa. Também um duto com 300 mm de diâmetro, submetido a 25 MPa de pressão interna, com dois defeitos de corrosão pite alinhados longitudinalmente, foram simulados. Plasticidade é levada em conta uma vez que o material é modelado como multilinear isotrópico com endurecimento. Após extenso estudo paramétrico, uma formulação que calcula a pressão de falha é derivada em função do diâmetro do duto, da espessura da parede e do fator de forma do pite. Conclui-se que a tensão máxima dentro do pite aumenta com o aumento do diâmetro do duto e do fator de forma do pite. A natureza concentradora de tensão do pite, mesmo para defeitos rasos é corroborada, bem como a relação direta entre o fator de forma e o fator de concentração de tensões.

Palavras Chaves: Pite de corrosão, transição pite para trinca, pressão de falha, análise por elementos finitos, tubulações de óleo e gás

LIST OF FIGURES

LIST OF TABLES

NOMENCLATURE

ABAQUS	Software suite for finite element analysis
AGA	American Gas Association
ANSYS®	Analysis System
API	American Petroleum Institute
ASME	American Society of Mechanical Engineering
ASTM	American Society for Testing Materials
BG Technology	British Gas Technology
CP	Cathodic protection
CPS	Corroded Pipe Strength
Cr	Chromium
DNV	Det Norske Veritas
DOT	Department of Transportation
EAC	Environmentally assisted cracking
ERW	eletric resistance welded
et al.	Latin short for *et alii* meaning “and others”
FEM	Finite element method
FORM	First-order reliability method
GNP	Gross National Product
GPa	Giga Pascal (10^9 Pascal)
INGAA	Interstate Natural Gas Association of America
ksi	kilopound per square inch
mm	millimeter (10^{-3} meter)
loc. cit.	Latin short for *loco citato* “meaning in the place cited”
LS-SVM	Least squares support vector machine
mm^2	square millimeter
μm	micrometer (10^{-6} meter)
Mo	Molybdenum
MPa	Mega Pascal (10^6 Pascal)
N	Newton
Ni	Nickel
op. cit.	Latin short for *opere citato* menaning “in the work cited”
p.	page
pp.	pages
ppm	parts per million
PDAM	Pipeline Defect Assessment Manual
PETROBRAS	Petróleo Brasileiro S.A.

PHMSA	Pipeline & Hazardous Materials Safety Administration
PPGEM	Programa de Pós-Graduação em Engenharia Mecânica
PUCPR	Pontifícia Universidade Católica do Paraná
RP	Recommended practice
SAW	Submerged arc weld
SCC	Stress corrosion cracking
SCF	Stress concentration factor
SINTAP	Structural Integrity Assessment Procedure
SMTS	Specified minimum tensile strength
SORM	Second-order reliability method
U.S.	United States of America
USSR	Union of Soviet Socialist Republics
V	Vanadium
WDD	Weighted Depth Difference
WYSIWYG	What You See Is What You Get
WYDSIWGY	What You Don’t See is What Gets You

LIST OF SYMBOLS

P	: internal pressure applied to a pipe, MPa
σ_{ref}	: reference stress, sometimes yield stress, MPa
t	: wall thickness of the pipe, mm
D	: pipe external diameter, mm
R_e	: external radius of the pipe, mm
R_i	: internal radius of the pipe, mm
A_0	: original cross-sectional area of the pipe at the defect ($L.t$), mm^2
M	: Folias bulging factor
P_f	: failure pressure, MPa
A	: projected area of defect on an axial plane through the wall thickness, mm^2
d_{max}	: maximum corrosion depth, mm
L	: length of the defect, mm
S	: safety factor
$\sigma_{y_{spec}}$	: specified yield stress, MPa
B	: parameter to calculate maximum length of the defect (ASME B31G)
σ_{flow}	: flow stress equals to σ_y + 68.948MPa, MPa
R_c	: rate of steady state corrosion, mm/year
Δd	: $d_T - d_0$ (difference between corrosion depth at time T and initial time)
d_T	: measurement of maximum corrosion depth at time T, mm
d_0	: initial measurement of maximum corrosion depth, mm
ΔT	: $T - T_0$ (difference between actual time and initial time)
T	: actual time of measurement d, year
T_0	: initial time of measurement d_0, year
D_{int}	: pipe internal diameter, mm
σ_u	: ultimate tensile strength, MPa
σ_s	: a chosen tensile strength, MPa
exp	: exponential function equal to e^x
R	: pipe external radius or D/2, mm
$P_{Long\ Groove}$	: failure pressure for a infinite long groove defect, MPa

σ_{crit} : critical stress, equivalent Von Mises stress, MPa

R_0 : pipe original internal radius, mm

t_{L0} : original ligament thickness (at the deepest point in the defect), mm

ε_{crit} : critical strain

$P_{plain\ pipe}$: failure pressure for a pipe without defect, MPa

g : function of the corrosion defect

z_{eval} : location of the evaluation point from an arbitrary origin

z_i : current position measured from the same arbitrary origin, mm

t_0 : original pipe wall thickness, mm

d^* : corrosion depth at a given location, mm

d_{eval} : corrosion depth at the evaluation point, mm

Δz : distance between adjacent measurements, mm

sech : hyperbolic secant function

$\sigma_{0.2}$: stress at 0.2% strain

F : force, N

K : constant of proportionality

k : parameter

δ : displacement, m

W : weight, N

A_s : cross sectional area, m^2

p : pressure, Pa

E : Young's modulus, MPa

σ : stress, MPa

ε : strain or total strain

x, y, z : Cartesian coordinates along axes X, Y and Z, respectively

E_1, E_2 : spring constants

Q : dumping constant

ε^e : elastic strain

ε^p : plastic strain

Γ : material property

$\boldsymbol{\sigma_{ij}}$: Cauchy stress tensor

$\boldsymbol{\sigma_{kk}}$: hydrostatic stress tensor

σ_m : mean stress

$\boldsymbol{S_{ij}}$: deviatoric stress tensor

l_0 : initial length

l : final length

$\boldsymbol{\varepsilon_{ij}}$: strain tensor

I_1, I_2, I_3 : invariants of the stress tensor

J_1, J_2, J_3 : invariants of the deviatoric stress tensor

$\sigma_1, \sigma_2, \sigma_3$: principal stress components

τ_{crit} : critical value of maximum shear stress

σ_t : tensile yield strength

W_D : elastic strain energy of distortion

G : elastic shear modulus

ω^p : work-hardening per unit volume

σ_e : equivalent stress

K_1, K_2, K_3 : invariants of the increment of plastic strain tensor

σ'_y : current yield stress

ν : Poisson ratio

$\{s\}$: deviatoric stress vector

$\{\sigma\}$: stress vector

σ_m : hydrostatic stress

Υ : yield criterion

σ_{max} : maximum stress inside the pit, MPa

a : depth of the pit corrosion, mm

$2c$: diameter of the pit corrosion, mm

$a/2c$: aspect ratio of the pit corrosion

α : parameter

β : parameter

σ_{hoop} : hoop stress, MPa

σ_{long} : longitudinal stress, MPa

σ_{radial} : radial stress, MPa

SUMMARY

1 INTRODUCTION

Pipelines are essential means of transportation for solid, liquid and gas bulk products since pipelines are cheap, safe and can operate at high capacity. The use of pipelines has spread during the industrial revolution, but their genesis could be far older. According to Watkins e Anderson (1999, p. 1), "buried conduits existed in prehistory when caves were protective habitat, and ganats[1] (tunnels back under mountains) were dug for water". According to Adib-Ramezani, et al.(2006a, p. 123) "pipelines are used as one of the most practical and low price methods for large oil and gas transport since 1950". However, Wright & Ashford (1989, p. 541) assert that "in 1865, Samuel Van Sychel built a two-inch pipeline to transport oil from a northwestern Pennsylvania oil field to a railroad terminal six miles away" and they continue: "Prior to this time, oil was transported by barrels in horse drawn wagons at a cost of about $0.30 per barrel-mile" (WRIGHT & ASHFORD, loc. cit.)

Not only cost shall be of primer concern, but safety and serviceability. As any other engineering project, pipelines are designed for a service life. They have to be maintained and inspected periodically to assure that they operate according to specified parameters. In addition, as any other engineering structure, pipelines suffer static and dynamic effects due to operation and to internal and external loads, stresses introduced by fabrication process and environmental effects. Finally, in the event of a defect, if no preventive or corrective measure is taken, all these effects together may cause the collapse of the pipeline with catastrophic consequences for the human life as well as for the environment.

Accidents may happen as a multitude of causes and the role of the engineer is to avoid those causes that can be inspected, predicted and prevented, such as the occurrence of defects in pipelines. Therefore knowledge of the subject is important, if not for safety or quality assurance, at least, as a professional duty.

This section will categorize pipeline defects into five types. Emphasis will be given to corrosion defects since it is the most common type of defect. Corrosion will be classified into types and a particular type of defect, known as pit corrosion will be addressed. The motivation of this work will then be described, its objectives and, finally, the organization of the work.

[1] *Ganat or Qanats*: "a form of subterranean aqueduct- or subsurface canal- engineered to collect groundwater and direct it through a gently sloping underground conduit to surface canals which provide water to agricultural fields". Lightfoot, 1996, apud (WESSELS & HOOGEVEEN, 2002).

1.1 PIPELINE DEFECTS

Five different types of defects can arise from any engineering structure, in the present discussion, pipelines. Those five types of defects are fabrication, construction, operation, environmental and combined defects. Fabrication defects can be divided into material defects and fabrication process defects. Construction defects can also be divided into handling and assembly defects (Figure 1).

Fabrication defects are those introduced during the fabrication of raw material or final product. In the case of pipes, these defects can be introduced during any phase of manufacturing from the production of ingots, to milling of the skelp[2] and the pipe itself or the welding process in the case of seam pipes. Construction defects include those introduced during the handling and transportation and assembly of the pipes, in other words, the placement of the pipe on its correct position according to drawings and its connection by mechanical connectors or by welding. Operation defects are those introduced by the daily operation of the pipeline. They comprise, mostly, of wear defects. Environmental defects are those introduced by environmental agents such as climate, water or soil, or by anthropomorphic actions, for instance, the action of the human element such as excavation on the vicinity of a buried pipeline, that may expose it. Finally, combined defects comprise two or more of the previous mentioned defects.

Figure 1 – Basic defects in engineering structures

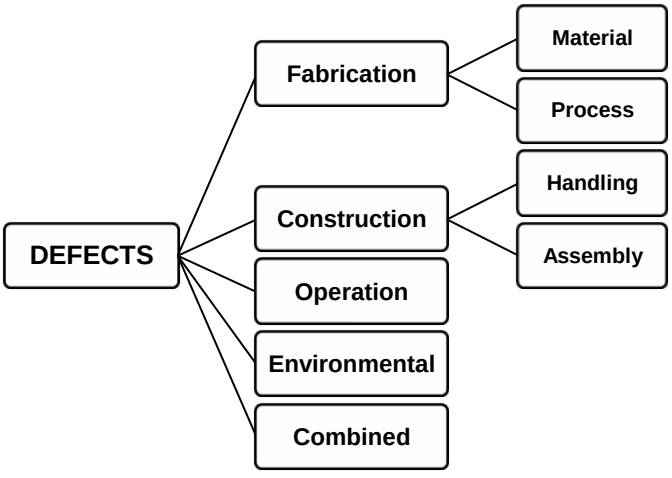

Source: BERTIN, 2015

[2] Skelp: plain sheet of iron or steel rolled into narrow strips in order to be transformed into pipe or tubing by being bent and welded.

Another classification of defects can be found in *Macaw's Pipeline Defects* (ARGENT, et al., 2003). It is a pictographical manual of all types of pipeline defects currently found on pressurized steel pipes.It divides pipeline defects into: fabrication defects (plate, seamless pipe, ERW – eletric resistance welded pipe and SAW – submerged arc weld/spiral defects), construction defects (girth welding, poor construction), operational defects (external corrosion, internal corrosion, erosion, fatigue, mechanical damage, ground movement and failure modes), coating and CP – cathodic protection (hot enamel, fusion bonded epoxy powder, polyolefin, liquid, cold applied tape, heat shrink materials and cathodic protection) and interaction defects.

1.1.1 Corrosion defect

Corrosion, as a defect, may occur as a result of environmental action and therefore be listed as an environmental defect. However corrosion may arise as consequence of all five previously listed types of defects. In fact, Argent (op. cit.) includes corrosion as operational defect, but also dedicates a section to defects of coating and cathodic protection. The opening words of his book's section on the subject are:

> "Coating defects do not usually create a direct risk of pipeline failure but do create the conditions in which corrosion may become active if the cathodic protection is deficient at the location of the coating defect or if the coating shields the exposed pipe surface from the action of the cathodic protection current" Argent (op. cit.).

In other words, corrosion is so important a defect that is cited as an operational defect as well as a coating and cathodic protection one.

The same view of the importance of corrosion is sponsored by Cosham et al.(2007, p. 1245): "the most common causes of damage and failures in onshore and offshore, oil and gas transmission pipelines in Western Europe and North America are external interference (mechanical damage) and corrosion". They also mentioned:

> Data for onshore gas transmission pipelines in Western Europe for the period from 1970 to 1997 indicates that 17% of all incidents resulting in a loss of gas were due to corrosion (Bolt R, Owen RW. *apud* (COSHAM, et al., 2007))

Callister (2001, p. S223) and Revie (2011, p. 6) classify metallic corrosion into eight categories (Figure 2): (1) uniform, (2) galvanic, (3) crevice, (4) pitting, (5) intergranular, (6) selective leaching (Callister) or dealloying (Revie), (7) erosion-corrosion and (8) environmentally assisted cracking (EAC) or stress corrosion cracking (SCC).

Figure 2 – Classification of corrosion according to Callister, 2001

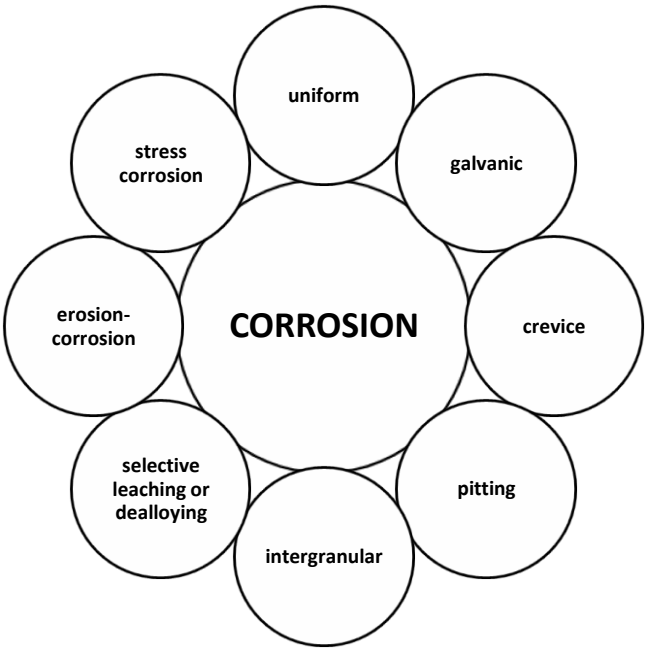

Source: BERTIN, 2015

1) **Uniform** galvanic corrosion may occur when the attack is uniformly distributed on the entire surface with equal intensity. This can lead to very high corrosion rates provided a right corrosive agent is present (for instance diluted nitric acid for carbon steel) or just a bad esthetic effect, when no structural damage is done to the metallic material but its surface appearance is altered.
2) **Galvanic corrosion** may appear when two different metals, a nobler and a less noble, are in contact and by exposition to an electrolyte, a current from one to the other is created. This type of corrosion is the basis for cathodic protection if the corrosion is forced to occur on a sacrificial anode.
3) **Crevice** is a type of localized corrosion and may occur when a recess, fracture or superposition of metal parts allow small amounts of solutions to accumulate under, inside and around recesses such as holes, lap joints, rivet heads, bolts, cracks and so forth.

4) **Pitting** may occur when a small portion of a protective passive layer is broken exposing a small region to a corrosive environment. "The mechanism for pitting is probably the same as for crevice corrosion in that oxidation occurs within the pit itself" (CALLISTER, 2001, p. S226).
5) **Intergranular** may occur in the space among grains of specific alloys such as stainless steel and in specific conditions such as temperatures between 500^0 and 800^0C when particles of chromium carbide may precipitate.
6) **Dealloying or selective leaching** may occur when in an alloy one of the components is leached out selectively. Two examples of this phenomenon are graphitic corrosion of cast iron where iron leaches from the iron-carbon matrix and dezincification of brass where zinc leaches from the zinc-copper matrix.
7) **Erosion-corrosion** may occur by chemical reaction plus mechanical abrasion as a result of fluid flow. At high speed, fluid motion may also cause cavitation on a previously corroded surface.
8) **Stress corrosion or SCC** may occur as a result of a combination of a corrosive environment and applied tensile stress. It tends to be unexpected and fundamental mechanism still not well understood, in the opinion of Revie (2011, p. 16).

From all the corrosion defects previously listed, special importance shall be given to those that are more difficult to detect because they embody the most potential risk of damage. On this category lies pit corrosion.

1.1.2 Pit Corrosion importance and mechanism

According to Pidaparti and Rao (2008, p. 1932) "pitting corrosion is known to be one of the major damage mechanisms affecting the integrity of many materials and structures in civil, nuclear and aerospace engineering". The minute dimensions (Figure 3) that makes detection difficult, the potential for crack initiation, the possibility to "assist in brittle failure, fatigue failure, environment-assisted cracking like stress corrosion cracking[3] (SCC), and corrosion fatigue by providing sites of stress concentration" (SCHWEITZER, 2010, p. 41) makes pit corrosion an important phenomenon in failure of metallic components.

[3] SCC – Stress Corrosion Cracking: "delayed failure of alloys by cracking when exposed to certain environments in the presence of static tensile stress. The stress level at which failure occurs is well below the stress required for a mechanical failure in the absence of corrosion". (SCHWEITZER, 2010, p. 46)

Figure 3 – Microscopic dimensions of pit corrosion on a specimen of 3% NiCrMoV

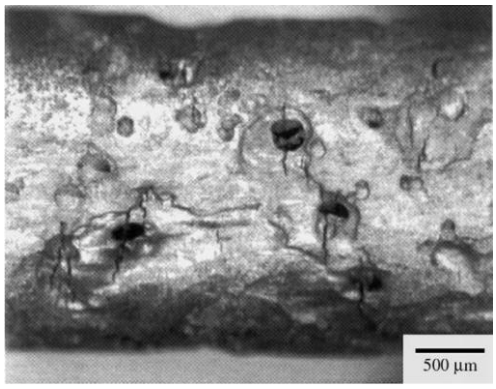

SOURCE: (TURNBULL & ZHOU, 2004, p. 1249)

For Callister (2001, pp. S-226) pit corrosion is "a very localized corrosion attack in which small pits or holes form" and for Ma (2012) pit corrosion is a "localized accelerated dissolution of metal that occurs as a result of a breakdown of the otherwise protective passive film[4] on metal surface" (MA, 2012, p. 139). The breaking of a passive film is also mentioned by Ok et al. (2007) when they relate the mechanics of pit corrosion to "areas where the highest stresses occur and which leads to coating break-down and stress corrosion cracking" (OK, et al., 2007, p. 2224).

Although the mechanics of pit corrosion initiation is out of the scope of the present work, the passive film appears to play an important role in the process. For instance, Szklarska-Smialowska (1999) distinguishes pit corrosion of aluminum as a four stage process:

> (1) processes occurring on the passive film, at the boundary of the passive film and the solution; (2) processes occurring within the passive film, when no visible microscopic changes occur in a film; (3) formation of so-called metastable pits which initiate and grow for a short period of time below the critical pitting potential and then repassivate (this is an intermediate step in pitting); and (4) stable pit growth, above a certain potential termed the critical pitting potential (SZKLARSKA-SMIALOWSKA, 1999, p. 1743).

On three of first four stages, processes on the passive film are mentioned. Passive film is also cited by Ma (2012) that relates the initiation of a pit to the formation of a passive oxide film on the surface of the metal as a result of:

[4] Passive film: thin protective corrosion product film present on the surface of metals and alloys resulting from reaction with the environment. (REVIE (Ed.), 2011, p. 1/16)

> (a) Mechanical damage of the passive film was caused by scratches. Anodic reaction starts on the metal surface exposed to the electrolyte. The passivity surrounding surface is act as the cathode. (b) Particles of a second phase emerging on the metal surface. These particles precipitating along the grains boundaries may function as local anodes causing localized galvanic corrosion and formation of initial pits. (c) Localized stresses in form of dislocations emerging on the surface may become anodes and initiate pits. (d) Non-homogeneous environment may dissolve the passive film at certain locations where initial pits form (MA, 2012, p. 142).

Jivkov (2004) modeled corrosion crack nucleation as three physical processes: (a) dissolution that accounts for the surface corrosion of a metal; (b) passivation or the formation of a thin protective layer of metallic oxide, or passive film, that prevents further attacks from the aggressive environment and (c) deformation caused by loading that breaks the protective film thus allowing the bare metal surface to be corroded again.

Turnbull and Zhou (2004) who performed experiments on steam turbine steel presented a five step process for the transition from pit to crack when pitting is the precursor to stress corrosion cracking: (a) pit initiation, (b) pit growth, (c) transition from pit to crack and (d) short crack growth and (e) long crack growth.

Summarizing, the presence of a passive film is important in the process of pit corrosion formation. The breaking of this film, although not the only mechanism, is responsible for pit growth. Depending on the level of stress the metal is undergoing, a stress corrosion crack initiates from a pit, breaking the passive film and causing corrosion to evolve or the crack to progress. In any case, the state of the defect becomes worse.

1.2 MOTIVATION

In pipelines, as in any steel structures, corrosion is always a major problem, the cause for increase probability of incidents and accidents, money loss, risk to human life and to the environment.

As for cost and human lives, Table 1 is a brief summary of a much larger spreadsheet, part of the Pipeline & Hazardous Materials Safety Administration – PHMSA report on All Reported Pipeline Incidents in the United States. The PHMSA, that is an agency of the United States of America Department of Transportation – DOT, reports an expenditure of US$ 298,924,350 per year in property damage over a period of 20 years from 1993 to 2012 as well as almost 19 deaths/yr and 74.5 injuries per year.

Table 1 – National All Pipeline Systems: All Reported Incident Details: 1993-2012

Reported Cause of Incident	Number	%	Fatalities	Injuries	Property Damage as Reported (US$)	% of Property Damage
Corrosion	1920	18.3%	25	86	620,018,283	10.3%
Excavation damage	1948	18.6%	146	505	472,386,184	7.9%
Incorrect operation	740	7.0%	18	158	145,489,330	2.4%
Material/weld/equip failure	2815	26.9%	19	155	2,070,341,509	34.6%
Natural force damage	714	6.8%	16	83	1,787,257,931	29.8%
Other outside force damage	766	7.3%	41	115	339,499,014	5.6%
All other causes	1539	14.7%	112	387	543,494,749	9.0%
Totals	10442	100.0%	377	1489	5,978,487,000	100.0%

SOURCE: (U.S. Department of Transportation, Pipeline & Hazardous Materials Safety Administration, 2013)

Although during this period corrosion had been responsible for 18.3% of all pipeline incidents in the United States and for 10.3% of property damage, or US$ 31,000,914 per year; it might be possible to add a fraction of the 0.3% due to environmental cracking-related incidents, include in the fourth row Material/weld/equip failure (see Attachment A), if it is assumed that some of the cracking could be related to corrosion.

The assumption that corrosion can lead to cracking by fatigue is supported by Kondo (1989, p. 7) that alerts: “pit initiation is the trigger for fatigue crack initiation”. Therefore it is reasonable to assume that at least part of the US$ 1,073,472,622 in property damage (U.S. Department of Transportation, Pipeline & Hazardous Materials Safety Administration, 2013), 17.9% of the total cost (see Attachment A), could be avoided by simply taking corrosion and pit corrosion into consideration.

Furthermore, approximately 5% of an industrialized nation’s income is spent on prevention, maintenance or replacement of corroded parts (CALLISTER, 2001, locus cit). The percentage mentioned by Callister is corroborated by Bennett et al. (1978) on a Report of the National Bureau of Standards to the Congress. They concluded at that time (1975) that “the total cost of corrosion in the United States is estimated to be $70 billion – about 4.2 percent of the Gross National Product” - GNP (BENNETT, et al., 1978, p. 30). In other countries the figures are not different from the United States. According to Revie (2011), in the United Kingdom a 1969 study by a committee appointed by the Ministry of Technology and headed by T. P. Hoar reported losses amounting approximately 3.5% of the GNP during 1969-70, whereas in West German the total cost during 1968-69 was 3% of the GNP, one percent more than former USSR - Union of Soviet Socialist Republics in 1969.

In computing, the acronym WYSIWYG - "What You See Is What You Get" refers to a system or software in which the image on the screen has the same appearance when printed. In maintenance, what you do not see is what gets you or WYDSIWGY, should the acronym exist in maintenance context. Among all types of corrosion, previously discussed, the smallest has the highest potential risk for failure since it goes undetected until its progress leads to unavoidable structural collapse or a deterioration of the structure operational condition or, at least, entails maintenance and substitution. Pit corrosion is one of such defects that can have microscopic dimensions. Acting as stress intensifier, pit corrosion can become a source for crack initiation. By breaking passive film, cracks expose the original material to the action of corrosive environment and to the progress of the problem. Small cracks, under sufficient stress, progress to become larger cracks that may affect the structural integrity of pipelines. To the knowledge of the author, as will be discussed in section 2 – Literature Review, there is not a formulation that beginning from Barlow's equation, calculates internal failure pressure that may lead to the progression of a single pit corrosion and incorporates the geometry of the defect, geometry of the pipe and material properties.

Furthermore, methods for appraisal of corroded pipelines are concerned with large corrosion defects, sometimes a colony of pits. These methods, as should be seen in item 2.1, tend to focus their attention on the remaining material to be corroded, hence the material that would still resist to the efforts arising from internal pressure. Apparently, no proper importance is given by those methods to the defect itself and its internal state of stress.

1.3 OBJECTIVE

1.3.1 Main objective

The objective of the present work is, based on finite element simulations, to derive a formulation to calculate internal failure pressure in the pipeline with a single pit corrosion defect that allows the defect to progress.

1.3.2 Specific objectives

a) To evaluate the maximum stress inside a single pit corrosion on the external surface of an oil or gas pipeline with respect to pipe diameter and pit depth.
b) To corroborate the stress concentrator nature of the pit.

c) To corroborate the relation between stress concentration factor – SCF and the pit corrosion aspect ratio.
d) To evaluate the influence of a second pit corrosion defect longitudinally aligned with the first one.
e) To obtain a parametric procedure to do the simulations rapidly and with good control of the intervenient variables.

1.4 ORGANIZATION

After an introductory discussion on pipelines as a mode of transportation and their safety, a topic on pipeline defects is addressed. Corrosion as a defect is then classified in order to raise the subject of pit corrosion in particular. Pit corrosion is defined and correlated to the process of corrosion progress. The motivation for this work is explained as well as some economic and social aspects of corrosion in the oil industry. The objectives of the present work are addressed as well as the organization of this text. Section 2, Literature Review, is presented and discussed covering the main methods for appraisal of corroded pipelines, corrosion in general and pit corrosion in particular. Section 3, Fundamental Concepts, explains some concepts of elasticity, plasticity and analyses methods for appraisal in respect to small or shallow defects. Section 4, Methodology, describes geometric modeling, material parameters and finite element modeling. Section 5, Analysis and Results, presents results, both on table and graphic format, and describe how the formulation to calculate internal failure pressure in pipelines with a single pit corrosion is derived and the assumptions made. Finally, in Section 6 conclusions are presented as well as recommendations for further research. Figures of maximum stress distribution for each of the 180 simulations are appended at the end with some relevant material.

1.5 SECTION SUMMARY

Very rarely locations of extraction of mineral resources are the same as their consumption. In fact, commonly they are separated by hundreds, sometimes thousands, of kilometers. Therefore it is essential to have reliable, cheap and safe means of transportation, implying one without, or at least, with as few defects as possible. This section has presented a broad view of all types of pipeline defects and centered on corrosion because of its

commonness. Corrosion was then classified into types and a particular type of defect, known as pit corrosion was addressed. The motivation of this work can be summarized by four arguments, as follows: (a) a defect, such as corrosion, in which vast amounts of money are spent worldwide is a defect worth to be studied; (b) small dimension of pit corrosion causing the defect to pass undetected, (c) the potential for pit corrosion, acting as stress intensifier, to break passive film, expose non corroded material to corrosive agents, forcing the defect to progress and (d) the apparent inadequacy of some of the most used methods for appraisal of corroded pipelines to deal with small defects. The main objective presented was to derive a formulation to calculate internal failure pressure of a pipeline with pit corrosion very small dimensions.

2 LITERATURE REVIEW

As previously mentioned on Section 1, pit corrosion can have microscopic dimensions, therefore it is suggested here that current methods for appraisal of corroded pipelines would not be suitable to predict failure pressure for pipelines with this type of defect. This section presents articles discussing and comparing those methods as an introduction to their presentation and explanation. Afterwards, literature is presented regarding the connection of pits with structural behavior or structural evaluation of pipes subjected to fatigue, cracks and stress concentration factor.

2.1 METHODS TO ASSESS PIPELINE DEFECTS

Cosham and Kirkwood (2000) discuss the need for fitness-for-purpose methods to assess defects in pipelines. They propose a methodology to assess defects and damage in transmission pipelines (Figure 4).

Figure 4 – Pipeline defect assessment - PDA

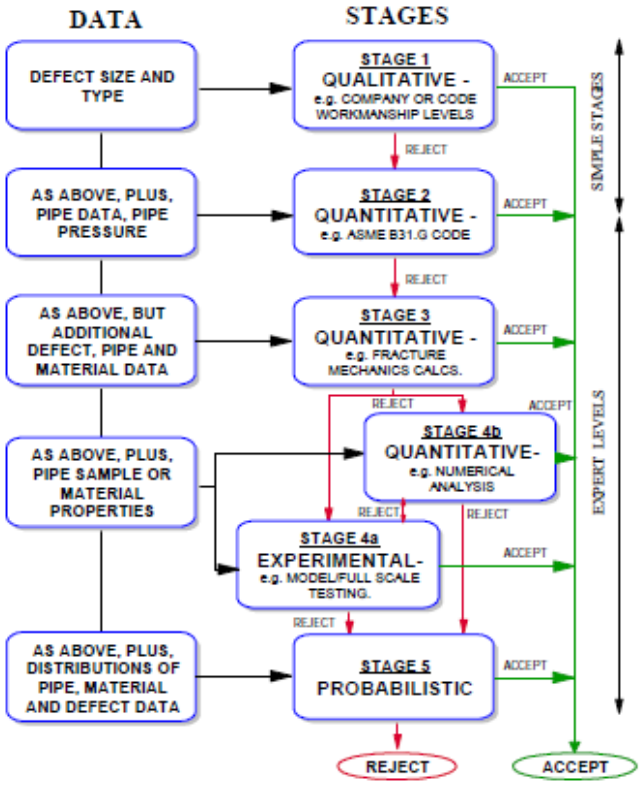

Source: (proposed by Cosham and Kirkwood (2000, p. 3))

They also discuss main defects, such as gouges, plain dents, smooth dents containing a defect, dents on welds, corrosion and girth welds providing formulations for each of them accordingly. On corrosion, they describe some of the methods of assessment, most of them detailed in section 2.1 of the present work. Finally, they describe a project to produce a version 2 of a Pipeline Defect Assessment Manual – PDAM.

A review of the methods for assessing corroded pipelines is also presented by Fu et al.(2001). The authors describe and discuss various methods and provide comprehensive tables summarizing the results of statistical analyses of each method for the ratio of actual failure pressure over predicted failure pressure. The study reaches seven conclusions:

1) The methods are not applicable to corrosion damage over pipe welds;
2) The methods may not be applicable to corroded pipes exhibiting toughness-dependent failure behavior;
3) Failure stress values are related to ultimate tensile strength, but test results shows that the use of specified minimum tensile strength – SMTS leads to accurate and consistent failure predictions;
4) The methods are only applicable to pipelines with internal pressure. However when detailed non-linear finite element analysis is used other loads can be used combined with internal pressure;
5) Accuracy of defect measurement is crucial to the defect assessment;
6) The guidelines for grouping the defects are empirical and based on engineering judgment; and
7) In general, the criteria for defect grouping are conservative.

Finally, the work recommends a three-level assessment methodology:

a) Level-1 assessment: criteria for defect grouping, screening level assessment for single defects and defect interaction assessment;
b) Level-2 assessment: assessment of complex-shaped defects; and
c) Level-3 assessment: case-by-case finite element analysis.

Cosham and Hopkins (2004) in their work briefly present the project PDAM, already mentioned in a previous work (COSHAM & KIRKWOOD, 2000), sponsored by fifteen international oil and gas companies. The rest of the paper describes various methods for the assessment of corrosion, lists the available full scale test data, identifies the best recognized methods for assessing corrosion and discusses their comparison, and presents considerations for the assessment of corrosion defect in a pipeline.

Cosham, Hopkins and Macdonald (2007) summarize the best practices for the assessment of corrosion in pipelines. They list published burst tests from 1972 to 2000, detailed the main parameters of these tests, giving, for instance, pipe diameter, wall thickness, defect geometry, material properties and burst pressure and also discussed the role of geometry and flow stress. Problems with the comparison of the methods are discussed and a flow chart of the assessment procedure for corrosion defects is presented and explained.

2.2 METHODS FOR APPRAISAL OF CORRODED PIPELINES

In 1837, Peter Barlow[5] published a book entitled "A Treatise on the Strength of Timber, Cast Iron, Malleable Iron, and Other Materials, with rules for application in Architecture, Construction of Suspension Bridges, Railways, etc., with an Appendix on the power of locomotive engines, and the effect of inclined planes and gradients, with seven plates" (BARLOW, 1837). In his book, from page 205 to 213, he published two articles: "124 – On the Strength of Hydrostatic Presses" and "125 – Application of this Rule for computing the proper Thickness of Metal in a Cylindric hydraulic Press of given Power and Dimensions". On article 124 he derives a method to calculate the thickness of a given pressure vessel as a function of its internal pressure, its diameter and the strength of the material used (Figure 5).

Figure 5 – Stress in thin-walled pipes undergoing internal pressure

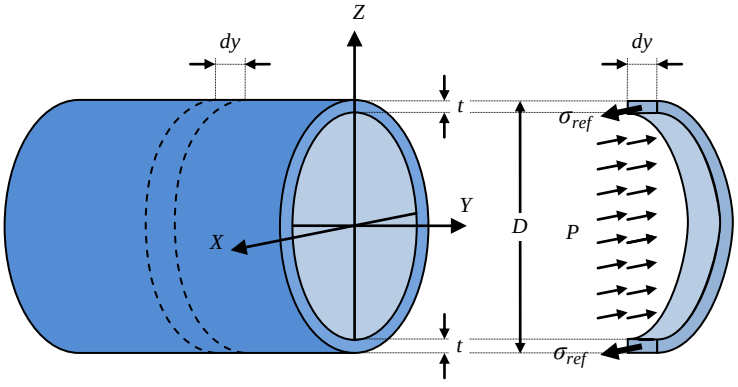

Source: Bertin, 2015, adapted from (HIBBELER, 2010), p. 300

[5] Peter Barlow (1776 – 1862) was an English mathematician, physicist, assistant mathematics master at the Royal Military Academy and fellow of the Royal Society.

On article 125 he gives an application example. The method of article 124 can be translated into a formula, now known as Barlow's equation and can be written as:

$$P = \frac{\sigma_{ref} \,.\, 2 \,.\, t}{D} \tag{1}$$

where:

P : internal pressure,

σ_{ref} : reference stress, yield stress or ultimate tensile strength, which is obtained in uniaxial test,

t : wall thickness of the pressure vessel, and

D : diameter of the vessel.

One shall note that Equation (1) is only applicable for thin-walled pipes (Figure 6 - a), in other words, if relation between thickness t and radius R (or $D/2$) is less than 1/10. For thick-walled (Figure 6 - b) pipes it is used an equation credited to Gabriel Lamé[6].

Figure 6 – Comparison of (a) thin and (b) thick-walled pipes

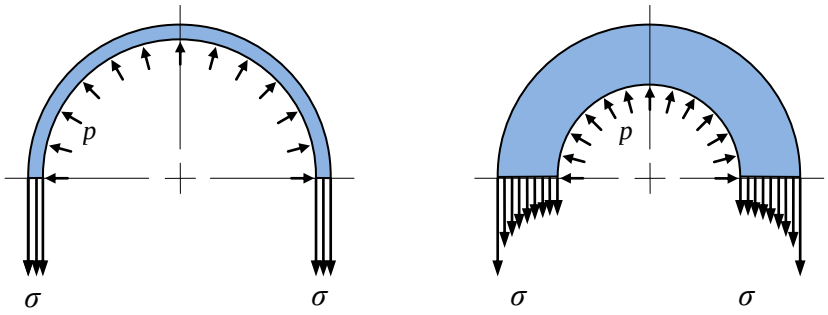

Source: Bertin, 2015

Although, according to Timoshenko[7] (TIMOSHENKO, 1983, p. 115) the discussion of the subject was first done by Lamé and Clapeyron[8] in a memoir entitled "*Sur l'équilibre interieur des corps solides homogènes*", it was in Lamé's book "*Leçons sur la théorie mathématique de l'élasticité des corps solides*" that he explains the elastic theory of hollow cylinders (LAMÉ,

[6] Gabriel Lamé[6] (1795 – 1870) was a French mathematician, engineer and professor of physique I at the Polytechnic School of Paris.

[7] Stephen Prokopovych Timoshenko (1878 – 1972) was a Ukrainian engineer and professor at University of Michigan, from 1927 to 1936 and after, at Stanford University, from 1936 to 1944.

[8] Benoît Clapeyron (1799 – 1864) was a French engineer, physicist and professor at *l'École des Transports*, Saint Petesburg, from 1820 to 1830.

1852, pp. 188-192). The equation can be arranged in a manner similar to Barlow's equation as follows:

$$P = \frac{\sigma_{ref} \cdot (R_e^2 - R_i^2)}{2R_e^2} \quad (2)$$

where:

P : internal pressure, yield stress or ultimate tensile strength,

σ_{ref} : reference stress, yield stress or ultimate tensile strength

R_e : external radius of the vessel, and

R_i : internal radius of the vessel.

Although less exact, Barlow's equation was used to calculate the internal maximum allowable pressure of a pipe subjected to corrosion defects on various methods. In a chronological way, some of the most used methods are described as follow.

2.2.1 AGA – NG 18

On late 1960 and early 1970, according to several authors, among them, (FERRAZ, 2007), (HIPPERT JR., 2004, p. 42), (FAN, et al., 2007, p. 239), (BJØRNØY & MARLEY, 2001, p. 93), to name but a few, the American Gas Association, based on a series of burst tests, proposed a semi-empirical equation, now known as NG-18. Quoting Quales (1970):

> Since its inception in 1953, the Line Pipe Research program (NG-18) has been one of the most complex and comprehensive efforts conducted by the American Gas Association's Pipeline Research Committee. NG-18 is a continuing research program into the properties of line pipe, conducted by Battelle Memorial Inst. Over the years the NG-18 program has been concerned with one general subject--mechanical properties of line pipe materials and how they perform during the service life of a line

The method adds a reductor to Barlow's equation. That reductor is expressed as a relation between projected corroded area, A, and undamaged area, A_0, or the depth of the defect, d, and the wall thickness, t. It also includes a bulging factor, M, known as Folias factor. The Folias factor, derived by Efthymios S. Folias, describes the bulging effect of a shell surface submitted to internal pressure when a portion of its wall is thinner than its surroundings. The formulation of NG-18 is:

$$P_f = \sigma_{flow} \frac{2t}{D} \left(\frac{1 - \frac{A}{A_0}}{1 - \frac{A}{A_0} \frac{1}{M}} \right) = \sigma_{flow} \frac{2t}{D} \left(\frac{1 - \frac{d_{max}}{t}}{1 - \frac{d_{max}}{t} \frac{1}{M}} \right) \quad (3)$$

and

$$M = \sqrt{1 + 0.6275 \left(\frac{L}{\sqrt{Dt}} \right)^2 - 0.003375 \left(\frac{L}{\sqrt{Dt}} \right)^4} \quad (4)$$

Figure 7 – Schematic view of a defect according to NG-18 method

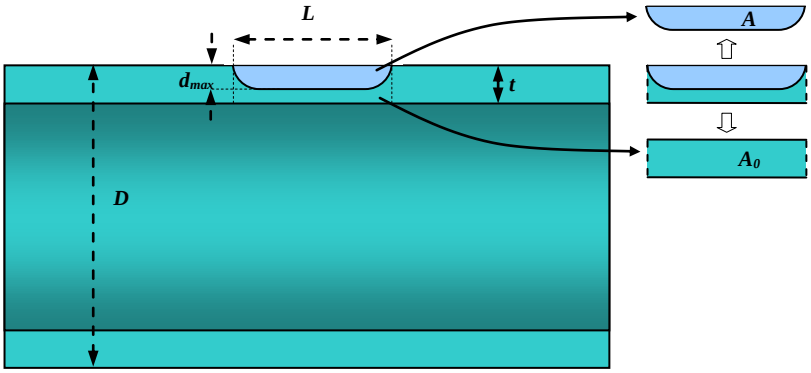

Source: BERTIN, 2015

where (view Figure 7):

A_0 : original cross-sectional area of the pipe at the defect ($L.t$), mm^2

A : projected area of defect on an longitudinal plane through the wall thickness, mm^2

M : Folias bulging factor

P_f : failure pressure, MPa

σ_{flow} : flow stress[9], equal to σ_y + 68.948 MPa (yield stress, σ_y, + 10 ksi),

D : pipe external diameter, mm

t : nominal pipe wall thickness, mm

d_{max} : maximum corrosion depth, mm

L : length of the defect, mm

[9] Flow stress: is the instantaneous value of stress required to continue deforming the material, in other words, to keep the metal flowing.

2.2.2 ASME B31G

The American Society of Mechanical Engineering or ASME issued the B31 Code for Pressure Piping in 1984. It was revised in 1989 and reissued as "Manual for Determining the Remaining Strength of Corroded Pipelines – a supplement to ASME 31 Code for Pressure Piping" in 1991 (ASME, 1991). According to Alves (2002) and Ahammed (1998, p. 321), it is the most used method presently because it provides conservative results. A report for INGAA Foundation - Interstate Natural Gas Association of America corroborates this by stating that, at least in the United States "ASME B31G is the standard for determining the remaining strength of steel pipelines that have experienced corrosion" (Process Performance Improvement Consultants, LLC, 2007, p. 21). However, B31G only applies "to defects in the body of line pipe which have relatively smooth contours and cause low stress concentration" (ASME, 1991, p. 1) which hands its application useless for defects such as pit corrosion unless they can be modeled as regular and smooth defects, only possible for shallow pits.

ASME B31G is a semi-empirical method for the determination of maximum allowable longitudinal extent of corrosion for pipes subjected to internal pressure only. The mathematical formulation of B31G is based on the NG18 equation. However, to account for experimental data and short defects, B31G assumes the projected corroded area A to be approximately parabolic (Figure 8), thus:

$$A = \frac{2}{3} d_{max} L \tag{5}$$

where:

A : is the projected area of defect on a longitudinal plane through the wall thickness,

d_{max} : is the maximum depth of the defect (Figure 8),

L : is the length of the defect.

Since the original cross-sectional area of the pipe at the defect is given by $A_0 = L.t$, it follows:

$$\frac{A}{A_0} = \frac{2}{3} \frac{d_{max}}{t} \tag{6}$$

Substituting (6) on (3), adding a safety factor *S* also called design factor, and substituting the flow stress, σ_{flow}, by 110% of a minimum specified yield stress SMYS or $\sigma_{y_{spec}}$, leads to:

$$P_f = S \times 1.1\sigma_{y_{spec}} \frac{2\mathrm{t}}{\mathrm{D}} \left(\frac{1 - \frac{2}{3}\frac{d_{max}}{t}}{1 - \frac{2}{3}\frac{d_{max}}{t}\frac{1}{M}} \right) \tag{7}$$

$$M = \sqrt{1 + 0.8\left(\frac{L}{\sqrt{\mathrm{Dt}}}\right)^2} \tag{8}$$

where:

S : safety factor

P_f : failure pressure, MPa

$\sigma_{y_{spec}}$: specified yield stress, MPa

D : pipe external diameter, mm

t : nominal pipe wall thickness, mm

d_{max} : maximum corrosion depth, mm

M : Folias bulging factor

L : length of the defect, mm

Figure 8 – Projected corroded area according to B31 G

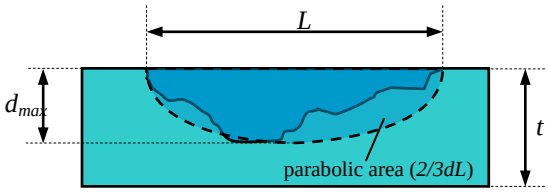

Source: BERTIN, 2015

B31G states that

> A contiguous corroded area having a maximum depth of more than 10% but less than 80% of the nominal wall thickness of the pipe should not extend along the longitudinal axis of the pipe for a distance greater than that calculated from (ASME, 1991, p. 9):

$$L = 1.12B\sqrt{Dt} \tag{9}$$

where:

L : is the extension of the corrosion defect along the longitudinal axis of the pipe,

B : is a parameter that may not exceed 4.0 (ASME, 1991, p. 9) and is given by:

$$B = \sqrt{\left(\frac{\frac{d_{max}}{\mathrm{t}}}{1.1\frac{d_{max}}{\mathrm{t}} - 0.15}\right)^2 - 1} \tag{10}$$

Making $B \leq 4.0$, L on (9) shall be:

$$L \leq \sqrt{20Dt} \tag{11}$$

which defines the maximum accepted extent of the corroded area for equations (7) and (8) to be valid.

In the case of $> \sqrt{20Dt}$, B31G (ASME, 1991, p. 42) defines failure pressure to be:

$$P_f = 1.1\sigma_{y_{spec}}\frac{2\mathrm{t}}{\mathrm{D}}\left(1 - \frac{d_{max}}{t}\right) \tag{12}$$

2.2.3 Modified ASME B31G or 85dL

To overcome the conservatism of the B31G, some modifications were introduced on the original formulation. It was proposed to return to the original NG18 formulation, but with a new method to appraise the defect. The parabolic area was replaced by, in the words of Cosham and Kirkwood (2000, p. 6), "a simple, arbitrary, geometric idealization … for hand calculations (a factor of 0.85 rather than 0.67…)" (Figure 9). The formulation, according to Cosham and Kirkwood (2000, p. 7), is given by:

$$P_f = \sigma_{\mathrm{flow}}\frac{2\mathrm{t}}{\mathrm{D}}\left(\frac{1 - 0.85\,\frac{d_{max}}{t}}{1 - 0.85\,\frac{d_{max}}{t}\,\frac{1}{M}}\right) \tag{13}$$

for $\frac{L^2}{Dt} \leq 50$

$$M = \sqrt{1 + 0.6275\left(\frac{L}{\sqrt{Dt}}\right)^2 - 0.003375\left(\frac{L}{\sqrt{Dt}}\right)^4} \quad (14)$$

for $\frac{L^2}{Dt} > 50$

$$M = 0.032\left(\frac{L}{\sqrt{Dt}}\right)^2 + 3.3 \quad (15)$$

where:

M : Folias bulging factor

P_f : failure pressure, MPa

σ_{flow} : flow stress equals to σ_y + 68.948 MPa

D : pipe external diameter, mm

t : nominal pipe wall thickness, mm

d_{max} : maximum corrosion depth, mm

L : length of the defect, mm

Figure 9 – Projected corroded area according to modified B31 G

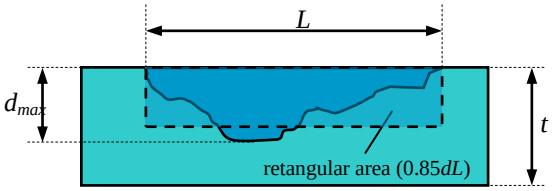

Source: BERTIN, 2015

Ahammed (1997) based on the same formulation of the modified ASME 31G proposed another formulation for the maximum allowable pressure incorporating a steady state rate of corrosion over a period of time, R_C:

$$R_c = \frac{\Delta d}{\Delta T} = \frac{d_T - d_0}{T - T_0} \quad (16)$$

where:

R_c : rate of steady state corrosion, mm/year

d_0 : initial measurement of maximum corrosion depth, mm

d_T : measurement of maximum corrosion depth at time *T*, mm

T_0 : initial time of measurement d_0, year

T : time of measurement d_T, year

Equation (16) can be modified to:

$$d_T = d_0 + R_c(T - T_0) \tag{17}$$

and substituted in Equation (13) without the consideration of defect area reduction by 0.85, giving:

$$P_f = \sigma_{flow} \frac{2t}{S \times D} \left\{ \frac{1 - \frac{[d_0 + R_c(T - T_0)]}{\mathrm{t}}}{1 - \frac{[d_0 + R_c(T - T_0)]}{t} \frac{1}{M}} \right\} \tag{18}$$

where:

M : Folias bulging factor, given by Equations (14) and (15)

P_f : failure pressure, MPa

σ_{flow} : flow stress equals to σ_y + 68.948MPa, MPa

D : pipe external diameter, mm

t : nominal pipe wall thickness, mm

S : safety factor

2.2.4 RPA Method

RPA – rectangular parabolic area method was proposed by Benjamin and Andrade (2003) based on laboratory tests. "An experimental study conducted by PETROBRAS has shown that the RSTRENG 085dL method gives unconservative results for long defects" (BENJAMIN & ANDRADE, 2003, p. 7), therefore for what they consider a long defect, $L^2/Dt > 20$, they proposed the following modification:

$$P_f = \sigma_{flow} \frac{2t}{D} \left(\frac{1 - k \frac{d_{max}}{t}}{1 - k \frac{d_{max}}{t} \frac{1}{M}} \right) \tag{19}$$

where:

$$k = 1 - 0.15\frac{64 \times 10^6}{\left(\frac{L^2}{Dt}\right)^6} \quad (20)$$

$$M = 2.1 + 0.07\frac{L^2}{Dt} \quad (21)$$

M : Folias bulging factor

P_f : failure pressure, MPa

σ_{flow} : flow stress equals to σ_y + 68.948MPa

D : pipe external diameter, mm

d_{max} : maximum corrosion depth, mm

t : nominal pipe wall thickness, mm

Figure 10 – Projected corroded area according to RPA Method

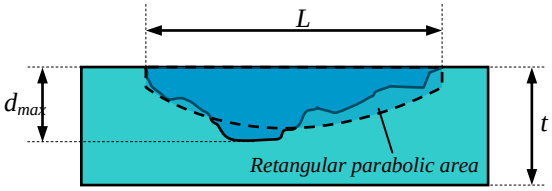

Source: BERTIN, 2015

The rectangular parabolic area (Figure 10) is "composed of an increasing depth rectangle plus a decreasing depth parabola" (BENJAMIN & ANDRADE, 2003, p. 8).

2.2.5 RSTRENG – effective area

RSTRENG method has the same formulation of NG-18 (Equation (3)) with the Folias factor calculated in the same manner (Equation (4)), but with the introduction of two significant modifications:

1) the area used is the area measured along the extent of the defect (Figure 11);

Figure 11 – Projected corroded area according to RSTRENG

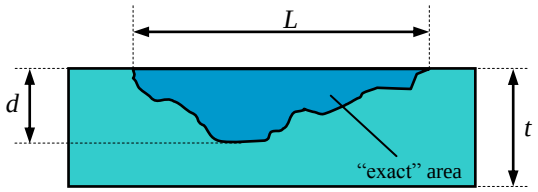

Source: BERTIN, 2015

2) the length of the defect is measured along the defect main axis in a manner called river-bottom (COSHAM, et al., 2007, p. 1255), opposing to the measurement of B31 G and B31 G modified that measure the defect along the longitudinal axis of the pipe (Figure 12). The length of the defect for RSTRENG therefore is bigger than other previous methods increasing the area of the defect considered.

However, in the opinion of Cosham et al.(2007, p. 1255) “the methods for assessing a river-bottom profile are also approximations, because a river-bottom profile is an idealization of the actual three-dimensional shape of a corroded area”.

Figure 12 – Length of the defect according to B31 G and to RSTRENG

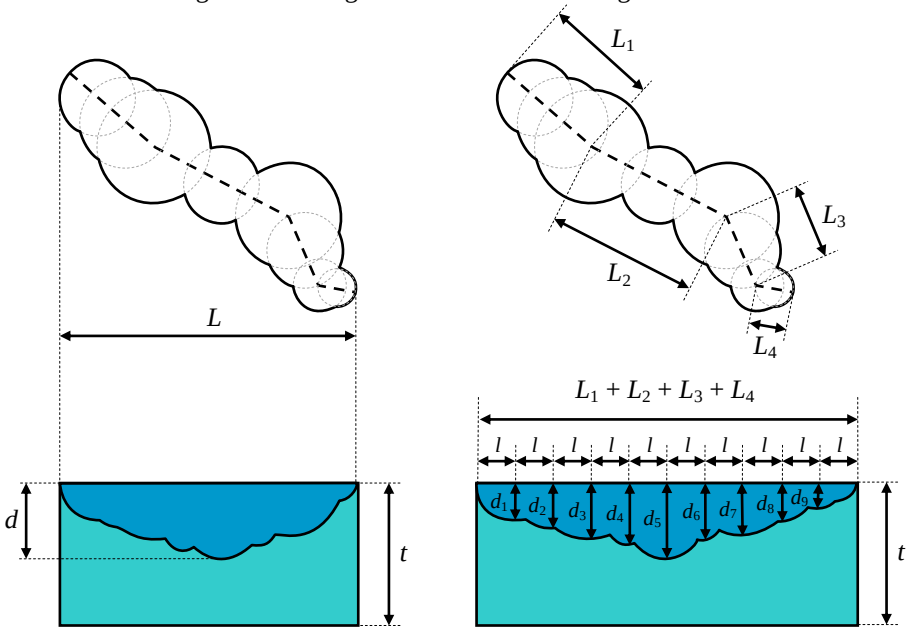

Source: BERTIN, 2015

2.2.6 DNV RP-F101

DNV RP-F101 is a recommended practice (RP) developed by a partnership between British Gas Technology and DNV - Det Norske Veritas, "an autonomous and independent foundation with the objectives of safeguarding life, property and the environment, at sea and onshore" (DET NORSKE VERITAS, 2010, p. 2). It is a semi-empirical method based both on burst tests done by BG Technology and DNV and on three dimensional non linear analysis done by FEM using software ABAQUS (ALVES, 2002). It is applicable to assess corrosion defects on carbon steel pipelines subjected to internal pressure only and internal pressure plus axial loading for a very complex arrangement of defects.

The method assumes a rectangular shape for the corroded defect as on Figure 13, but uses the river-bottom approach do measure the length. In other words, RP-F101 envelopes the defect in a rectangular box. The simplified formulation is very similar to NG-18 with three modifications to be noted: a) a safety factor of 1.05 is used "determined from comparison with laboratory test results with rectangular shaped metal loss defects" (DET NORSKE VERITAS, 2010, p. 9); b) the use of ultimate tensile strength instead of flow stress; and c) the use of average diameter or $D - t$

Figure 13 – Projected corroded area according to DNV RP-F101

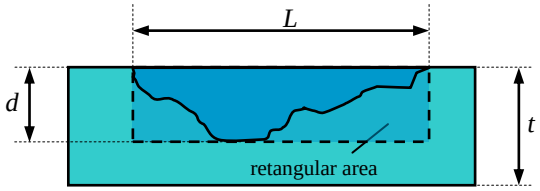

Source: BERTIN, 2015

$$D - t = \frac{D + D_{\text{int}}}{2} \tag{22}$$

where:

D : pipe external diameter, mm

t : nominal pipe wall thickness, mm

D_{int} : pipe internal diameter, mm

The simplified allowed pressure or failure pressure is given by:

$$P_f = 1.05 \times \sigma_u \frac{2t}{D-t}\left(\frac{1-\frac{d_{max}}{\mathrm{t}}}{1-\frac{d_{max}}{\mathrm{t}}\frac{1}{M}}\right) \quad (23)$$

Folias bulging factor is also modified based on test trials:

$$M = \sqrt{1+0.31\left(\frac{\mathrm{L}}{\sqrt{\mathrm{Dt}}}\right)^2} \quad (24)$$

where:

M : Folias bulging factor
P_f : failure pressure, MPa
σ_u : ultimate tensile strength, MPa
D : pipe external diameter, mm
t : nominal pipe wall thickness, mm
d_{max} : maximum corrosion depth, mm
L : length of the defect, mm

The method has nine limitations listed under item 1.8 Exclusions (DET NORSKE VERITAS, 2010, p. 7), as follows:

1) Materials other than carbon linepipe steel.
2) Linepipe grades in excess of X80.
3) Cyclic loading.
4) Sharp defects (i.e. cracks).
5) Combined corrosion and cracking.
6) Combined corrosion and mechanical damage.
7) Metal loss defects attributable to mechanical damage (e.g. gouges).
8) Fabrication defects in welds.
9) Defect depths greater than 85% of the original wall thickness (i.e. remaining ligament[10] is less than 15% of the original wall thickness).

For more detailed analysis, RP-F101 recommends two different approaches: Part A uses the calibrated safety factor approach, comprising of a probabilistic treatment to account for uncertainties regard defect depth and material properties. It provides guidance to assess single defect, interacting defects and complex shape defects by step to step instructions. Part B uses the allowable stress approach to calculate failure pressure. The background of the

[10] Ligament: remaining material after a corrosion attack on a duct normally referred as remaining thickness or remaining area.

development of the DNV-RP-F101 is summarized on a paper by Bjornoy, Sigurdsson and Marley (2001).

2.2.7 PCORR

PCORRC, according to Cosham and Hopkins (2004) and Squarcio (2009) or PCORR, according to Janelle (2005) and Fu et al.(2001) or yet simply Batelle for Caleyo, Gonzáles and Hallen (2002) is a method developed by Batelle Memorial Institute (STEPHENS and LEIS, 2000 *apud* (BJØRNØY & MARLEY, 2001)), the same institution that developed NG-18. Differently from other methods, PCORR is an analytical formulation based on finite element analysis only and not on burst tests. PCORR in fact is a finite element analysis tool. The formulation goes as follows:

$$P_f = \sigma_u \frac{2t}{D}\left(1 - \left(\frac{d_{max}}{t}\right)\left(1 - \exp\left(-0.157\frac{L}{\sqrt{R_e(t - d_{max})}}\right)\right)\right) \quad (25)$$

where:

P_f : failure pressure, MPa

σ_u : ultimate tensile strength, MPa

D : pipe external diameter, mm

t : nominal pipe wall thickness, mm

d_{max} : maximum corrosion depth, mm

L : length of the defect, mm

exp : exponential function equal to e^x

R_e : pipe external radius or $D/2$, mm

2.2.8 WDD – Weighted Depth Difference Method

Cosham and Hopkins (2004) mention a method developed by Cronin and Pick, named CPS or Corroded pipe Strength. The method is mentioned again in Cosham et al. (2007). According to Souza (2003) CPS is a computer software that helps the application of Cronin and Pick´s (2002) method WDD - Weighted Depth Difference (SOUZA, 2003, pp. 17-18). The authors reason that there are two limits for the failure pressure of a pipeline. The upper

limit is the failure of the plain pipe without any defects and the lower limit is the failure pressure of a pipe with a infinite long defect in the form of a groove. The depth of the groove is the maximum depth of the corrosion defect. The method uses the Ramberg-Osgood material model to characterize pipeline steel and derives the following equation for failure pressure of a long groove:

$$P_{Long\ Groove} = \frac{\sigma_{\text{crit}}}{R_0\sqrt{\frac{3}{4}}} t_{\text{L0}} \exp\left(-\sqrt{\frac{3}{4}}\varepsilon_{\text{crit}}\right) \tag{26}$$

for: $\frac{t_{\text{L0}}}{t_0} \geq 0.2$

where:

$P_{Long\ Groove}$	: failure pressure for an infinite long groove defect, MPa
σ_{crit}	: critical stress, equivalent von Mises stress, MPa
R_0	: pipe original internal radius, mm
t_{L0}	: original ligament thickness (at the deepest point in the defect), mm
t_0	: original pipe wall thickness, mm
exp	: exponential function equal to e^x
$\varepsilon_{\text{crit}}$	: critical strain, calculated by the Ramberg-Osgood equation for σ_{crit}

Assuming the upper and lower limits, the failure pressure of a corrosion defect is given by:

$$P_f = P_{\text{Long Groove}} + \left(P_{\text{plain pipe}} - P_{\text{Long Groove}}\right) \times g \tag{27}$$

where:

P_f	: failure pressure, MPa
$P_{\text{Long Groove}}$	: failure pressure for a infinite long groove defect, MPa
$P_{\text{plain pipe}}$	: failure pressure for a pipe without defect, MPa
g	: function of the corrosion defect

with g, function of the corrosion defect, varying from 1.0 to 0.0 and calculated by:

$$g = \frac{\text{Sum WDD}}{\text{Max WDD}} \tag{28}$$

where:

a) the effect of the corrosion is evaluated by summing the weighed depth difference or WDD for a set of measurements, as in equation (29):

$$\text{Sum WDD} = \sum_{\text{i=1}}^{\text{n}} \left\{ \text{sech} \left[\frac{z_{\text{eval}} - z_i}{\sqrt{D(t_0 - d_{\max})}} \right] \times \left[\left(1 - \frac{d^*}{t_0} \right) - \left(1 - \frac{d_{\text{eval}}}{t_0} \right) \right] \Delta z \right\} \quad (29)$$

and

b) the maximum weighed depth difference is given by equation (30) which is similar to equation (29) except the fact that corrosion depth d^* is set to 0.0 corresponding to a pipe without defects. Max WDD is determined at all locations except the evaluated point.

$$\text{Max WDD} = \sum_{\text{i=1}}^{\text{n}} \left\{ \text{sech} \left[\frac{z_{\text{eval}} - z_i}{\sqrt{D(t_0 - d_{\max})}} \right] \times \left[\left(1 - \frac{0.0}{t_0} \right) - \left(1 - \frac{d_{\text{eval}}}{t_0} \right) \right] \Delta z \right\} \quad (30)$$

where:

z_{eval}	: location of the evaluation point from an arbitrary origin
z_{i}	: current position measured from the same arbitrary origin, mm
D	: diameter of the pipe, mm
t_0	: original pipe wall thickness, mm
d^*	: corrosion depth at a given location, mm
$d_{\max}$	: maximum corrosion depth, mm
d_{eval}	: corrosion depth at the evaluation point, mm
Δz	: distance between adjacent measurements, mm
sech	: hyperbolic secant function

The idea, given the complexity of the corrosion defects, is to weigh the depth of the defect on one location against a defined point depth, called evaluation point. It uses the same principle of several measurements as RSTRENG, but weighing them against one measurement that could be the deepest one.

Figure 14 – WDD measurement method

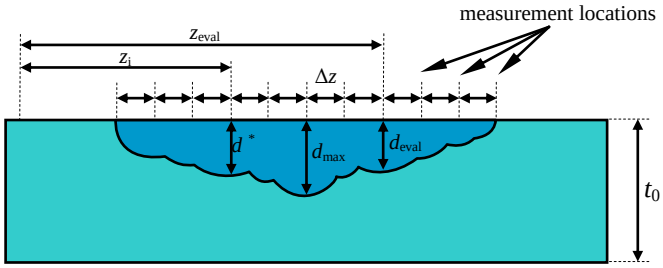

Source: (adapted from (CRONIN & PICK, 2002))

2.2.9 Choi *et al*

Fitness-for-purpose, mentioned by Cosham and Kirkwood (2000) is also discussed by Choi et al. (CHOI, et al., 2003). They performed a series of burst tests on machined corrosion-like defects and compared the results with finite element simulations in order to derive a failure criterion. A limit load solution for corroded API (American Petroleum Institute) X65 pipes, in good agreement with burst test results, is obtained as a function of defect depth, length and pipe geometry, as follows:

for $\frac{L}{\sqrt{Rt}} < 6$

$$P_f = 0.9\sigma_u \frac{2t}{D}\left[C_2\left(\frac{1}{\sqrt{R_e t}}\right)^2 + C_1\left(\frac{1}{\sqrt{R_e t}}\right) + C_0\right] \quad (31)$$

where:

$$C_2 = 0.1163\left(\frac{d_{max}}{t}\right)^2 - 0.1053\left(\frac{d_{max}}{t}\right) + 0.0292 \quad (32)$$

$$C_1 = -0.6913\left(\frac{d_{max}}{t}\right)^2 + 0.4548\left(\frac{d_{max}}{t}\right) - 0.1447 \quad (33)$$

$$C_0 = 0.06\left(\frac{d_{max}}{t}\right)^2 - 0.1035\left(\frac{d_{max}}{t}\right) + 1.0 \quad (34)$$

for $\frac{L}{\sqrt{R_e t}} \geq 6$

$$P_f = 0.9\sigma_u \frac{2t}{D}\left[C_1\left(\frac{1}{\sqrt{R_e t}}\right) + C_0\right] \quad (35)$$

where:

$$C_1 = 0.0071\left(\frac{d_{max}}{t}\right) - 0.0126 \quad (36)$$

$$C_0 = -0.9847\left(\frac{d_{max}}{t}\right) + 1.1101 \quad (37)$$

P_f : failure pressure, MPa
σ_u : ultimate tensile strength, MPa
D : pipe external diameter, mm
t : pipe wall thickness, mm
d_{max} : maximum corrosion depth, mm
R_e : pipe external radius or D/2, mm

A summary of the equations of failure pressure and bulging factors, where applied, is presented in appendix E, Table 25. These equations are not suitable to calculate internal failure pressure for pit corrosion, since its dimensions are too small. However, if calculated for the worst pit corrosion dealt in the present work, the pit with 1 mm of diameter and 4 mm of depth, the resulting pressure would be higher if compared to internal failure pressure, for undamaged pipe, calculated by Barlow's equation (1), and presented in the two first rows of Table 2 as reference.

Table 2 – Internal failure pressure for pipe with pit corrosion - calculated by assessment methods

Assessment Methods	parameters	Pipe diameter (mm)		
		300	400	500
Result from Barlow's equation	P_f *	48.7	36.53	29.22
	P_f **	59.7	44.78	35.82
NG18	P_f *	55.19	41.70	33.36
	M	1.00007	1.000052	1.000042
B31G	P_f *	53.13	40.18	32.14
	M	1.000089	1.000067	1.000053
85dL	P_f *	55.19	41.70	33.36
	M	1.00007	1.000052	1.000042
RSTRENG	P_f *	55.19	41.70	33.36
	M	1.00007	1.000052	1.000042
DNV F101	P_f **	65.98	48.84	38.77
	M	1.000034	1.000026	1.000021
PCORR	P_f **	59.64	44.74	35.79
Choi *et al*	P_f **	52.39	39.30	31.45
	C_0	0.976667	0.976667	0.976667
	C_1	-0.07258	-0.07258	-0.07258
	C_2	0.00939	0.00939	0.00939

* Internal pressure P_f (MPa), calculated for yield stress, σ_y = 487 MPa
** Internal pressure P_f (MPa), calculated for ultimate tensile strength, σ_u = 597 MPa
Failure pressures calculated for a defect 1 mm – diameter and 4 mm – depth.
SOURCE: Bertin, 2015

Most of the corrosion assessment methods relate internal failure pressure to the remaining metal that would have to support loadings. High values of internal failure pressure are obtained for two main reasons: a) equations are not derived for single pit corrosion of small dimensions and b) little volume of metal is lost, hence no substantial modification in the remaining metal volume is perceived.

Again, there is no intention of comparing the formulations of the various assessment methods with the formulation present at the end of this work. The sole purpose of Table 2 is to emphasize that those equations are not suited for very small defects such as pit corrosion because they, in general, give values of internal failure pressure greater than values for pipes without any defect. WDD is not included in Table 2 because since the method presupposes a long and complex defect, it is not applicable for a single pit. In section 4 a better discussion on this topic will be carried on.

Comparing with ASME B31G, modified ASME B31G, DNV RP-F101 and Choi et al. formulation (CHOI, et al., 2003), Adib-Ramezani, et al. (2006b) studied the integrity of gas pipelines by means of SINTAP – Structural Integrity Assessment Procedure for semi-spherical, semi-elliptical and elongated groove defects. Analyses were conducted by means of nonlinear FEM and used mainly SINTAP modified by notch-based failure assessment diagram or 'NFAD'. The authors concluded that "SINTAP procedure and NFAD concept using notch stress intensity point of view provide safety factors, which are located between lower and upper bound estimates by other codified methods for chosen defects" (ADIB-RAMEZANI, et al., 2006b).

Adib-Ramezani et al. (2007) also studied safety factor of gas pipelines with an elongated corrosion defect. SINTAP curves and the safety factor were calculated by means of elastic-plastic finite element simulations. SINTAP was modified to take into account the fact that the defect is a curved surface and not a crack. Safety factor was also calculated by probabilistic methods, in this case, Monte Carlo simulation, first-order reliability method – FORM and second-order reliability method – SORM. FORM and SORM had similar results, therefore only the second one is used. Safety factor calculated by deterministic approach were well in range of the minimum safety factor. SORM also performed well but Monte Carlo Simulation was unable to deliver results "in a fast and economic way" (ADIB-RAMEZANI, et al., 2007, p. 131).

2.3 LITERATURE ON PIT CORROSION

Apart from corrosion assessment methods, literature related to pit corrosion and its influence on structural capacity of pipes is concentrated on five main areas: (a) the formation of cracks inside the pit and their propagation; (b) pit corrosion and SCF – stress concentration factor and (c) influence of the relative position for single elongated or two defects; (d) safety factor and pit corrosion and (e) Pit corrosion and fatigue.

2.3.1 Pit Corrosion and cracks

The formation of cracks inside the pit may lead to the evolution of the defect in one of two ways: the breaking of the passive film exposing the undamaged metal to corrosive

environment, as already explained in section 1 or the actual formation of fissures and cracks leading to the ultimate failure of the pipe and bursting.

Turnbull and Zhou (2004) exposed a steel disc from a steam turbine to three environmental conditions: aerated water, non-aerated water and aerated water with 1.5 ppm[11] of chloride ion. They observed pit corrosion on all samples and crack initiation on aerated water and the chloride aerated solution. They concluded that the transition from pit to crack was described by a Weibull cumulative distribution function.

Turnbull, McCartney, & Zhou (2006), conducting experiments on a disc steel (3NiCrMoV) in a simulated condensate environment, concluded that "quantitatively, 43% of cracks extended beyond the base of the pit and also broke the surface in the expected manner. However, 50% broke the surface but the pit base was deeper than the crack, and 7% extended beyond the pit base but did not break the surface".

Turnbull, Horner and Connolly (2008) examined X-ray tomographic images of pits and cracks showing cracks initiating at the mouth of the pit. They also conducted a Finite Element Analysis on a solid cylindrical specimen with a single "bullet-shaped" pit defect to simulate the same experimental results. The model was loaded with uniform stress at one end. Von Mises material model was used to ensure elastic-plastic behavior of the material. The model showed inconsistencies with the morphology of the pits and cracks. They concluded that "the evolution of a stress corrosion crack from a pit is a highly complex process" (TURNBULL, et al., 2008, p. 640).

Turnbull, Wright and Crocker (2010) conducted finite element analysis on a cylindrical specimen of 3NiCrMoV steel with U-shaped pit corrosion on its surface. Pit mouth opening adopted was 666 μm and depths of 100 and 500 μm. They used a linear tetrahedron element and refined around the pit region. The elastic-plastic character of the material was ensured by a von Mises material model. They try to model pit corrosion growth using "three concentric pits of slightly different radii" (TURNBULL, et al., 2010, p. 1493) and a command of ABAQUS® that allows the removal of elements form a mesh. The cylindrical specimen was fixed at one end and loaded with a uniform stress of 90% of $\sigma_{0.2}$ at the other end. They concluded that maximum "plastic strain is localized on the pit walls below the pit mouth rather than at the base" (TURNBULL, et al., 2010, p. 1497), but stress was maximized at the pit base. However, for low applied stress in the absence of plastic deformation maximum

[11] ppm – parts per million

stress was found on the pit walls below the pit mouth, in accordance with the findings of Cerit, Genel and Eksi (2009), ahead detailed.

Bertin, R.J., Abdalla Filho, J.E. & Machado, R.D. (2010) numerically compared maximum stress on curved and plane surfaces, considering plasticity. They devised a formulation to correlate maximum stress inside the pit, σ_{max}, its aspect ratio, $a/2c$, the ultimate tensile strength, σ_u, and the applied load, σ, either longitudinal traction stress, for flat steel plate, or hoop stress, for a curved steel plate.

$$\sigma_{max}/\sigma_u = \alpha \ln(a/2c) + \beta \tag{38}$$

where:

σ_{max} : is the maximum stress inside the pit;

σ_u : is the ultimate tensile strength;

$a/2c$: is the strain aspect ratio of the pit, its depth, a, divide by its aperture, $2c$;

α : is a parameter related to applied stress and is represented by a quadratic equation of the type $y = ax^2 + bx + c$;

β : is a parameter related to applied stress and is represented by a quadratic equation of the type $y = ax^2 + bx + c$.

For plane surface subjected to a longitudinal traction load σ, values of α and β are:

$$\begin{aligned} \alpha &= -2.017 \times 10^{-6}\sigma^2 + 9.905 \times 10^{-4}\sigma + 2.438 \times 10^{-3} \qquad (R^2 = 99{,}8\%)^{12} \\ \beta &= -6.361 \times 10^{-6}\sigma^2 + 5.126 \times 10^{-3}\sigma - 1.268 \times 10^{-2} \qquad (R^2 = 84{,}9\%) \end{aligned} \tag{39}$$

For curved surface subjected to hoop stress σ, values of α and β are:

$$\begin{aligned} \alpha &= -3.344 \times 10^{-4}\sigma^2 + 1.604 \times 10^{-2}\sigma - 1.120 \times 10^{-2} \qquad (R^2 = 90.5\%) \\ \beta &= -5.068 \times 10^{-5}\sigma^2 + 7.559 \times 10^{-2}\sigma - 2.232 \times 10^{-2} \qquad (R^2 = 98.8\%) \end{aligned} \tag{40}$$

For both cases combined, values of α and β are:

[12] R^2 is the statistical coefficient of determination, given by:

$$R^2 \equiv 1 - \frac{residual\ sum\ of\ squares}{total\ sum\ of\ squares} \equiv 1 - \frac{\sum_i (y_i - f_i)^2}{\sum_i (y_i - \bar{y})^2}$$

$$\alpha = -4.070 \times 10^{-6}\sigma^2 + 4.529 \times 10^{-3}\sigma - 3.848 \times 10^{-2} \qquad (R^2 = 98.1\%)$$
$$\beta = -1.368 \times 10^{-6}\sigma^2 + 8.723 \times 10^{-4}\sigma - 7.588 \times 10^{-3} \qquad (R^2 = 75.5\%) \tag{41}$$

Horner et al. (2011) made a stress corrosion test on a 3 NiCrMoV steel taken from a steam turbine disc. They submitted six cylindrical specimens to stress corrosion testing in aerated water containing 1.5 ppm of chloride ion. The resulting cracked specimens were examined with computed X-ray microtomography. Finite element simulations were also used, as previously mentioned in Turnbull, Wright and Crocker (2010). They concluded that "the unique images of pits and stress corrosion cracks at different exposure times show convincingly that the preferred site for crack initiation is on the pit wall close to the pit mouth" (HORNER, et al., 2011, p. 3483).

Turnbull and Zhou (2012) made fatigue experiments with a sample of steel from a turbine blade. Samples were pre-cracked and submitted to cyclic load in a chemically aggressive environment of chloride and sulfuric ion aerated solution. They measured corrosion potential and cracks growth rate. They concluded that for the material tested "there was no effect of crack size on the corrosion fatigue crack growth" in deaerated solution (TURNBULL & ZHOU, 2012). However, short crack growth rate was 20 times higher that long crack in aerated solution.

Rajabipour and Melchers (2013), partially based on Bertin, R.J., Abdalla Filho, J.E. and Machado, R.D. (2010) modeled a small section of a pipe under increasing axial load and constant internal pressure and placed an elliptical pit defect on the exterior surface of the pipe. Plasticity was considered. They concluded stress required for plasticity initiation depended on the aspect ratio of the pit mouth. They also concluded that "fracture around the pipe wall can be associated with a critical plastic section" (RAJABIPOUR & MELCHERS, 2013).

2.3.2 Pit Corrosion and Stress Concentration Factor – SCF

Cerit, Genel and Eksi (2009) simulated on ANSYS® pit corrosion of various diameters and depths on a solid metal block to which was applied a tension of 1.0 MPa. They concluded that the pit aspect ratio $a/2c$ is a main parameter affecting the value of SCF for a elastic linear analysis. They found maximum stress at the pit wall below the pit mouth for that low applied stress condition. A formulation for stress concentration factor – SCF was proposed.

Cerit (2013) analyzed the stress distribution inside a semi elliptical pit corrosions on a cylindrical solid under torsion. Torsional load was applied so that the resulting maximum shear stress did not exceeded 1MPa. The shape of the pit corrosion was obtained by means of a series of scanning electron microscope micrographs. He concluded that the SCF for this case is a function of the depth and diameter of the pit, in other words, the aspect ratio $a/2c$ is a governing factor is the main parameter affecting SCF.

Ji et al. (2015) investigate the SCF of single elliptical pit corrosion using finite element analysis. Their intent is to quantify the effect of the geometry of the pit on SCF by means of least square support vector machine – LS-SVM and compare these results with those of FEM. They developed a predictive model for SCF using LS-SVM, "as surrogate to the computationally intensive 3-D FE analysis … in good agreement for a variety of testing examples" (JI, et al., 2015).

2.3.3 Influence of the relative position for single elongated or two defects

The shape of corrosion defect, specifically elongated ones defined as grooves, and its position with respect to the longitudinal direction of the pipe was studied by Lee and Kim (2000). They had compared Von Mises[13] stress results obtained by FEM with those obtained by methods B 31G and B 31G modified. They had suggested that FEM analysis may result in better failure prediction on pipes subjected to internal pressure. They also had demonstrated that the depth and length of corrosion defect has considerable effect on failure and, furthermore, for identical defects the angle of the defects with respect to the longitudinal axis of the pipe is of some significance.

According to Chouchaoui and Pick (1996, p. 17) "corrosion occurs as individual pits, colonies of pits, general wall-thickness reduction, or in combination". These authors analyzed a series of results of burst tests on pipes with longitudinally aligned defects. Those tests had been conducted on samples of API X46 pipe, in service since 1956, with 304.8 mm average diameter and 6.35 mm average nominal thickness of the wall. A modulus of elasticity of 207 GPa was used and tests were conducted to obtain hoop and longitudinal stresses for 0.2% deformation normally associated to yield stress. Hoop stresses varied from 356 MPa to 381 MPa with average of 372 MPa and standard deviation of 10.34 MPa. Longitudinally yield stresses varied from 320 MPa to 341 MPa with average of 327 MPa and standard deviation of

[13] Richard Edler von Mises (1883 – 1953) was an Austro-Hungarian scientist, mathematician, and Professor of Aerodynamics and Applied Mathematics at Harvard University

8.98 MPa. Defects were created by electro erosion with an approximate elliptic shape with average length of 19.98 mm, width of 20.81 mm and depth of 58% of the wall thickness. Defects had been arranged longitudinally, in two rows at either side of the seam. Separation among defects ranged from 0 to 6 times thickness of the pipe wall. Two series of tests had been conducted, with closed extremity and open extremity. The conclusion was that in pits of different depths failure occurs in the ligament of the deepest pit. When depths are similar, there is tendency that failure extends among defects that could be treated as one long defect if they touch each other. Finally, the pressure of rupture calculated through the criterion of local plastic collapse, for the case of opened extremities, has good correlation with experimental results.

Chen et al. (2015) investigate failure pressure of high strength pipeline with single and multiple corrosions defects using non-linear finite element analysis. They, based on several papers including (ABDALLA FILHO, et al., 2014) developed regression equations to predict failure pressure in good agreement with experimental data from literature. They proposed an assessment procedure for high strength pipes with multiple corrosion defects.

Chen et al. (2015) investigate failure pressure of X80 pipeline with interacting defects. Again, based on several papers including (ABDALLA FILHO, et al., 2014), they developed regression equations to predict failure pressure and compared with experimental data from literature, this time for a specific pipe.

2.4 SECTION SUMMARY

Section 2 reviewed articles discussing and comparing methods for appraisal of corroded pipelines. All of them use Barlow's equation for thin wall pipes under internal pressure multiplied by a reduction factor. However, some of them, when applied to small or shallow defects, may produce results of failure pressure greater than the one for a pipe without any defect. Several articles (TURNBULL & ZHOU, 2004), (TURNBULL, et al., 2006), (TURNBULL, et al., 2008), (TURNBULL, et al., 2010), (BERTIN, et al., 2010), (HORNER, et al., 2011) and (RAJABIPOUR & MELCHERS, 2013) report formation of cracks as a result of the stress state inside or emanating from the pit or the level of stress that could induce cracks. Fissures, as explained on Section 1, may lead to rupture of passive film and exposition of untouched metal to corrosion attack. Cracks can also be the cause of the

rupture of the pipe and consequent leakage or, worst, its catastrophic failure and burst. Although using a very small load, two articles (CERIT, et al., 2009) and (CERIT, 2013), describe the importance of the pit aspect ratio, $a/2c$, on its SCF (JI, et al., 2015). Also using aspect ratio as key parameter developed a prediction model for SCF (LEE & KIM, 2000), (CHOUCHAOUI & PICK, 1996) and (CHEN, et al., 2015) studied the effect of multiple corrosion defects on pipelines.

3 FUNDAMENTAL CONCEPTS

Because all the simulations and analyses performed in the present work were done considering plastic deformation, this section, discusses plasticity. Elasticity is also discussed as an introduction to plasticity. The plastic material model used here in simulations, multilinear isotropic hardening, is explained. The use of true strain, yield criteria, von Mises criterion and hardening rules are also explained. Section 2 presented the methods of appraisal of corroded pipelines. In the last topic of this Section 3, failure pressures are calculated, as numerical examples, for six of those methods. Results are compared with failure pressure for undamaged pipe.

3.1 ELASTICITY

Elasticity denotes the property of a material that returns to its original dimensions after the load to it applied is removed. It expresses the linear relationship between stress and strain and is known as Hooke's Law. The concept was first proposed by Robert Hook[14] and latter developed in its present form by Thomas Young[15]. Mathematically Hooke's law can be formulated as:

$$\sigma = E\varepsilon \tag{42}$$

where:

E : is the modulus of elasticity mentioned by Young,

σ : is the stress or "pressure", and

ε : is the strain or the ratio of the deformation by the original length of the "column of the same substance".

For a three-dimensional state of stress where components σ_x, σ_y, σ_z, τ_{xy}, τ_{yz} and τ_{zx} (or in terms of continuum mechanics, σ_{ij}) produce strains ε_x, ε_y, ε_z, γ_{xy}, γ_{yz} and γ_{zx} at a point (or ε_{kl}),

[14] Robert Hooke (1635 – 1703) was a British polymath, architect and natural philosopher. He was curator of experiments of the Royal Society and Gresham Professor of Geometry.
[15] Thomas Young (1773 – 1829) was a British physician, polymath and Egyptologist. He is most known by his work on wave theory of light, physiology of the vision and solid mechanics.

Equation (42) can be generalized as a series of linear equations that, in the context of continuum mechanics, is written:

$$\begin{gathered}\bar{\bar{\sigma}} = \bar{\bar{\bar{\bar{C}}}}\bar{\bar{E}} \\ that\ is, \\ \sigma_{ij} = c_{ijkl}\varepsilon_{kl}\end{gathered} \tag{43}$$

where coefficients c_{ijkl} represent material properties directly related to the material for which the equations are formulated, σ_{ij} are the three normal stress components and the three tangential components and ε_{kl} are the three normal strains and the three angular strains.

Another way of representing the relation between stress and strain is a stress strain diagram resulting from tensile-tests. According to Timoshenko, it was Jean-Victor Poncelet[16] in his book "*Mécanique industrielle*" from 1839 that introduced tensile-test diagrams (TIMOSHENKO, 1983, p. 88). Ever since, these diagrams have been used currently in sciences of materials and engineering.

Figure 15 depict an example of a diagram for a metallic alloy. Equation (42) is represented by the slope of $\overline{OA}$ and gives the value of the elastic modulus.

Figure 15 – Diagram stress – strain for a metallic alloy

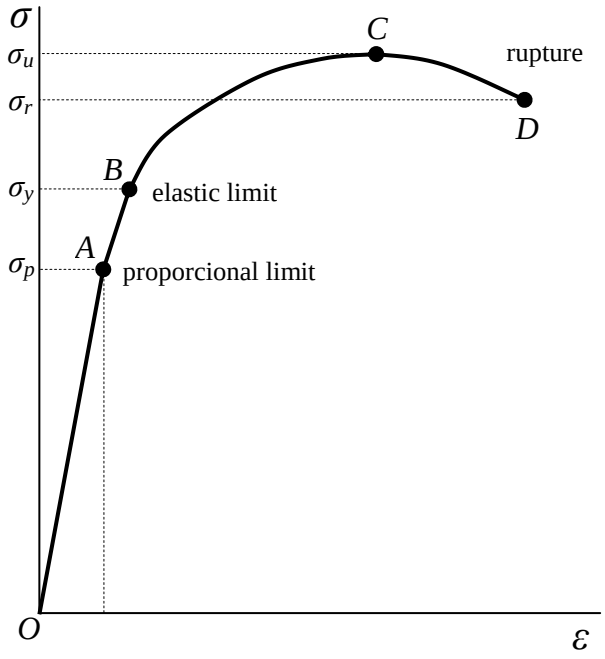

SOURCE: Bertin, 2015

[16] Jean-Victor Poncelet (1788 – 1867) was a French engineer, mathematician, professor at the *Faculté des Sciences* at the University of Paris and commandant general of the *École Polytechnique*.

Point *A* marks the end of the linear behavior of the material and is called proportional limit, associated to proportional stress σ_p. From *A* to *B,* although not linear, the relation of stress and strain still is in the elastic domain providing the removal of the load would still not cause permanent deformation. Point B is called elastic limit and is associated to yield stress σ_y. From point O to B, deformation on the body is recoverable. In atomic scale, as explained by Callister, "macroscopic elastic strain is manifested as small changes in the interatomic spacing and the stretching of interatomic bonds" (CALLISTER, 2001, p. 155).

3.2 PLASTICITY

After point B, interatomic bonds are broken from one atom and established with its neighbor. Once a certain amount of atoms or molecules are moved in relation to others, they do not return to their original positions, hence rendering deformation permanent. This is "accomplished by means of a process called slip, which involves the motion of dislocations" (CALLISTER, 2001, p. 160). From point B, stress is not proportional to strain anymore and part of the deformation undergone by the material is permanent. If stress is increased it will build at its maximum value at point *C*, corresponding to ultimate stress σ_u and from *C* stress will progress until rupture at point *D*, associated to stress of rupture σ_r.

In order to better study the problem of elasticity and plasticity of materials a series of simplified models were proposed by an assemblage of springs and dashpots, with displacement representing strain and force representing stress. Several plastic behaviors of materials, some hypothetical, were developed such as: rigid-perfectly plastic, rigid plastic with linear hardening, also known as Kelvin[17] model, elastic-perfectly plastic, or Maxwell[18] model and elasto-plastic with linear hardening, or as "standard solid" model (LUBLINER, 2008, p. 62). This last arrangement, in the form of multilinear isotropic hardening will be used on the material modeling for finite analysis simulations and explained in more detail.

3.2.1 Elasto-plastic with linear hardening

Suppose the behavior of a material can be modeled as an assemblage of a spring of elastic constant E_1 arranged in series with another spring of elastic constant E_2 mounted in

[17] William Thomson (1824 – 1907), 1st Baron Kelvin, was an Irish mathematical physicist and engineer. The absolute scale of temperature is named after him.
[18] James Clerk Maxwell (1831 – 1879) was a Scottish theoretical physicist known for electromagnetic theory.

parallel with a dashpot of damping constant *Q* (Figure 16). The system showed in Figure 16 presents a bilinear behavior, since an elastic (and instantaneous) displacement occurs due to the spring (E_1) followed by an additional and progressive displacement due to the system spring (E_2) and dashpot.

Figure 16 – Elasto-plastic model or "standard solid"

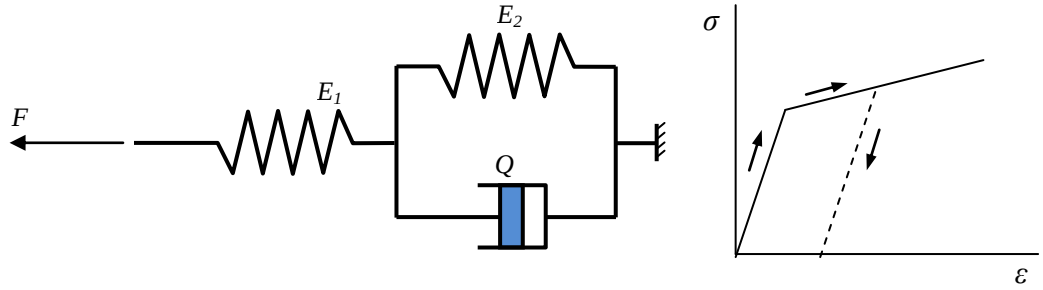

SOURCE: Bertin, 2015

Static equilibrium requires that force *F* on the left-hand spring is equal to the sum of forces of the right-hand spring and dashpot and since a single body with the same area is being modeled, the problem can be equated as:

$$E_1\varepsilon^e = E_2\varepsilon^p + Q\frac{d\varepsilon^p}{dt} \tag{44}$$

for total strain:

$$\varepsilon = \frac{\sigma}{E_1} + \varepsilon^p \tag{45}$$

And for the rate of the plastic strain equation is:

$$\frac{d\varepsilon^p}{dt} = \frac{1}{Q}\sigma - \frac{E_2}{Q}\varepsilon^p \tag{46}$$

Given an increment of stress as a function of time, the differential equation for inelastic strain can be solved for ε^p(t):

$$\varepsilon^p(t) = \frac{1}{K}\int_{-\infty}^{t} e^{-\frac{(t-t')}{\Gamma}}\sigma(t')dt' \tag{47}$$

where:

- $-\infty$: is a convenient reference time were $\varepsilon^p = 0$,
- Γ : is a material property constant with dimension of time and equals to Q/E_2,
- t : time at final configuration,
- t' : time at initial configuration,
- σ : applied stress

For multilinear isotropic hardening, several Γ constants are calculated representing each change of slope of the stress-strain curve.

Figure 17 – Multilinear isotropic hardening model

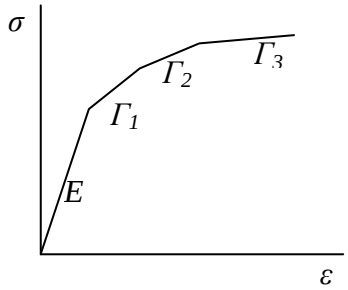

SOURCE: Bertin, 2015

3.2.2 Stress and strain

Stress given by Equation (43) can be written in matrix format originating the Cauchy stress tensor:

$$\boldsymbol{\sigma_{ij}} = \begin{bmatrix} \sigma_{xx} & \tau_{xy} & \tau_{xz} \\ \tau_{yx} & \sigma_{yy} & \tau_{yz} \\ \tau_{zx} & \tau_{zy} & \sigma_{zz} \end{bmatrix} \tag{48}$$

where σ_{xx}, σ_{yy}, σ_{zz}, τ_{xy}, τ_{yz}, τ_{zx} are, respectively, the three normal stress components and the three tangential components, remembering that $\tau_{ij} = \tau_{ji}$.

The stress tensor, by its turn, can be decomposed into:

a) a mean hydrostatic stress tensor, $\boldsymbol{\sigma_{kk}}$, responsible for changes of volume of the stressed body;

$$\boldsymbol{\sigma_{kk}} = \begin{bmatrix} \sigma_m & 0 & 0 \\ 0 & \sigma_m & 0 \\ 0 & 0 & \sigma_m \end{bmatrix} \tag{49}$$

where σ_m is the mean stress, or:

$$\sigma_m = \frac{1}{3}\left(\sigma_{xx} + \sigma_{yy} + \sigma_{zz}\right) \tag{50}$$

b) a deviatoric stress tensor, $\boldsymbol{S_{ij}}$, responsible for distorting the body.

$$\boldsymbol{S_{ij}} = \begin{bmatrix} S_{xx} & S_{xy} & S_{xz} \\ S_{yx} & S_{yy} & S_{yz} \\ S_{zx} & S_{zy} & S_{zz} \end{bmatrix} = \begin{bmatrix} \sigma_{xx} & \tau_{xy} & \tau_{xz} \\ \tau_{yx} & \sigma_{yy} & \tau_{yz} \\ \tau_{zx} & \tau_{zy} & \sigma_{zz} \end{bmatrix} - \begin{bmatrix} \sigma_m & 0 & 0 \\ 0 & \sigma_m & 0 \\ 0 & 0 & \sigma_m \end{bmatrix} \tag{51}$$

When dealing with the possibility of large-strain, the concept of true strain[19] is necessary. According to Rees (2006, p. 55) true strain or logarithmic strain was first used by Prandtl[20] and Hencky[21] and is characterized by incremental displacement:

$$\varepsilon = \int \frac{dl}{l} = \ln\left(\frac{l}{l_0}\right) \tag{52}$$

Generalizing the incremental infinitesimal displacement concept for three dimensions it is possible to determine the increase of strain in an arbitrary point inside a solid body by means of the strain tensor, $\boldsymbol{\varepsilon_{ij}}$ (for $\varepsilon_{ij} = \varepsilon_{ji}$), given by:

$$\boldsymbol{\varepsilon_{ij}} = \begin{bmatrix} \varepsilon_{xx} & \varepsilon_{xy} & \varepsilon_{xz} \\ \varepsilon_{yx} & \varepsilon_{yy} & \varepsilon_{yz} \\ \varepsilon_{zx} & \varepsilon_{zy} & \varepsilon_{zz} \end{bmatrix} = \frac{1}{2}\left(\frac{\partial u_i}{\partial x_j} + \frac{\partial u_j}{\partial x_i}\right) \tag{53}$$

[19] True strain: is the strain originated by true stress. True stress is the applied load divided by the actual cross-sectional area that changes with time. True strain is also known as Hencky strain while engineering strain, the one originated by engineering stress (applied load divided by original cross-sectional area that is considered constant over time), is known as Cauchy strain.

[20] Ludwig Prandtl (1875 – 1953) was a German engineer and professor at the Technical University Hannover, at that time Technical School.

[21] Heinrich Hencky (1885 – 1951) is a German engineer and professor at University of Delft (Netherland), at the Massachusetts Institute of Technology, USA and at the Chemistry & Technology Institute in Kharkov, Russia.

3.2.3 Yield criteria

When the concept of plasticity is applied to metals, the most used yield criteria are based on two hypothesis: a) the influence of hydrostatic stress is negligible and b) for isotropic material yield must depend on the intensity of the applied stress and not affected by axis rotation. For hypothesis a) a yield function would be written as a function of the stress invariants I_1, I_2 and I_3 of the stress tensor.

$$I_1 = tr(\boldsymbol{\sigma_{kk}}) = \delta_{ij}\sigma_{ij} \text{ (trace of the stress tensor)} \tag{54}$$

where δ_{ij} is the Kronecker delta ($\delta_{ij} = 1$, if $i = j$ and $\delta_{ij} = 0$, if $i \neq j$).

$$I_2 = \frac{1}{2}\left(\sigma_{ij}\sigma_{ij} - \sigma_{ii}\sigma_{kk}\right) \tag{55}$$

$$I_3 = \det\left(\boldsymbol{\sigma_{ij}}\right) \text{ (determinant of the stress tensor)} \tag{56}$$

For hypothesis b) a yield function would be written through the deviatoric stress invariants J_2 and J_3.

$$J_2 = \frac{1}{2}\left(\sigma_{ij}\sigma_{ij}\right) \tag{57}$$

$$J_3 = \det\left(S_{ij}\right) \text{ (determinant of the deviatoric stress tensor)} \tag{58}$$

When applied to soils, rocks, and concrete, the yield criterion hypothesis that hydrostatic stress is negligible is not possible; therefore plasticity theory is dependent of the mean stress.

For ductile metals, such as steel, two criteria are usually used: Tresca criterion and von Mises criterion.

3.2.4 Tresca Criterion

Tresca[22] yield criterion, proposed in his 1864 work "*Mémoire sur l'écoulement des corps solides soumis à de fortes pressions*", admits that plastic deformation begins when maximum shear stress attains a critical value, in this case, yield stress in pure shear:

$$\frac{1}{2}(\sigma_1 - \sigma_3) \geq \tau_{crit} = \frac{\sigma_t}{2} \tag{59}$$

where:

τ_{crit} : is the critical value of maximum shear stress equals to the yield stress in pure shear,

σ_1 : is the maximum principal normal stress,

σ_3 : is the minimum principal normal stress,

σ_t : is the tensile yield strength.

3.2.5 Von Mises Criterion

Von Mises criterion, proposed in his 1913 work "*Mechanik der festen Körper im plastisch deformablen Zustand*", admits that plastic deformation begins when the value of elastic strain energy of distortion reaches a critical value, in mathematical terms:

$$\frac{J_2}{2G} \geq W_D \tag{60}$$

where:

W_D : is the elastic strain energy of distortion,

J_2 : is the second invariant of the deviatoric stress tensor,

G : is the elastic shear modulus.

In terms of principal stresses, von Mises criterion would be written as:

$$\frac{1}{12G}[(\sigma_1 - \sigma_2)^2 + (\sigma_2 - \sigma_3)^2 + (\sigma_1 - \sigma_3)^2] \geq W_D \tag{61}$$

[22] Henri Édouard Tresca (1814 – 1885) was a French mechanical engineer and professor at the *Conservatoire National des Arts et Métiers*.

where σ_1, σ_2, and σ_3 are principal stresses. Tensile yield strength, σ_t, in this case would be given by:

$$\sigma_t = \sqrt{\frac{(\sigma_1 - \sigma_2)^2 + (\sigma_2 - \sigma_3)^2 + (\sigma_1 - \sigma_3)^2}{2}} \tag{62}$$

3.2.6 Tresca criterion compared to von Mises criterion

Graphic representation of elastic surfaces of Tresca and von Mises are done in the tridimensional stress of Haig-Westergaard, where Tresca's surface corresponds to a infinite hexagonal prism and von Mises' surface corresponds to a infinite cylinder. Both surfaces are centered on a spacial diagonal that passes through the origin of the system of coordinates σ_i, σ_j, σ_k, in other words, surfaces circumscribe the hydrostatic axis. Inside the surfaces elastic deformation occurs, while over the surface deformation is plastic. On plane stress, when σ_k = 0, Tresca's and von Mises' tridimensional surfaces are projected on σ_i, σ_j plane, respectively, as a distorted hexagon and as an ellipsis (Figure 18).

Figure 18 – Yield locus for plane stress for Tresca and von Mises yield condition

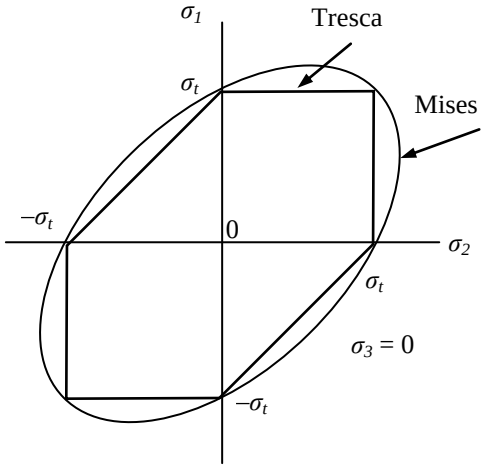

SOURCE: Bertin, 2015 (adapted from (MARCINIAK, et al., 2002))

3.2.7 Hardening rules

When, due to increasing load, the initial yield stress is attained, a new yield surface is necessary to express the current flow stress for the material. Since there is plastic strain outside the initial yield surface, it becomes necessary to account for the effect of plasticity. If loading occurs on a steady state basis, the yield surface may expand uniformly and the hardening is said to be isotropic. If loading occurs cyclically, the yield surface may translate from its previous position and the hardening is called kinematic.

For von Mises' criterion, the two hardening rules could be displayed graphically for plane stress as:

Figure 19 – Yield locus according to isotropic hardening and kinematic hardening rules

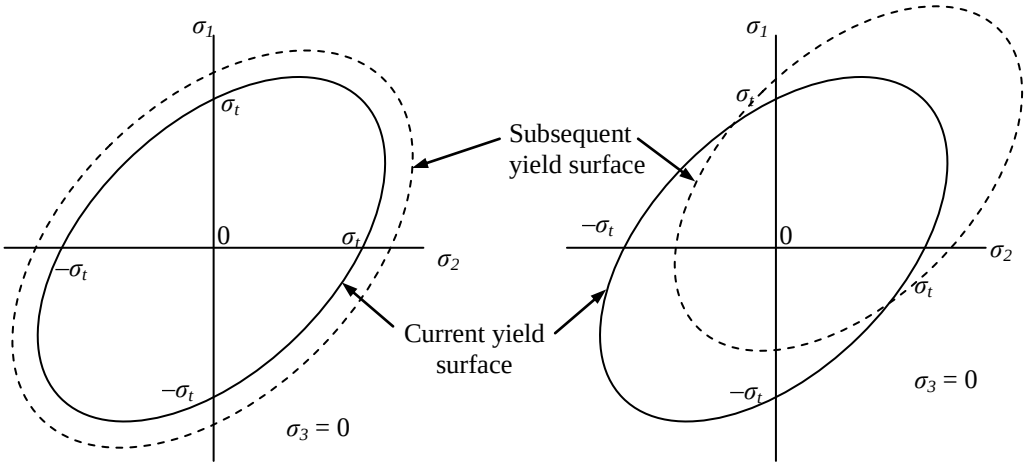

SOURCE: Bertin, 2015

3.2.8 Isotropic Hardening

Work-hardening is the work of plastic deformation done to a body and it is not recoverable, as opposed to elastic work. If the amount of work-hardening per unit volume is symbolized as ω^p, the increment of energy to produce plastic deformation, $d\omega^p$ is given by:

$$d\omega^p = \boldsymbol{\sigma_{ij}} d\varepsilon_{ij}^p \tag{63}$$

where:

$\boldsymbol{\sigma_{ij}}$: is the stress tensor,

$d\varepsilon_{ij}{}^{p}$: is the plastic components of the strain tensor resulting from the increment of strain.

Total plastic work-hardening done, ω^p, can be calculated by the integral of $d\omega^p$ as follows:

$$\omega^p = \int \sigma_{ij} d\varepsilon_{ij}^p \tag{64}$$

Work of plastic deformation may be correlated to an equivalent stress, σ_e. For von Mises' criterion the equivalent stress is given by:

$$\sigma_e = \sqrt{3J_2} = \sqrt{\frac{3}{2} S_{ij} S_{ij}} \tag{65}$$

where:

σ_e : is the equivalent stress,

J_2 : is the second invariant of the deviatoric stress tensor,

S_{ij} : is the deviatoric stress tensor.

Assuming that for isotropic materials the deviatoric stress tensor and plastic strain increment tensor have identical properties and provided the shear strain tensors are used, then invariants of deviatoric stress tensor (J_1, J_2 *and* J_3) are proportional to those of the increment of plastic strain tensor (K_1, K_2 *and* K_3) (REES, 2006, p. 287). For von Mises' criterion the increment of equivalent plastic strain, $d\varepsilon_e^p$, can be calculated as follows:

$$d\varepsilon_e^p = \sqrt{\frac{4}{3} K_2} = \sqrt{\frac{2}{3} d\varepsilon_{ij}^p d\varepsilon_{ij}^p} \tag{66}$$

where:

K_2 : is the second invariant of increment of plastic strain tensor,

$d\varepsilon_{ij}{}^{p}$: is the increment of plastic strain;

and integrated as:

$$\varepsilon_e^p = \int d\varepsilon_e^p = \sqrt{\frac{2}{3}\varepsilon_{ij}^p \varepsilon_{ij}^p} \tag{67}$$

The increment of plastic energy, $d\omega^p$ can also be calculated by the equivalent values of stress and strain:

$$d\omega^p = \sigma_e d\varepsilon_e^p \tag{68}$$

For isotropic hardening the yield criterion in terms of equivalent stress is given by:

$$\sigma_e - \sigma'_y = 0 \Rightarrow \sqrt{\frac{3}{2}S_{ij}S_{ij}} - \sigma'_y = 0 \tag{69}$$

where:

σ_e : is the equivalent stress,

S_{ij} : is the deviatoric stress tensor,

σ'_y : is the current yield stress.

For each increment of increment of plastic strain a new yield stress shall be calculated.

3.3 METHODS OF APPRAISAL AND PIT CORROSION

As previously stated, methods for appraisal of corroded pipelines do not perform well for defects with a small diameter and for shallow defects. Six of the most common methods of appraisal of corroded pipelines are compared, namely: NG18, B31G, 85dL, RSTRENG, DNV F101 and PCORR.

Failure pressure for each appraisal method is calculated for pit corrosion defects ranging from depths of 1 mm to 14.9 mm and for diameters, ranging from 1 mm to 200 mm. Pipe diameter was set to 300 mm and wall thickness to 15 mm. Failure pressure for a pipe without any defect is given by Barlow's equation (1). Two maximum reference stresses were used, yield stress, σ_y, and ultimate tensile stress, σ_u, according to the method used and the material chosen. When $\sigma_{ref} = \sigma_y = 483$ MPa, $t = 15$ mm and $D = 300$ mm, the resulting failure pressure is $P_f = 48.3$ MPa. Otherwise, when $\sigma_{ref} = \sigma_u = 597$ MPa, same wall thickness and pipe diameter, the resulting failure pressure is $P_f = 59.7$ MPa.

Two methods are not compared, RPA and WDD. Method RPA is not be dealt here since for short defects in which $L \leq \sqrt{20Dt}$ failure pressure is calculated by the same equation as 85dL. In the present case, it is being analyzed lengths of defects ranging from 1 to 200 mm. For pipe diameter, D = 300 mm, and wall thickness, t = 15 mm, L would have to be greater than 300 mm in order for RPA equations to be applicable. WDD analyzes complex defects with a multitude of depths by summing weighed depth differences. Since the present work analyses simple defects, this method is not compared.

3.3.1 NG 18

For NG 18, it is used flow stress, σ_{flow} = 551.948 MPa, which is the yield stress, σ_y = 483 MPa added to 68.948 MPa, as already mentioned in the method description, item 2.1.1. Equation (3), leading to the following formulation:

$$P_f = 551.948 \frac{2 \times 15}{300} \left(\frac{1 - \frac{d_{max}}{15}}{1 - \frac{d_{max}}{15} \frac{1}{M}} \right) \tag{70}$$

With Folias factor equal to:

$$M = \sqrt{1 + 0.6275 \left(\frac{L}{\sqrt{300 \times 15}} \right)^2 - 0.003375 \left(\frac{L}{\sqrt{300 \times 15}} \right)^4} \tag{71}$$

Or, after suitable calculations:

$$M = \sqrt{1 + 1.3944 \times 10^{-4} (L)^2 - 1.6667 \times 10^{-10} (L)^4} \tag{72}$$

Failure pressure, P_f, is calculated by previous Equation (70) varying depth of the defect, 1 mm $\leq d_{max} \leq$ 14.9 mm and diameter of the defect, 1 mm $\leq L \leq$ 200 mm. Values of Folias' factor, M, calculated by Equation (72) are presented on the third line of Table 3. Values on the left side above the thin line are greater than P_f = 48.3 MPa, previously calculated, indicating that there is a range of values of L and d_{max} inside which failure pressure calculated by NG 18 gives pressures above maximum pressure allowed for pipes without any defect. Values in

bold face on the right side below the thin line are smaller than failure pressure for perfect pipes.

Table 3 – Failure Pressure NG 18

	L (mm)														
	1	2	3	4	5	10	15	20	25	30	40	50	100	150	200
M	1.00	1.00	1.00	1.00	1.00	1.01	1.02	1.03	1.04	1.06	1.11	1.16	1.54	2.01	2.51
1	55.19	55.19	55.19	55.19	55.19	55.17	55.13	55.09	55.03	54.97	54.82	54.65	53.84	53.28	52.92
2	55.19	55.19	55.19	55.19	55.18	55.14	55.06	54.97	54.85	54.71	54.39	54.04	52.36	51.23	50.52
3	55.19	55.19	55.19	55.18	55.17	55.10	54.98	54.83	54.64	54.41	53.91	53.35	50.74	49.03	**47.98**
4	55.19	55.19	55.18	55.17	55.16	55.06	54.89	54.66	54.39	54.07	53.34	52.55	48.94	**46.66**	**45.28**
5	55.19	55.19	55.18	55.16	55.15	55.01	54.78	54.47	54.09	53.66	52.68	51.62	**46.94**	**44.10**	**42.43**
6	55.19	55.18	55.17	55.15	55.13	54.94	54.64	54.23	53.73	53.16	51.89	50.53	**44.72**	**41.33**	**39.39**
7	55.19	55.18	55.16	55.14	55.11	54.86	54.46	53.93	53.29	52.56	50.93	49.23	**42.21**	**38.32**	**36.15**
8	55.19	55.18	55.16	55.12	55.09	54.76	54.24	53.56	52.73	51.80	49.76	**47.65**	**39.38**	**35.04**	**32.70**
9	55.19	55.17	55.14	55.10	55.05	54.63	53.95	53.06	52.01	50.82	**48.27**	**45.70**	**36.14**	**31.45**	**29.01**
10	55.19	55.16	55.13	55.07	55.00	54.44	53.55	52.39	51.02	49.52	**46.33**	**43.22**	**32.41**	**27.51**	**25.04**
11	55.18	55.15	55.10	55.03	54.93	54.17	52.96	51.41	49.62	**47.68**	**43.70**	**39.97**	**28.07**	**23.15**	**20.79**
d_{max} (mm) 12	55.18	55.13	55.06	54.95	54.81	53.71	52.01	49.86	**47.44**	**44.90**	**39.92**	**35.51**	**22.94**	**18.32**	**16.20**
13	55.17	55.09	54.97	54.80	54.58	52.83	50.20	**47.02**	**43.61**	**40.21**	**34.04**	**29.04**	**16.80**	**12.92**	**11.24**
14	55.14	54.98	54.71	54.35	53.88	50.33	**45.45**	**40.15**	**35.10**	**30.62**	**23.60**	**18.77**	**9.32**	**6.86**	**5.85**
14.1	55.13	54.95	54.66	54.25	53.73	49.81	**44.51**	**38.89**	**33.64**	**29.07**	**22.09**	**17.41**	**8.48**	**6.21**	**5.29**
14.2	55.13	54.92	54.59	54.12	53.54	49.17	**43.39**	**37.42**	**31.98**	**27.35**	**20.46**	**15.96**	**7.62**	**5.56**	**4.72**
14.3	55.12	54.88	54.50	53.97	53.30	48.38	**42.04**	**35.69**	**30.07**	**25.42**	**18.69**	**14.41**	**6.75**	**4.89**	**4.15**
14.4	55.10	54.83	54.38	53.76	52.98	**47.35**	**40.35**	**33.61**	**27.86**	**23.23**	**16.75**	**12.76**	**5.85**	**4.22**	**3.57**
14.5	55.08	54.75	54.21	53.47	52.55	**45.99**	**38.21**	**31.08**	**25.25**	**20.73**	**14.63**	**11.00**	**4.93**	**3.54**	**2.99**
14.6	55.05	54.64	53.96	53.04	51.90	**44.09**	**35.40**	**27.92**	**22.14**	**17.85**	**12.29**	**9.11**	**3.99**	**2.85**	**2.40**
14.7	55.01	54.45	53.55	52.34	50.86	**41.25**	**31.52**	**23.88**	**18.38**	**14.49**	**9.71**	**7.09**	**3.03**	**2.15**	**1.81**
14.8	54.91	54.08	52.75	50.99	48.90	**36.54**	**25.87**	**18.52**	**13.71**	**10.53**	**6.83**	**4.90**	**2.04**	**1.44**	**1.21**
14.9	54.63	52.99	50.48	**47.34**	**43.84**	**27.22**	**16.81**	**11.07**	**7.78**	**5.78**	**3.62**	**2.55**	**1.03**	**0.73**	**0.61**

SOURCE: Bertin, 2015

3.3.2 B31G

Same procedure used to analyze NG 18 is used for B31G. It is used flow stress, $\sigma_{y_{spec}} = 483$ MPa, safety factor, S = 1, same t and D. Inputting all values on Equation (3), leads to the following formulation for P_f and M:

$$P_f = 1 \times 1.1 \times 483 \times \frac{2 \times 15}{300}\left(\frac{1 - \frac{2}{3}\frac{d_{max}}{15}}{1 - \frac{2}{3}\frac{d_{max}}{15}\frac{1}{M}}\right) \tag{73}$$

$$M = \sqrt{1 + 0.8\left(\frac{L}{\sqrt{300 \times 15}}\right)^2} \Rightarrow \mathrm{M} = \sqrt{1 + 1.778 \times 10^{-4}\mathrm{L}^2} \quad (74)$$

Results are presented in Table 4. Again, values of the left side above the thin line are greater than P_f = 48.3 MPa maximum pressure allowed for pipes without any defect, while values in bold face bellow the thin line are smaller than P_f.

Table 4 – Failure Pressure calculated by B31G method

		L (mm)														
		1	2	3	4	5	10	15	20	25	30	40	50	100	150	200
	M	1.00	1.00	1.00	1.00	1.00	1.01	1.02	1.03	1.05	1.08	1.13	1.20	1.67	2.24	2.85
	1	53.13	53.13	53.13	53.13	53.12	53.11	53.08	53.05	53.00	52.95	52.84	52.72	52.16	51.80	51.57
	2	53.13	53.13	53.13	53.12	53.12	53.08	53.03	52.96	52.87	52.76	52.53	52.27	51.13	50.41	49.97
	3	53.13	53.13	53.12	53.12	53.11	53.06	52.97	52.86	52.71	52.55	52.19	51.79	50.05	48.97	48.31
	4	53.13	53.13	53.12	53.11	53.10	53.03	52.91	52.74	52.55	52.32	51.81	51.27	48.90	**47.46**	**46.59**
	5	53.13	53.12	53.12	53.11	53.10	53.00	52.84	52.62	52.36	52.07	51.40	50.70	**47.68**	**45.88**	**44.82**
	6	53.13	53.12	53.11	53.10	53.09	52.96	52.76	52.49	52.16	51.78	50.95	50.07	**46.38**	**44.24**	**42.99**
	7	53.13	53.12	53.11	53.10	53.08	52.92	52.67	52.33	51.93	51.47	50.45	49.38	**45.00**	**42.52**	**41.09**
	8	53.13	53.12	53.11	53.09	53.07	52.87	52.57	52.16	51.67	51.11	49.89	48.62	**43.52**	**40.71**	**39.12**
	9	53.13	53.12	53.10	53.08	53.05	52.82	52.45	51.96	51.37	50.71	49.27	**47.78**	**41.94**	**38.82**	**37.09**
	10	53.13	53.11	53.10	53.07	53.04	52.76	52.32	51.73	51.03	50.25	48.56	**46.84**	**40.25**	**36.84**	**34.97**
	11	53.13	53.11	53.09	53.06	53.02	52.69	52.16	51.47	50.64	49.73	**47.76**	**45.78**	**38.43**	**34.75**	**32.78**
d_{max} *(mm)*	12	53.12	53.11	53.08	53.04	53.00	52.60	51.98	51.16	50.19	49.12	**46.83**	**44.57**	**36.46**	**32.56**	**30.51**
	13	53.12	53.10	53.07	53.03	52.97	52.50	51.75	50.78	49.64	48.39	**45.76**	**43.20**	**34.34**	**30.25**	**28.14**
	14	53.12	53.10	53.06	53.01	52.94	52.37	51.48	50.33	48.99	**47.53**	**44.51**	**41.62**	**32.03**	**27.81**	**25.68**
	14.1	53.12	53.10	53.06	53.00	52.93	52.36	51.45	50.28	48.92	**47.44**	**44.37**	**41.45**	**31.79**	**27.56**	**25.43**
	14.2	53.12	53.10	53.06	53.00	52.93	52.34	51.42	50.23	48.84	**47.34**	**44.23**	**41.27**	**31.54**	**27.31**	**25.18**
	14.3	53.12	53.10	53.06	53.00	52.93	52.33	51.39	50.18	48.77	**47.24**	**44.09**	**41.09**	**31.30**	**27.05**	**24.93**
	14.4	53.12	53.10	53.05	53.00	52.92	52.31	51.36	50.12	48.69	**47.14**	**43.94**	**40.91**	**31.05**	**26.80**	**24.67**
	14.5	53.12	53.10	53.05	52.99	52.92	52.30	51.32	50.07	48.61	**47.03**	**43.79**	**40.73**	**30.80**	**26.54**	**24.42**
	14.6	53.12	53.10	53.05	52.99	52.91	52.28	51.29	50.01	48.53	**46.93**	**43.64**	**40.55**	**30.55**	**26.28**	**24.16**
	14.7	53.12	53.09	53.05	52.99	52.91	52.27	51.25	49.95	48.44	**46.82**	**43.49**	**40.36**	**30.29**	**26.02**	**23.90**
	14.8	53.12	53.09	53.05	52.99	52.90	52.25	51.22	49.89	48.36	**46.71**	**43.33**	**40.16**	**30.04**	**25.76**	**23.64**
	14.9	53.12	53.09	53.05	52.98	52.90	52.23	51.18	49.83	**48.27**	**46.60**	**43.17**	**39.97**	**29.78**	**25.50**	**23.38**

SOURCE: Bertin, 2015

3.3.3 85dL

Same procedure used to analyze NG 18 is used for 85dL. Input values are: σ_{flow} = 551.948 MPa, same as NG18, same t and D and M satisfying the condition that $L^2/Dt \leq 50$. Equation (13) results:

$$P_f = 551.948 \frac{2 \times 15}{300} \left(\frac{1 - 0.85 \frac{d_{max}}{t}}{1 - 0.85 \frac{d_{max}}{t} \frac{1}{M}} \right) \tag{75}$$

And after calculation:

$$P_f = 55.1948 \left(\frac{1 - 0.85 \frac{d_{max}}{t}}{1 - 0.85 \frac{d_{max}}{t} \frac{1}{M}} \right) \tag{76}$$

In the same way, replacing variables in the bulging factor equation by suitable parameters leads to:

$$M = \sqrt{1 + 0.6275 \left(\frac{L}{\sqrt{300 \times 15}} \right)^2 - 0.003375 \left(\frac{L}{\sqrt{300 \times 15}} \right)^4} \tag{77}$$

And finally:

$$M = \sqrt{1 + 1.3944 \times 10^{-4} L^2 - 1.6667 \times 10^{-10} L^4} \tag{78}$$

In a similar way as previously done, values on the left side and above the thin line of Table 5 are greater than P_f = 48.3 MPa, maximum pressure allowed for pipes without any defect. Boldface values, below the thin line, are smaller than the failure pressure for undamaged pipes.

Table 5 – Failure Pressure calculated by 85dL method

		L (mm)														
		1	2	3	4	5	10	15	20	25	30	40	50	100	150	200
M		1.00	1.00	1.00	1.00	1.00	1.01	1.02	1.03	1.04	1.06	1.11	1.16	1.54	2.01	2.51
	1	55.19	55.19	55.19	55.19	55.19	55.17	55.14	55.11	55.06	55.01	54.88	54.74	54.05	53.58	53.27
	2	55.19	55.19	55.19	55.19	55.18	55.15	55.09	55.01	54.91	54.79	54.53	54.23	52.82	51.86	51.25
	3	55.19	55.19	55.19	55.18	55.18	55.12	55.02	54.89	54.74	54.55	54.13	53.67	51.49	50.04	49.14
	4	55.19	55.19	55.18	55.18	55.17	55.08	54.95	54.77	54.54	54.28	53.69	53.04	50.04	**48.10**	**46.92**
	5	55.19	55.19	55.18	55.17	55.16	55.04	54.86	54.62	54.32	53.97	53.18	52.33	48.46	**46.04**	**44.59**
	6	55.19	55.19	55.18	55.16	55.15	55.00	54.76	54.44	54.06	53.61	52.60	51.52	**46.73**	**43.83**	**42.13**
	7	55.19	55.18	55.17	55.15	55.13	54.95	54.64	54.24	53.75	53.19	51.93	50.59	**44.84**	**41.47**	**39.55**
	8	55.19	55.18	55.17	55.14	55.12	54.88	54.50	54.00	53.39	52.69	51.14	49.51	**42.74**	**38.94**	**36.82**
	9	55.19	55.18	55.16	55.13	55.10	54.80	54.33	53.70	52.94	52.09	50.20	**48.24**	**40.41**	**36.22**	**33.94**
	10	55.19	55.17	55.15	55.11	55.07	54.70	54.11	53.33	52.39	51.35	49.06	**46.73**	**37.82**	**33.29**	**30.89**
	11	55.19	55.17	55.14	55.09	55.04	54.57	53.83	52.85	51.70	50.41	**47.65**	**44.90**	**34.90**	**30.12**	**27.65**
d_{max} *(mm)*	12	55.19	55.16	55.12	55.06	54.99	54.40	53.45	52.23	50.78	49.20	**45.87**	**42.64**	**31.60**	**26.67**	**24.22**
	13	55.18	55.15	55.10	55.02	54.93	54.15	52.93	51.35	49.53	**47.57**	**43.55**	**39.78**	**27.83**	**22.92**	**20.57**
	14	55.18	55.14	55.06	54.96	54.83	53.77	52.13	50.05	**47.71**	**45.24**	**40.38**	**36.03**	**23.50**	**18.83**	**16.67**
	14.1	55.18	55.13	55.06	54.95	54.82	53.72	52.03	49.89	**47.48**	**44.95**	**39.99**	**35.59**	**23.03**	**18.40**	**16.27**
	14.2	55.18	55.13	55.05	54.94	54.80	53.67	51.92	49.72	**47.24**	**44.65**	**39.60**	**35.14**	**22.55**	**17.96**	**15.86**
	14.3	55.18	55.13	55.05	54.93	54.79	53.61	51.80	49.53	**46.99**	**44.34**	**39.19**	**34.67**	**22.07**	**17.52**	**15.45**
	14.4	55.18	55.13	55.04	54.92	54.77	53.56	51.68	49.34	**46.72**	**44.01**	**38.76**	**34.19**	**21.57**	**17.08**	**15.04**
	14.5	55.18	55.12	55.04	54.91	54.76	53.49	51.56	49.14	**46.45**	**43.66**	**38.32**	**33.69**	**21.07**	**16.63**	**14.63**
	14.6	55.18	55.12	55.03	54.90	54.74	53.43	51.42	48.92	**46.15**	**43.30**	**37.85**	**33.18**	**20.57**	**16.18**	**14.21**
	14.7	55.18	55.12	55.02	54.89	54.72	53.36	51.28	48.70	**45.85**	**42.92**	**37.37**	**32.64**	**20.05**	**15.72**	**13.79**
	14.8	55.17	55.11	55.02	54.88	54.70	53.28	51.12	48.46	**45.52**	**42.52**	**36.87**	**32.09**	**19.53**	**15.26**	**13.37**
	14.9	55.17	55.11	55.01	54.86	54.68	53.20	50.96	**48.20**	**45.18**	**42.10**	**36.35**	**31.52**	**18.99**	**14.80**	**12.94**

SOURCE: Bertin, 2015

3.3.4 RSTRENG

This method used the same formulation as NG-18, but instead of defect depth, it uses its actual cross sectional area. This area, *A*, is compared with the original cross-sectional area of the pipe at the defect point ($A_0 = Lt$). The defect is modeled, described on the following item 4.2.2, as a semi-ellipsoidal surface. The cross section of this three dimension surface is a semi-ellipse, Figure 20, with horizontal axis as diameter, *L* according to the notation used so far, and vertical axis as depth of defect, *d*.

Figure 20 – Dimensions of the steel pipe containing a pit

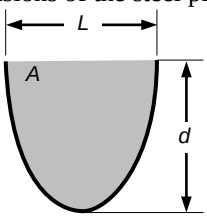

SOURCE: Bertin, 2015

Equation for this semi-elliptical area is:

$$A = \frac{\pi \times \frac{L}{2} \times d}{2} = \frac{\pi L d}{4} \tag{79}$$

Hence

$$P_f = \sigma_{flow} \frac{2t}{D} \left(\frac{1 - \frac{A}{A_0}}{1 - \frac{A}{A_0} \frac{1}{M}} \right) \tag{80}$$

And, substituting Equation (79) into (80), it results:

$$P_f = \sigma_{flow} \frac{2t}{D} \left(\frac{1 - \frac{\pi d}{4t}}{1 - \frac{\pi d}{4t} \frac{1}{M}} \right) \tag{81}$$

Or

$$P_f = 551.948 \frac{2 \times 15}{300} \left(\frac{1 - \frac{\pi d}{4 \times 15}}{1 - \frac{\pi d}{4 \times 15} \frac{1}{M}} \right) \Rightarrow P_f = 55.1948 \left(\frac{1 - \frac{\pi d}{60}}{1 - \frac{\pi d}{60} \frac{1}{M}} \right) \tag{82}$$

Folias factor is the same as NG-18 give by Equation (72) already mentioned and is presented in the third line of Table 6, indicated by *M*.

Table 6 – Failure Pressure calculated by RSTRENG Method

	L (mm)														
	1	2	3	4	5	10	15	20	25	30	40	50	100	150	200
M	1.00	1.00	1.00	1.00	1.00	1.01	1.02	1.03	1.04	1.06	1.11	1.16	1.54	2.01	2.51
1	55.19	55.19	55.19	55.19	55.19	55.17	55.15	55.11	55.07	55.02	54.90	54.78	54.14	53.70	53.42
2	55.19	55.19	55.19	55.19	55.18	55.15	55.10	55.02	54.93	54.83	54.58	54.31	53.02	52.13	51.56
3	55.19	55.19	55.19	55.18	55.18	55.12	55.04	54.92	54.78	54.61	54.23	53.81	51.80	50.46	49.63
4	55.19	55.19	55.19	55.18	55.17	55.09	54.97	54.81	54.60	54.37	53.83	53.24	50.49	48.70	**47.60**
5	55.19	55.19	55.18	55.17	55.16	55.06	54.90	54.68	54.41	54.09	53.38	52.61	49.08	**46.84**	**45.48**
6	55.19	55.19	55.18	55.17	55.15	55.02	54.81	54.53	54.18	53.78	52.88	51.90	**47.54**	**44.85**	**43.27**
7	55.19	55.19	55.17	55.16	55.14	54.98	54.71	54.35	53.92	53.42	52.30	51.10	**45.87**	**42.75**	**40.94**
8	55.19	55.18	55.17	55.15	55.13	54.92	54.59	54.15	53.61	53.00	51.64	50.18	**44.04**	**40.50**	**38.49**
9	55.19	55.18	55.16	55.14	55.11	54.86	54.45	53.91	53.25	52.51	50.86	49.13	**42.03**	**38.10**	**35.92**
10	55.19	55.18	55.16	55.13	55.09	54.78	54.28	53.62	52.82	51.92	49.94	**47.90**	**39.81**	**35.54**	**33.22**
11	55.19	55.17	55.15	55.11	55.06	54.68	54.07	53.26	52.29	51.21	48.85	**46.45**	**37.36**	**32.78**	**30.37**
d_{max} (mm) 12	55.19	55.17	55.14	55.09	55.03	54.56	53.80	52.81	51.63	50.32	**47.51**	**44.72**	**34.62**	**29.82**	**27.36**
13	55.19	55.16	55.12	55.06	54.99	54.39	53.45	52.22	50.77	49.18	**45.85**	**42.61**	**31.55**	**26.63**	**24.18**
14	55.18	55.15	55.10	55.03	54.93	54.17	52.97	51.42	49.62	**47.69**	**43.72**	**39.98**	**28.09**	**23.17**	**20.81**
14.1	55.18	55.15	55.10	55.02	54.93	54.14	52.91	51.32	49.49	**47.51**	**43.47**	**39.68**	**27.72**	**22.81**	**20.46**
14.2	55.18	55.15	55.09	55.02	54.92	54.11	52.85	51.22	49.35	**47.33**	**43.21**	**39.38**	**27.34**	**22.45**	**20.11**
14.3	55.18	55.15	55.09	55.01	54.91	54.08	52.78	51.12	49.20	**47.14**	**42.95**	**39.06**	**26.96**	**22.08**	**19.76**
14.4	55.18	55.15	55.09	55.01	54.90	54.05	52.72	51.01	49.05	**46.94**	**42.68**	**38.74**	**26.57**	**21.71**	**19.40**
14.5	55.18	55.15	55.09	55.00	54.89	54.02	52.65	50.90	48.89	**46.74**	**42.41**	**38.41**	**26.18**	**21.34**	**19.05**
14.6	55.18	55.14	55.08	55.00	54.89	53.99	52.58	50.78	48.73	**46.53**	**42.12**	**38.07**	**25.78**	**20.96**	**18.69**
14.7	55.18	55.14	55.08	54.99	54.88	53.95	52.51	50.66	48.56	**46.32**	**41.83**	**37.73**	**25.38**	**20.58**	**18.33**
14.8	55.18	55.14	55.08	54.98	54.87	53.91	52.43	50.54	48.38	**46.09**	**41.52**	**37.37**	**24.97**	**20.20**	**17.96**
14.9	55.18	55.14	55.07	54.98	54.86	53.88	52.35	50.41	**48.20**	**45.86**	**41.21**	**37.00**	**24.56**	**19.81**	**17.60**

SOURCE: Bertin, 2015

Values on the left side and above the thin line are greater than P_f = 48.3, while values in bold face on the right side and below the thin line are smaller than the failure pressure for undamaged pipes.

3.3.5 DNV F101

The simplified version of this method calculates the failure pressure taking into account the ultimate tensile strength, σ_u, instead of flow stress or the yield stress. It also calculates the average pipe diameter by subtracting wall thickness t from external diameter D. Using the ultimate tensile strength as σ_u = 597 MPa and the other parameters already mentioned, Equation (23) becomes:

$$P_f = 1.05 \times 597 \frac{2 \times 15}{300 - 15} \left(\frac{1 - \frac{d_{max}}{15}}{1 - \frac{d_{max}}{15} \frac{1}{M}} \right) \tag{83}$$

Allowing:

$$P_f = 65.98 \left(\frac{1 - \frac{d_{max}}{15}}{1 - \frac{d_{max}}{15} \frac{1}{M}} \right) \tag{84}$$

Introducing the diameter of the pipe and wall thickness into Equation (24), the bulging factor is:

$$M = \sqrt{1 + 0.31 \left(\frac{\mathrm{L}}{\sqrt{300 \times 15}} \right)^2} \Rightarrow \mathrm{M} = \sqrt{1 + 6.89 \times 10^{-5} \times \mathrm{L}^2} \tag{85}$$

Combining the two Equations, P_f and M, it results in data of Table 7. Bold face values below the thin line are failure pressure values smaller than 59.7 MPa which is the maximum allowed pressure for pipes without defects, considering ultimate tensile strength as the governing parameter. Values on the left side above the thin line are greater than the mentioned failure pressure.

Table 7 – Failure Pressure calculated by DNV F101 Method

		L (mm)														
		1	2	3	4	5	10	15	20	25	30	40	50	100	150	200
	M	1.00	1.00	1.00	1.00	1.00	1.00	1.01	1.01	1.02	1.03	1.05	1.08	1.30	1.60	1.94
d_{max} (mm)	1	65.98	65.98	65.98	65.98	65.98	65.97	65.95	65.92	65.89	65.84	65.75	65.63	64.92	64.27	63.78
	2	65.98	65.98	65.98	65.98	65.98	65.95	65.91	65.85	65.77	65.68	65.47	65.22	63.72	62.40	61.41
	3	65.98	65.98	65.98	65.98	65.97	65.93	65.86	65.76	65.64	65.50	65.15	64.75	62.39	60.35	**58.86**
	4	65.98	65.98	65.98	65.97	65.96	65.90	65.80	65.66	65.49	65.28	64.78	64.20	60.88	**58.09**	**56.11**
	5	65.98	65.98	65.97	65.97	65.96	65.87	65.73	65.54	65.30	65.02	64.35	63.56	**59.16**	**55.59**	**53.13**
	6	65.98	65.98	65.97	65.96	65.95	65.83	65.65	65.40	65.08	64.71	63.82	62.79	**57.19**	**52.82**	**49.89**
	7	65.98	65.98	65.97	65.95	65.93	65.79	65.54	65.21	64.80	64.32	63.17	61.85	**54.91**	**49.72**	**46.35**
	8	65.98	65.97	65.96	65.94	65.92	65.73	65.41	64.98	64.45	63.82	62.35	60.69	**52.23**	**46.23**	**42.48**
	9	65.98	65.97	65.95	65.93	65.90	65.65	65.23	64.67	63.98	63.18	61.30	**59.20**	**49.03**	**42.28**	**38.23**
	10	65.98	65.97	65.94	65.91	65.87	65.54	64.99	64.25	63.34	62.29	59.88	**57.24**	**45.16**	**37.76**	**33.53**
	11	65.98	65.96	65.93	65.88	65.83	65.37	64.62	63.62	62.40	61.01	**57.88**	**54.53**	**40.38**	**32.54**	**28.31**
	12	65.98	65.95	65.90	65.84	65.76	65.09	64.02	62.60	60.90	**58.99**	**54.82**	**50.54**	**34.33**	**26.45**	**22.47**
	13	65.97	65.93	65.85	65.75	65.62	64.55	62.85	60.66	**58.11**	**55.33**	**49.57**	**44.09**	**26.41**	**19.24**	**15.92**
	14	65.95	65.86	65.70	65.48	65.20	62.96	**59.59**	**55.50**	**51.07**	**46.64**	**38.52**	**31.89**	**15.61**	**10.59**	**8.49**
	14.1	65.95	65.84	65.67	65.42	65.11	62.62	**58.91**	**54.47**	**49.73**	**45.07**	**36.70**	**30.04**	**14.31**	**9.62**	**7.69**
	14.2	65.94	65.82	65.62	65.35	64.99	62.20	**58.09**	**53.23**	**48.16**	**43.24**	**34.65**	**28.01**	**12.96**	**8.64**	**6.88**
	14.3	65.94	65.80	65.57	65.25	64.84	61.67	**57.05**	**51.72**	**46.27**	**41.10**	**32.34**	**25.77**	**11.56**	**7.64**	**6.06**
	14.4	65.93	65.77	65.50	65.12	64.65	60.97	**55.74**	**49.84**	**43.97**	**38.56**	**29.69**	**23.29**	**10.10**	**6.62**	**5.23**
	14.5	65.92	65.72	65.40	64.95	64.38	60.02	**53.99**	**47.42**	**41.12**	**35.49**	**26.64**	**20.52**	**8.59**	**5.57**	**4.39**
	14.6	65.90	65.65	65.25	64.68	63.98	**58.65**	**51.57**	**44.20**	**37.46**	**31.70**	**23.08**	**17.42**	**7.01**	**4.51**	**3.54**
	14.7	65.87	65.54	65.00	64.25	63.32	**56.50**	**47.97**	**39.71**	**32.63**	**26.91**	**18.87**	**13.91**	**5.37**	**3.42**	**2.67**
	14.8	65.82	65.32	64.51	63.40	62.04	**52.64**	**42.11**	**33.01**	**25.94**	**20.67**	**13.84**	**9.92**	**3.65**	**2.30**	**1.79**
	14.9	65.65	64.66	63.07	60.98	**58.49**	**43.68**	**30.81**	**21.91**	**16.06**	**12.19**	**7.68**	**5.33**	**1.87**	**1.16**	**0.90**

SOURCE: Bertin, 2015

3.3.6 PCORR

PCORR method has three noticeable characteristics for the present discussion. Firstly it also uses ultimate tensile strength similar to DNV F101, but without the safety factor of 1.05. Second, it does not use Folias bulging factor. Third, all values resulting from the calculations are smaller than the failure pressure for a pipe without defects. Therefore, it is the only method suitable for defects with minute dimensions such as pit corrosion. Hence, for the same parameters of previous methods, Equation (25) would be:

$$P_f = 597\frac{2\times15}{300}\left(1-\left(\frac{d_{max}}{15}\right)\left(1-\exp\left(-0.157\frac{L}{\sqrt{150(15-d_{max})}}\right)\right)\right) \quad (86)$$

And:

$$P_f = 59.7\left(1-\left(\frac{d_{max}}{15}\right)\left(1-\exp\left(-0.157\frac{L}{\sqrt{150(15-d_{max})}}\right)\right)\right) \quad (87)$$

Table 8 – Failure Pressure calculated by PCORR method

		L (mm)														
		1	2	3	4	5	10	15	20	25	30	40	50	100	150	200
d_{max} (mm)	1	**59.69**	**59.67**	**59.66**	**59.65**	**59.63**	**59.57**	**59.50**	**59.44**	**59.37**	**59.31**	**59.19**	**59.07**	**58.55**	**58.10**	**57.73**
	2	**59.67**	**59.64**	**59.62**	**59.59**	**59.56**	**59.42**	**59.29**	**59.15**	**59.02**	**58.89**	**58.64**	**58.40**	**57.32**	**56.41**	**55.65**
	3	**59.66**	**59.61**	**59.57**	**59.52**	**59.48**	**59.27**	**59.06**	**58.85**	**58.64**	**58.45**	**58.06**	**57.68**	**56.01**	**54.61**	**53.46**
	4	**59.64**	**59.58**	**59.52**	**59.46**	**59.40**	**59.10**	**58.80**	**58.52**	**58.23**	**57.96**	**57.42**	**56.90**	**54.60**	**52.70**	**51.13**
	5	**59.62**	**59.54**	**59.46**	**59.38**	**59.30**	**58.91**	**58.53**	**58.15**	**57.78**	**57.42**	**56.72**	**56.05**	**53.07**	**50.63**	**48.65**
	6	**59.60**	**59.50**	**59.40**	**59.30**	**59.20**	**58.70**	**58.22**	**57.74**	**57.28**	**56.83**	**55.95**	**55.11**	**51.40**	**48.40**	**45.98**
	7	**59.57**	**59.45**	**59.32**	**59.20**	**59.08**	**58.47**	**57.87**	**57.29**	**56.72**	**56.16**	**55.08**	**54.05**	**49.55**	**45.96**	**43.09**
	8	**59.55**	**59.39**	**59.24**	**59.09**	**58.94**	**58.19**	**57.47**	**56.76**	**56.07**	**55.39**	**54.09**	**52.85**	**47.47**	**43.25**	**39.94**
	9	**59.51**	**59.33**	**59.14**	**58.96**	**58.77**	**57.87**	**57.00**	**56.14**	**55.31**	**54.50**	**52.93**	**51.45**	**45.10**	**40.22**	**36.46**
	10	**59.47**	**59.25**	**59.02**	**58.80**	**58.58**	**57.48**	**56.42**	**55.39**	**54.39**	**53.41**	**51.54**	**49.78**	**42.33**	**36.74**	**32.55**
	11	**59.42**	**59.14**	**58.87**	**58.59**	**58.32**	**56.98**	**55.69**	**54.43**	**53.22**	**52.04**	**49.80**	**47.70**	**38.98**	**32.66**	**28.07**
	12	**59.35**	**59.00**	**58.65**	**58.31**	**57.96**	**56.29**	**54.68**	**53.13**	**51.63**	**50.19**	**47.46**	**44.93**	**34.72**	**27.68**	**22.81**
	13	**59.23**	**58.77**	**58.31**	**57.86**	**57.41**	**55.22**	**53.12**	**51.12**	**49.21**	**47.38**	**43.96**	**40.84**	**28.86**	**21.24**	**16.40**
	14	**58.99**	**58.29**	**57.60**	**56.91**	**56.24**	**53.00**	**49.95**	**47.10**	**44.42**	**41.91**	**37.35**	**33.33**	**19.44**	**12.13**	**8.27**
	14.1	**58.95**	**58.20**	**57.47**	**56.75**	**56.03**	**52.61**	**49.40**	**46.41**	**43.61**	**41.00**	**36.27**	**32.14**	**18.11**	**10.98**	**7.34**
	14.2	**58.90**	**58.10**	**57.32**	**56.55**	**55.79**	**52.15**	**48.77**	**45.62**	**42.68**	**39.95**	**35.04**	**30.79**	**16.67**	**9.77**	**6.40**
	14.3	**58.83**	**57.98**	**57.14**	**56.32**	**55.50**	**51.62**	**48.01**	**44.68**	**41.59**	**38.73**	**33.62**	**29.24**	**15.08**	**8.50**	**5.44**
	14.4	**58.76**	**57.83**	**56.92**	**56.03**	**55.15**	**50.96**	**47.10**	**43.55**	**40.28**	**37.27**	**31.95**	**27.44**	**13.34**	**7.18**	**4.48**
	14.5	**58.66**	**57.65**	**56.65**	**55.66**	**54.70**	**50.13**	**45.96**	**42.15**	**38.67**	**35.49**	**29.94**	**25.30**	**11.41**	**5.79**	**3.53**
	14.6	**58.53**	**57.39**	**56.27**	**55.17**	**54.10**	**49.04**	**44.47**	**40.33**	**36.60**	**33.23**	**27.42**	**22.68**	**9.25**	**4.37**	**2.60**
	14.7	**58.35**	**57.02**	**55.73**	**54.47**	**53.24**	**47.49**	**42.38**	**37.83**	**33.78**	**30.19**	**24.14**	**19.35**	**6.83**	**2.94**	**1.74**
	14.8	**58.04**	**56.42**	**54.85**	**53.32**	**51.83**	**45.02**	**39.12**	**34.00**	**29.57**	**25.72**	**19.51**	**14.85**	**4.15**	**1.60**	**0.99**
	14.9	**57.34**	**55.08**	**52.91**	**50.82**	**48.82**	**39.94**	**32.68**	**26.76**	**21.92**	**17.97**	**12.12**	**8.21**	**1.43**	**0.53**	**0.42**

SOURCE: Bertin, 2015

All values in Table 8 are smaller than the failure pressure calculated using the ultimate tensile strength which is P_f = 59.7 MPa.

3.3.7 Choi et al

Choi developed two formulation based on burst tests, one for small defects in which $/\sqrt{R_e t} < 6$, and the other in which the same parameter is greater than 6. The same concept, distinct equations for different defect lengths, is also used by RPA method. For the present analysis, since it is being used lengths of defects smaller than 200 mm, values of the parameter $L/\sqrt{R_e t}$ ranges from 0.002, for L = 1 mm, to 4.22, for L = 200 mm. Therefore just one of the formulations is here presented and analyzed. For ultimate tensile strength σ_u = 597 MPa, external radius R_e = 150 mm and the other parameters already mentioned, Equation (23) becomes:

$$P_f = 0.9 \times 597 \frac{2 \times 15}{300}\left[C_2\left(\frac{1}{\sqrt{150 \times 15}}\right)^2 + C_1\left(\frac{1}{\sqrt{150 \times 15}}\right) + C_0\right] \tag{88}$$

and, after calculation:

$$P_f = 53.73\left[C_2\left(\frac{1}{47.434165}\right)^2 + C_1\left(\frac{1}{47.434165}\right) + C_0\right] \tag{89}$$

where:

$$C_0 = 0.06\left(\frac{d_{max}}{15}\right)^2 - 0.1035\left(\frac{d_{max}}{15}\right) + 1.0 \tag{90}$$

$$C_1 = -0.6913\left(\frac{d_{max}}{15}\right)^2 + 0.4548\left(\frac{d_{max}}{15}\right) - 0.1447 \tag{91}$$

$$C_2 = 0.1163\left(\frac{d_{max}}{15}\right)^2 - 0.1053\left(\frac{d_{max}}{15}\right) + 0.0292 \tag{92}$$

Two aspects of these equations shall be noticed: bulging factor is not used, although the formulation was partially developed by means of burst tests, and the length of the defect is

not incorporated directly in the formulation, therefore values of failure pressure are the same regardless of diameter defect up to the limit of this analysis which is 200 mm.

Table 9 – Failure Pressure calculated by Choi et al. formulation

d_{max} (mm) \ L (mm)	1	2	3	4	5	10	15	20	25	30	40	50	100	150	200
1	**53.24**	**53.24**	**53.24**	**53.24**	**53.24**	**53.24**	**53.24**	**53.24**	**53.24**	**53.24**	**53.24**	**53.24**	**53.24**	**53.24**	**53.24**
2	**52.94**	**52.94**	**52.94**	**52.94**	**52.94**	**52.94**	**52.94**	**52.94**	**52.94**	**52.94**	**52.94**	**52.94**	**52.94**	**52.94**	**52.94**
3	**52.65**	**52.65**	**52.65**	**52.65**	**52.65**	**52.65**	**52.65**	**52.65**	**52.65**	**52.65**	**52.65**	**52.65**	**52.65**	**52.65**	**52.65**
4	**52.39**	**52.39**	**52.39**	**52.39**	**52.39**	**52.39**	**52.39**	**52.39**	**52.39**	**52.39**	**52.39**	**52.39**	**52.39**	**52.39**	**52.39**
5	**52.16**	**52.16**	**52.16**	**52.16**	**52.16**	**52.16**	**52.16**	**52.16**	**52.16**	**52.16**	**52.16**	**52.16**	**52.16**	**52.16**	**52.16**
6	**51.94**	**51.94**	**51.94**	**51.94**	**51.94**	**51.94**	**51.94**	**51.94**	**51.94**	**51.94**	**51.94**	**51.94**	**51.94**	**51.94**	**51.94**
7	**51.74**	**51.74**	**51.74**	**51.74**	**51.74**	**51.74**	**51.74**	**51.74**	**51.74**	**51.74**	**51.74**	**51.74**	**51.74**	**51.74**	**51.74**
8	**51.57**	**51.57**	**51.57**	**51.57**	**51.57**	**51.57**	**51.57**	**51.57**	**51.57**	**51.57**	**51.57**	**51.57**	**51.57**	**51.57**	**51.57**
9	**51.42**	**51.42**	**51.42**	**51.42**	**51.42**	**51.42**	**51.42**	**51.42**	**51.42**	**51.42**	**51.42**	**51.42**	**51.42**	**51.42**	**51.42**
10	**51.29**	**51.29**	**51.29**	**51.29**	**51.29**	**51.29**	**51.29**	**51.29**	**51.29**	**51.29**	**51.29**	**51.29**	**51.29**	**51.29**	**51.29**
11	**51.18**	**51.18**	**51.18**	**51.18**	**51.18**	**51.18**	**51.18**	**51.18**	**51.18**	**51.18**	**51.18**	**51.18**	**51.18**	**51.18**	**51.18**
12	**51.09**	**51.09**	**51.09**	**51.09**	**51.09**	**51.09**	**51.09**	**51.09**	**51.09**	**51.09**	**51.09**	**51.09**	**51.09**	**51.09**	**51.09**
13	**51.03**	**51.03**	**51.03**	**51.03**	**51.03**	**51.03**	**51.03**	**51.03**	**51.03**	**51.03**	**51.03**	**51.03**	**51.03**	**51.03**	**51.03**
14	**50.98**	**50.98**	**50.98**	**50.98**	**50.98**	**50.98**	**50.98**	**50.98**	**50.98**	**50.98**	**50.98**	**50.98**	**50.98**	**50.98**	**50.98**
14.1	**50.98**	**50.98**	**50.98**	**50.98**	**50.98**	**50.98**	**50.98**	**50.98**	**50.98**	**50.98**	**50.98**	**50.98**	**50.98**	**50.98**	**50.98**
14.2	**50.98**	**50.98**	**50.98**	**50.98**	**50.98**	**50.98**	**50.98**	**50.98**	**50.98**	**50.98**	**50.98**	**50.98**	**50.98**	**50.98**	**50.98**
14.3	**50.97**	**50.97**	**50.97**	**50.97**	**50.97**	**50.97**	**50.97**	**50.97**	**50.97**	**50.97**	**50.97**	**50.97**	**50.97**	**50.97**	**50.97**
14.4	**50.97**	**50.97**	**50.97**	**50.97**	**50.97**	**50.97**	**50.97**	**50.97**	**50.97**	**50.97**	**50.97**	**50.97**	**50.97**	**50.97**	**50.97**
14.5	**50.97**	**50.97**	**50.97**	**50.97**	**50.97**	**50.97**	**50.97**	**50.97**	**50.97**	**50.97**	**50.97**	**50.97**	**50.97**	**50.97**	**50.97**
14.6	**50.97**	**50.97**	**50.97**	**50.97**	**50.97**	**50.97**	**50.97**	**50.97**	**50.97**	**50.97**	**50.97**	**50.97**	**50.97**	**50.97**	**50.97**
14.7	**50.97**	**50.97**	**50.97**	**50.97**	**50.97**	**50.97**	**50.97**	**50.97**	**50.97**	**50.97**	**50.97**	**50.97**	**50.97**	**50.97**	**50.97**
14.8	**50.96**	**50.96**	**50.96**	**50.96**	**50.96**	**50.96**	**50.96**	**50.96**	**50.96**	**50.96**	**50.96**	**50.96**	**50.96**	**50.96**	**50.96**
14.9	**50.96**	**50.96**	**50.96**	**50.96**	**50.96**	**50.96**	**50.96**	**50.96**	**50.96**	**50.96**	**50.96**	**50.96**	**50.96**	**50.96**	**50.96**

SOURCE: Bertin, 2015

In the same way as PCORR, all values in Table 9 area smaller than the failure pressure for perfect pipes, P_f = 59.7 MPa.

3.4 SECTION SUMMARY

In Section 3, the material model used on the pit corrosion defect finite element analysis of the present work, as well as, plasticity criterion and hardening rules were explained. Numerical examples of failure pressure calculated by some of the methods for appraisal of corroded pipelines were compared with the failure pressure for a perfect undamaged pipe, utilizing yield stress and ultimate tensile strength accordingly. As previously said, except for the method formulated by Choi et al. and PCORR, all the others overestimate failure pressure for small or shallow defects.

4 METHODOLOGY

In order to investigate maximum stress levels inside a corrosion pit located on the external surface of a pipe, a finite element simulation is conducted for a single pit with a constant diameter of 1.0 mm and depth varying from 0.1 mm to 4 mm. The influence of a second pit, longitudinally aligned with the first one, and its proximity with the first one is also investigated. Depths of the second pit vary similarly to single pit and spacing between first pit and second one vary from 0.1 mm to 5.0 mm.

4.1 MATERIAL PARAMETERS

Material was modeled as carbon steel as specified by the American Petroleum Institute – API, specification 5L (2004). It is chosen the API 5L X60 steel from Dotta and Ruggieri (2004). The following material properties at room temperature (20^0 C) are used: Young's Modulus E = 210,000 MPa, Poisson's ratio ν = 0.3, yield stress σ_y = 483 MPa at 0.2% strain, ultimate tensile strength σ_u = 597 MPa at 29% strain (DOTTA & RUGGIERI, 2004). For the type of simulation conducted in this work, chemical composition is not relevant, however, for information purpose only, chemical composition of API 5L X60 is presented in Table 10.

Table 10 – Chemical composition of steel API 5L X60

Grade & Class	Carbon	Manganese	Phosphorus		Sulfur	Titanium
	maximum	maximum	minimum	maximum	maximum	maximum
X60	0.28	1.4	0.045	0.030	0.030	0.04

SOURCE: API 5L, (2008)

4.2 GEOMETRICAL MODELING

4.2.1 Pipeline modeling

A 600 mm segment of a steel pipe is modeled with three different diameters. Pipes for the oil and gas industry are sold in various diameter and wall thickness depending on,

specification, use and manufacturer. Since a finite element analysis is conducted it is considered not relevant to simulate specific diameters of real pipes. Therefore the pipe is modeled with diameter of 300, 400 and 500 mm. As for wall thickness it is maintained constant during the whole simulation at 15 mm since the deepest pit corrosion modeled has 4 mm or 26.7%, leaving 73.3% of ligament. The pit is centered longitudinally on the external surface as shown on Figure 21. Applying symmetry, only ¼ of the pipe is modeled with half the length or 300mm.

Figure 21 – Dimensions of the steel pipe segment containing a pit

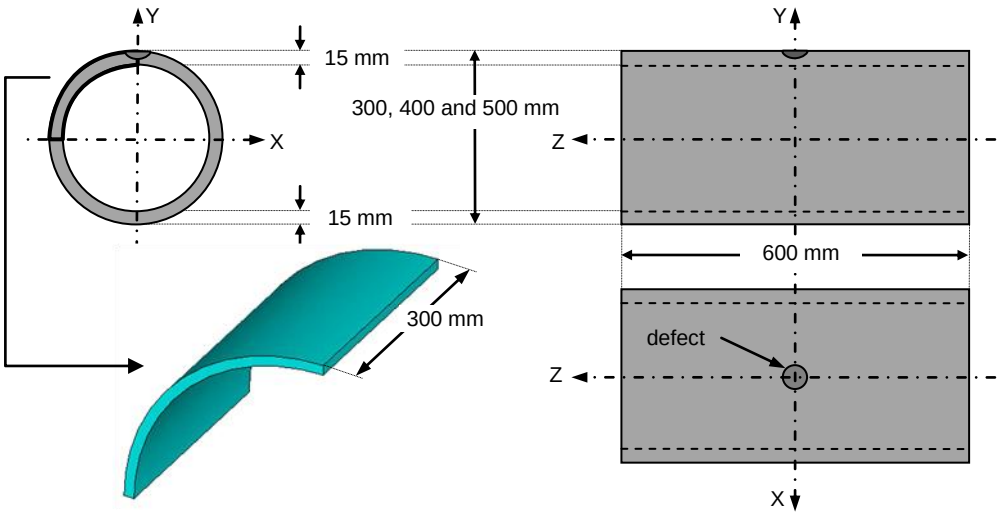

SOURCE: Bertin, 2015

4.2.2 Pit modelling

Pit can occur in different shapes. The American Society for Test of Materials – ASTM guide G46 (ASTM G46 *appud* HOEPPNER, 2011) list seven different shapes (Figure 22): narrow, elliptical, wide, subsurface, undercutting, horizontal and vertical. The first three may be grouped as elliptical. Narrow might be deep elliptical and wide might be shallow elliptical.

Figure 22 – ASTM Standard G46 Portion Showing Variation of Pit Character

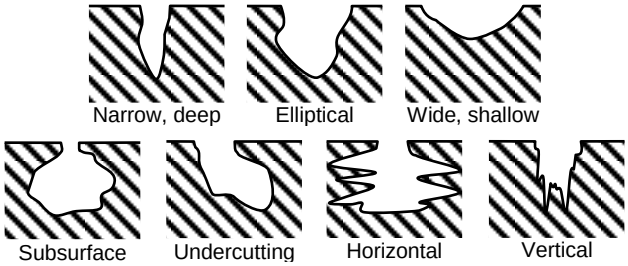

SOURCE: ASTM G46 *appud* HOEPPNER, 2011

In the present work pit corrosion was modeled as elliptical, ranging from shallow to deep. Internal surface of the pit was modeled as a semi-ellipsoidal surface with circular cross section (Figure 23).

Figure 23 – Semi-elliptical surface modeling of the pit

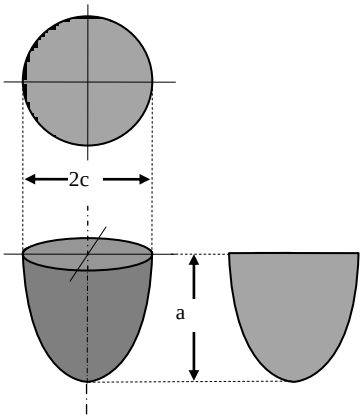

SOURCE: Bertin, 2015

Since only ¼ of the pipe is modeled, in the same way, only ¼ of a semi-ellipsoidal pit was used. The quarter pit was positioned on the upper corner of the quarter pipe as shown in Figure 24.

Figure 24 – Model of ¼ pipe with pit corrosion

SOURCE: Bertin, 2015

In the case of single pit analyses, the diameter, 2*c*, of the pit is 1.0 mm and the depths, *a*, are 0.1, 0.2, 0.3, 0.4, 0.5, 1.0, 1.5, 2.0, 2.5, 3.0, 3.5 and 4.0 mm. For this diameter, aspect ratio *a*/2*c* has the same value as depth. In the case of double pit, the diameter of the first pit, on the corner of the quarter pipe, was maintained as 2*c* = 1.0 mm with depth *a* = 1.0 mm as well. Depths of the second pit were set to 0.1, 0.2, 0.3, 0.4, 0.5, 1.0, 2.0, 3.0 and 4.0 mm. Spacing, *e*, between borders of pits also varied, assuming the following values: 0.1, 0.2, 0.3, 0.4, 0.5, 1.0, 2.0, 3.0, 4.0 and 5.0 mm. A total of 90 different simulations were performed. Figure 25 depicts four of the 90 cases, from upper left figure and working clockwise depth, *a*, and spacing, *e*, of the border of the second pit relative to the border of the first one are: 0.1 and 0.1 mm; 4.0 and 0.1 mm; 0.1 and 5.0 mm; 4.0 and 5.0 mm, respectively.

Figure 25 – Double pit maximum and minimum sizes and relative position

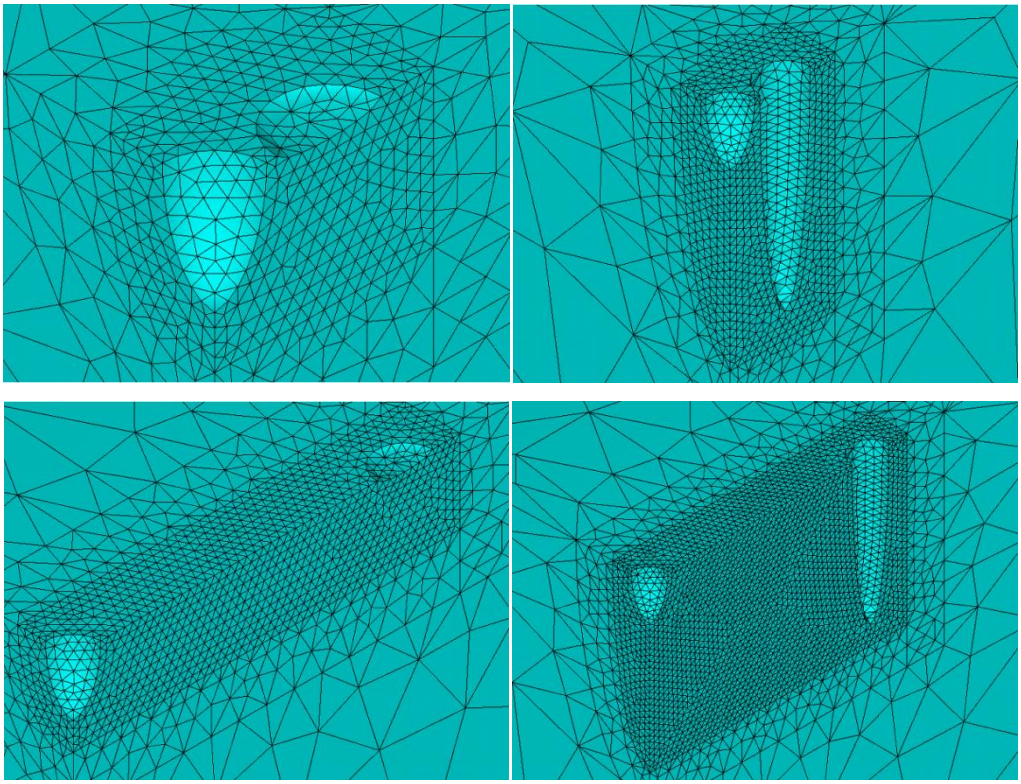

SOURCE: Bertin, 2015

4.3 FINITE ELEMENT MODELING

Simulations are performed using the finite element program ANSYS®, release 14.0.

4.3.1 Pipe and pit modeling

The 3-D model used in ANSYS® 14 was constructed parametrically by means of three scripts in Ansys Parametric Design Language – APDL (Appendices A, B and C). The first script was for preprocessing, the second one is for solving and the last one is for post processing. In this way, each process is done separately allowing more control on debugging and error correction.

Two approaches are available in ANSYS® to model any element: top down and bottom up. For the present case, the top down approach, if used, the model would be implemented by creating the volume of the pipe as a hollow quarter of a cylinder and by subtracting the pit hole, in this case a sphere scaled to the proper depth of the defect. Although simpler the approach gives little control on the creation of the refining volumes. Therefore the bottom up approach is used in this work. In the bottom up approach the model is implemented by defining the position of each keypoint given by their x, y and z coordinates. Mathematical equations are applied to change these coordinates and the entire model. Keypoints are then linked forming lines (Figure 26 and Figure 27)

Figure 26 – Keypoints and lines of quarter pipe model and pit corrosion refining volumes

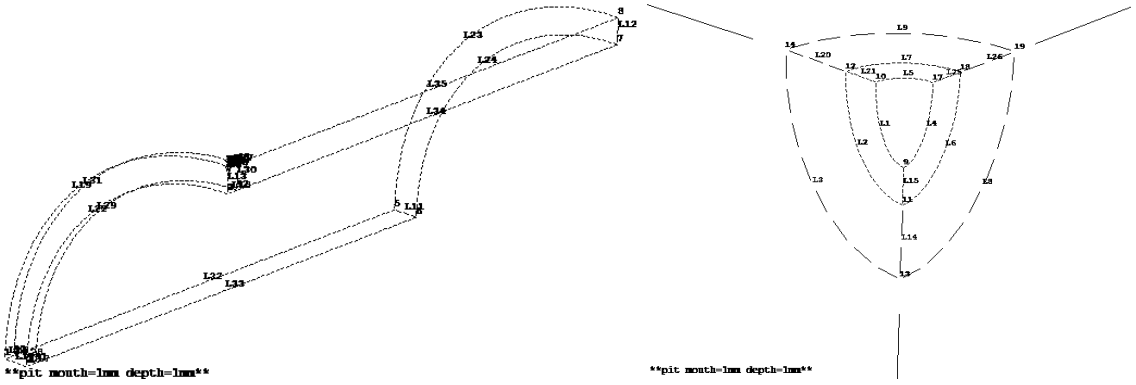

SOURCE: Bertin, 2015

Figure 27 – Keypoints and lines double pit corrosion refining volumes

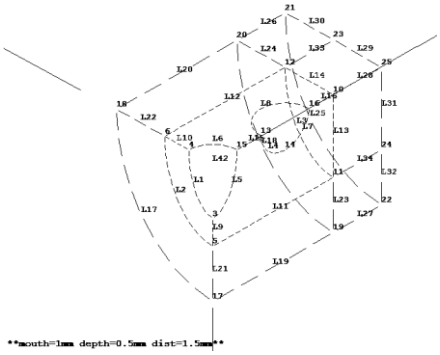

SOURCE: Bertin, 2015

Areas and volumes (Figure 28 and Figure 29) are also constructed using parametric commands. This approach permits more control over each individual parameter and allows a better design of the model and the volumes of refinement around the pit corrosion.

Figure 28 – Volumes of the model of (a) quarter pipe and (b) around the pit

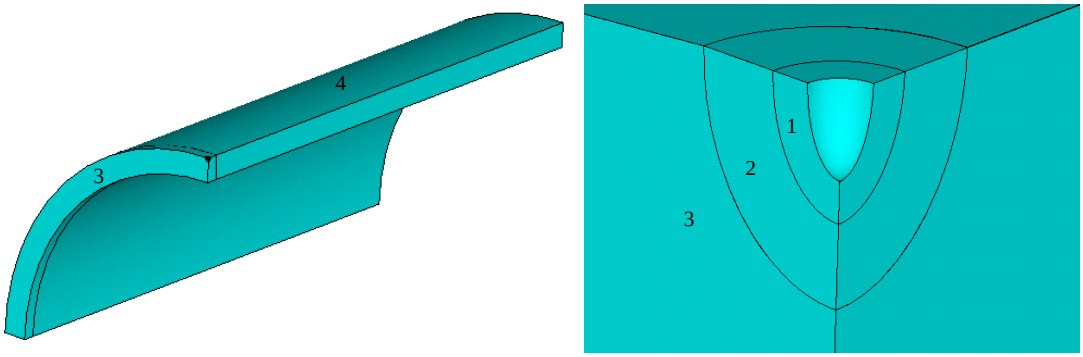

(a) (b)

SOURCE: Bertin, 2015

Figure 29 – Volumes of the model around the double pit

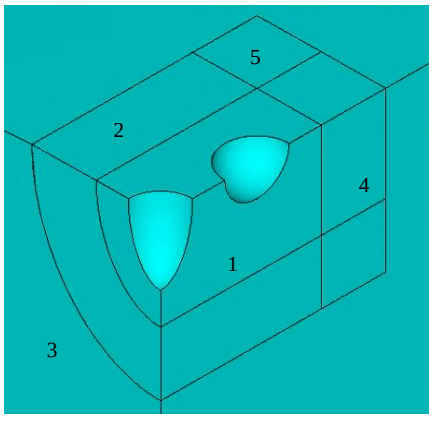

SOURCE: Bertin, 2015

Displacement restrictions are applied on axis X, Y and Z to simulate the continuity of the pipe in accordance to the symmetry conditions. Pressure is applied on the entire internal surface of the pipe (Figure 30). No other load is applied.

Figure 30 – 3D model of ¼ pipe oriented along XYZ global coordinates

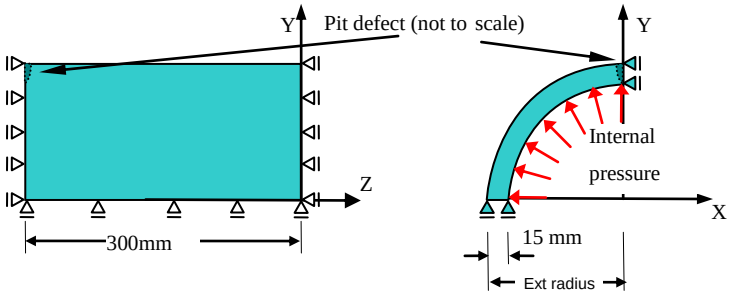

SOURCE: Bertin, 2015

4.3.2 Material modeling

Material is modeled as non linear material using ANSYS® 14 option Multilinear Isotropic Hardening. This option uses the von Mises yield criterion with the associated flow rule and isotropic hardening with the following equation:

$$\sigma_e = \frac{3}{2}[\{s\}^T[N]\{s\}]^{\frac{1}{2}} \tag{93}$$

where:

σ_e : equivalent stress; stress calculated in each point of the stress – strain curve above the yield point,

$\{s\}$: deviatoric stress vector, given by

$$\{s\} = \{\sigma\} - \sigma_m[1 \quad 1 \quad 1 \quad 0 \quad 0 \quad 0]^T \tag{94}$$

$[N]$: is given by

$$[N] = \begin{bmatrix} 1 & 0 & 0 & 0 & 0 & 0 \\ 0 & 1 & 0 & 0 & 0 & 0 \\ 0 & 0 & 1 & 0 & 0 & 0 \\ 0 & 0 & 0 & 2 & 0 & 0 \\ 0 & 0 & 0 & 0 & 2 & 0 \\ 0 & 0 & 0 & 0 & 0 & 2 \end{bmatrix} \quad (95)$$

$\{\sigma\}$: stress vector given by:

$$\{\sigma\} = [\sigma_x \quad \sigma_y \quad \sigma_z \quad \tau_{xy} \quad \tau_{yz} \quad \tau_{xz}] \quad (96)$$

σ_m : hydrostatic stress, given by:

$$\sigma_m = \frac{1}{3}(\sigma_x + \sigma_y + \sigma_z) \quad (97)$$

When the material yields the criterion adopted is:

$$Y = \sigma_e - \sigma_y \quad (98)$$

Working hardening or flow rule and isotropic hardening, σ_k, is determined directly from the equivalent plastic equivalent plastic strain, $\hat{e}^{pl}$, by the amount of plastic work done. Table 11 and

Figure 31 present the stress-strain curve used in the material model:

Table 11 – Stress – strain data used in material model

Strain	Stress (MPa)
0.0	0.0
0.0023	483.0
0.01	483.0
0.05	536.0
0.1	559.0
0.15	573.0
0.2	584.0
0.25	592.0
0.29	597.0

SOURCE: Bertin, 2015

Figure 31 – Stress – strain piecewise curve used in material model

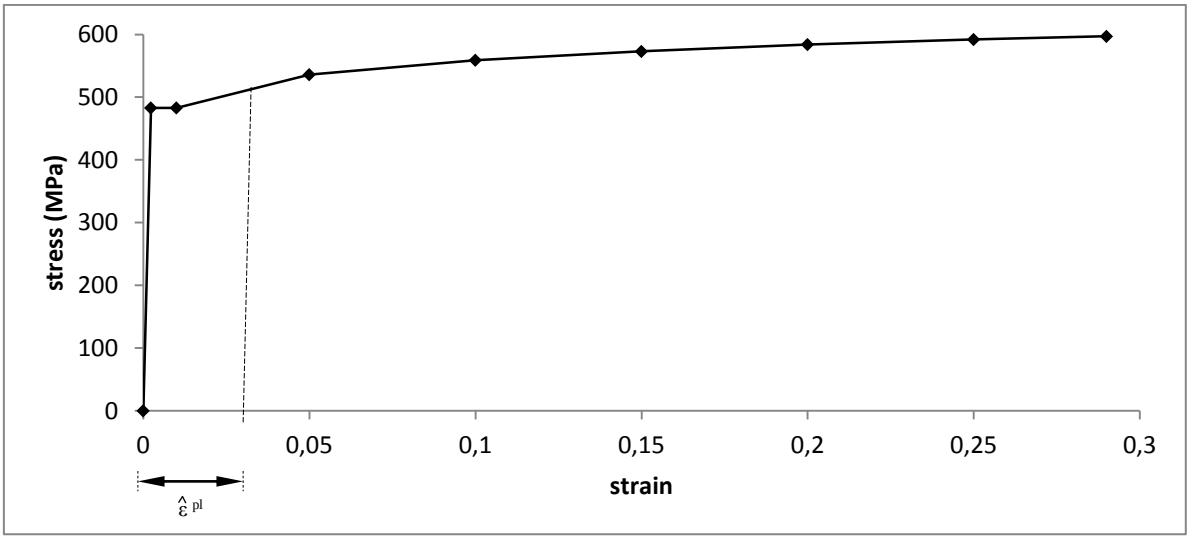

SOURCE: Bertin, 2015

4.3.3 Geometric non linearity modeling

Since the model was loaded up to the point of ultimate tensile strength it is expected significant stiffness change, therefore large displacements are allowed in the model and loading is carried on step by step automatically. It is considered that 20 substeps are adequate. A Newton-Raphson algorithm was used.

4.3.4 Element choice

On early stage of the research it was used a 20 node parallelogram structural solid, but it was discarded since for pit corrosion with depths greater than 2 mm, there was a risk of high deformation or torsion of the element that assumed a well known hourglass shape. Therefore a 10 node tetrahedron structural solid element is used. The element, (Figure 32), has a quadratic displacement behavior. Due to its tetrahedral shape, it is suited to model irregular meshes. As long as it is not flatted enough so that internal dihedral angles became too small or too large, assuming the shape of a chip, the element performs well as a solid. The element has plasticity, hyperelasticity, creep, stress stiffening, large deflection, and large strain capabilities. Each of the 10 nodes has three translational degrees of freedom in the nodal *x*, *y* and *z* directions.

Figure 32 –10 node tetrahedron structural solid element

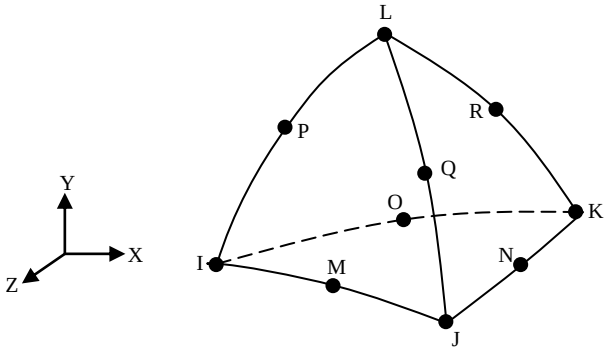

SOURCE: (HUGHES, 2000) adapted

The shape functions for the 10 node tetrahedron structural solid element in the volume natural coordinates are given as follows:

$$N_i = (2L_i - 1)L_i \text{ for corner nodes } i = \text{I, J, K, L}$$

$$\left.\begin{aligned} N_M &= 4L_{\mathrm{I}}L_{\mathrm{J}} \\ N_N &= 4L_{\mathrm{J}}L_{\mathrm{K}} \\ N_O &= 4L_{\mathrm{I}}L_{\mathrm{K}} \\ N_P &= 4L_{\mathrm{I}}L_{\mathrm{L}} \\ N_Q &= 4L_{\mathrm{J}}L_{\mathrm{L}} \\ N_R &= 4L_{\mathrm{K}}L_{\mathrm{L}} \end{aligned}\right\} \text{ for mid-edge nodes} \tag{99}$$

where:

N_i : are shape functions,

L_i : for i = I, J, K, L is given by:

$$L_i = \frac{1}{6V}(a_i + b_i x + c_i y + d_i z) \tag{100}$$

where the volume of the tetrahedron element V can be obtained by:

$$V = \frac{1}{6} det \begin{bmatrix} 1 & x_I & y_I & z_I \\ 1 & x_J & y_J & z_J \\ 1 & x_K & y_K & z_K \\ 1 & x_L & y_L & z_L \end{bmatrix} \tag{101}$$

and coefficients a_i, b_i, c_i and d_i are given by:

$$a_i = det\begin{bmatrix} x_j & y_j & z_j \\ x_k & y_k & z_k \\ x_l & y_l & z_l \end{bmatrix}, \quad b_i = -det\begin{bmatrix} 1 & y_j & z_j \\ 1 & y_k & z_k \\ 1 & y_l & z_l \end{bmatrix}$$
$$c_i = -det\begin{bmatrix} y_j & 1 & z_j \\ y_k & 1 & z_k \\ y_l & 1 & z_l \end{bmatrix}, \quad d_i = -det\begin{bmatrix} y_j & z_j & 1 \\ y_k & z_k & 1 \\ y_l & z_l & 1 \end{bmatrix} \tag{102}$$

in which the subscript i = I, J, K, L and subscripts j, k, l are determined by a cyclic permutation in the order of i, j, k, l. For example, if i = I, then j = J, k = K and l = L. Cycling, when i = J, then j = K, k = L and l = I, and so on. In Equations (104) and (102), x_I, x_J, x_K, x_L, y_I, y_J, … to z_L are Cartesian coordinates of the nodal points I, J, K and L (Figure 32).

The displacement field is then given by:

$$u = u_I N_I + u_J N_J + u_K N_K + u_L N_L + u_M N_M + u_N N_N + u_O N_O + u_P N_P + u_Q N_Q + u_R N_R \tag{103}$$

$$v = v_I N_I + v_J N_J + v_K N_K + v_L N_L + v_M N_M + v_N N_N + v_O N_O + v_P N_P + v_Q N_Q + v_R N_R \tag{104}$$

$$w = w_I N_I + w_J N_J + w_K N_K + w_L N_L + w_M N_M + w_N N_N + w_O N_O + w_P N_P + w_Q N_Q + w_R N_R \tag{105}$$

where u_I, u_J, u_K, u_L, … v_I, v_J, … to w_R are displacements, respectively, of nodes I, J, … to R in the x, y and z directions.

4.3.5 Meshing

At the beginning of the research, meshing was done automatically by the software with its most refined mesh; however results were inaccurate, due to the fact that the refinement was too coarse to properly capture stress distribution around the pit. Figure 33 illustrates (a) that mesh on the entire quarter pipe model and (b) a detailed view around the pit.

Figure 33 – Course mesh at early stage of the research

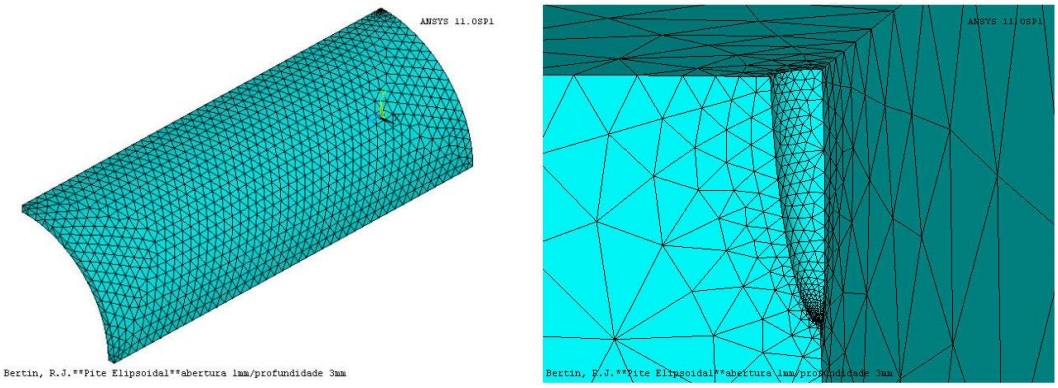

(a) (b)

SOURCE: Bertin, 2015

To overcome this problem, the model is meshed in four different volumes (Figure 28) with different sizes of element. The region around the pit (Figure 34b) is refined in two volumes (thicker black line), thus reducing computing effort and the number of nodes. The first volume, closer to pit surface, is 0.5 of pit diameter, *c*, wide and it is composed of elements with size 1/14 of the pit diameter or 71 μm. The second volume is one pit diameter, 2*c*, wide with elements varying from 71 μm to 0.45 mm . In total a volume 1.5 radius, 3*c*, wide is refined.

Figure 34 – Detail of the refined mesh around the pit in two volumes

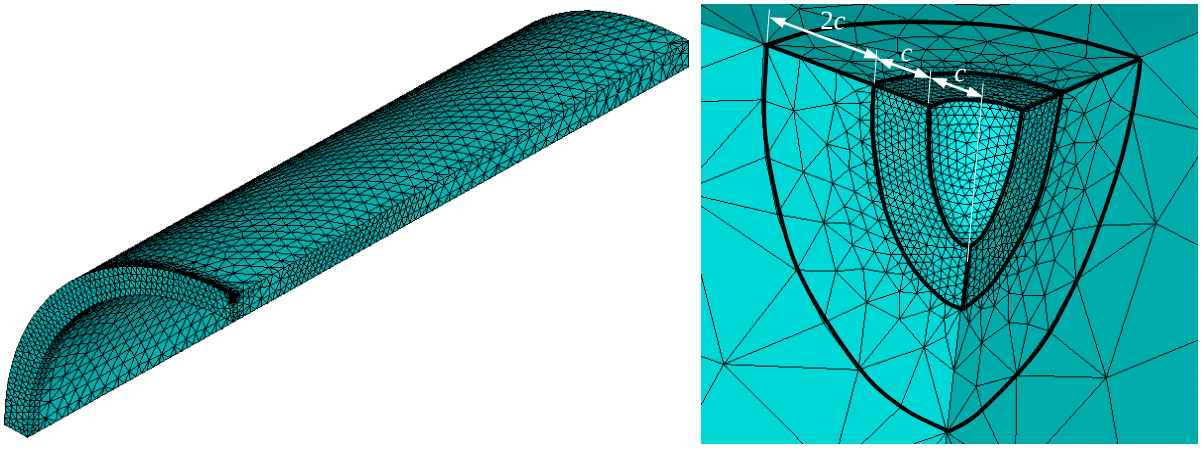

(a) (b)

SOURCE: Bertin, 2015

Volume 3, the dark band on the left end of the meshed model Figure 34a, is refined to capture boundary condition occurring outside the two previous volumes. It would be better to refine a parallelepipedal volume, but due to the complexity of the APDL script a slice of the pipe is modeled instead. Elements in volume 3 have average dimension of 1.25 mm. Volume 4, the remaining of the pipe, is automatic meshed by ANSYS® with the smallest mesh size available to ensure good transition, despite the computational effort. Table summarizes the number of elements and number of nodes of each simulation.

Table 12 – Number of elements and number of nodes for refined meshes used

pit depth (mm)	number of elements			number of nodes		
	300 mm	400 mm	500 mm	300 mm	400 mm	500 mm
0.1	27703	32517	38631	46317	54780	65280
0.2	27343	32187	39784	45896	54408	66862
0.3	27327	32972	40006	45862	55431	67169
0.4	28397	33777	40572	47400	56608	68014
0.5	29032	34783	41363	48327	58009	69136
1.0	34374	39449	48535	55780	64554	79055
1.5	40111	47254	53983	63740	75279	86642
2.0	45311	52811	56953	71074	83125	90990
2.5	48714	54188	63402	75863	85194	99829
3.0	53760	59260	65972	82985	92353	103650
3.5	59079	65042	73539	90476	100444	114160
4.0	65097	68344	77318	98801	105167	119498

SOURCE: Bertin, 2015

The model with double pit is meshed in three different volumes (Figure 35) with different sizes of element. The region close to the pits is refined in two volumes (thicker black line. The first volume, closer to pits surface, similar to the single pit, is half pit diameter, *c*, wide and it is composed of elements with size 1/14 of the pit diameter or 71 μm. This refined volume extends laterally to involve the second pit and surpass it by half diameter, *c*. The second volume is one pit diameter, 2*c*, wide with elements varying from 71 μm to 0,45 mm. The volume surpasses the previous one by one diameter, 2*c*. Both volume increase and decrease parametrically with pit depth and the spacing between them. The remaining volume that encompasses the rest of the quarter pipe is meshed similarly to volume 4 of the single pit model.

Figure 35 – Detail of the refined mesh around double pit in two volumes

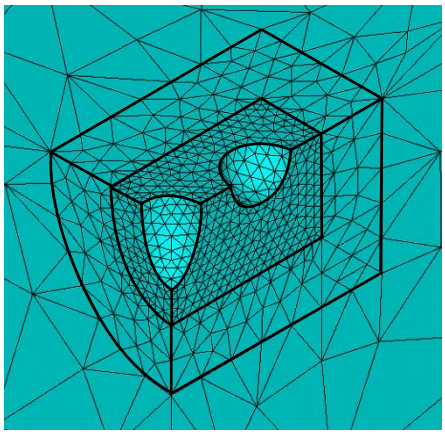

SOURCE: Bertin, 2015

Table 13 summarizes the number of elements and number of nodes of each model of the double pit.

Table 13 – Number of elements and number of nodes – double pit

pit	spacing between pit borders (mm)									
depth	0.1	0.2	0.3	0.4	0.5	1.0	2.0	3.0	4.0	5.0
(mm)	number of nodes									
0.1	99584	100327	100798	101202	101384	104724	109894	116218	119647	126221
0.2	99442	100153	100919	100954	101233	104255	110320	116072	119262	126623
0.3	99132	99558	100271	100522	101137	104119	109796	115747	119201	126170
0.4	99970	100159	100912	100658	101362	103998	110025	115733	119218	125935
0.5	99295	99794	100330	100500	101271	103868	110119	116053	119323	126336
1.0	98547	98947	99770	99740	100555	103384	109236	114947	118707	125342
2.0	104454	105128	106094	106365	107688	111753	120614	129493	135395	145676
3.0	109876	110676	112209	113014	114441	119691	130212	141131	152448	164500
4.0	114798	114962	118226	118774	120466	127109	141452	156138	169075	184047
	number of elements									
0.1	64212	64763	65091	65373	65479	67866	71525	76044	78409	83069
0.2	64123	64664	65202	65209	65377	67536	71863	75956	78130	83368
0.3	63879	64147	64652	64861	65302	67424	71466	75710	78080	83047
0.4	64516	64633	65182	64961	65479	67336	71643	75694	78096	82861
0.5	63995	64363	64733	64838	65400	67233	71705	75941	78166	83168
1.0	63450	63736	64332	64284	64898	66885	71060	75115	77700	82418
2.0	67600	68106	68780	68956	69918	72836	79158	85498	89620	96971
3.0	71411	71984	73085	73665	74700	78438	85951	93754	101831	110446
4.0	74824	74909	77318	77688	78901	83677	93966	104503	113749	124457

SOURCE: Bertin, 2015

4.3.6 Simulation

Analyses are done for internal pressures from 5 to 25 MPa with 5 MPa intervals. Internal pressure is applied incrementally over several load steps. Large deflections and large strain are allowed. Automatic time stepping feature, that reduces the load step size after a load step with plastic strain greater than 15% is encountered, is also allowed. A total of 180 simulations are performed. It is obtained, for each simulation, a list of the nodal solutions in the domain of principal stresses. Since the interest is on maximum stress, the greatest value of the first principal stress is retrieved. A picture displaying the distribution of first principal stress was also saved.

For double pit, only internal pressures of 25 MPa were used. The rest of the simulation was performed much in the same way as for single pit. A total of 90 simulations were performed. The greatest value of the first principal stress was retrieved, similar to single pit

4.4 SECTION SUMMARY

In Section 4, it was described the methodology of the research. Two cases were considered: single pit corrosion defect located on the external surface of an oil pipe and double pit corrosion defect with similar location. Both cases were modeled geometrically by means of parametric equations to simplify and speed up analyses. Material was modeled as steel conform to the API 5L X60 seamless pipe specification. Finite element analyses were conducted using a multilinear isotropic hardening model with von Mises yield criterion. Large displacements were used and loading were applied in steps. It was used a solid 10 node quadratic tetrahedron. Meshing was applied in separate volumes to allow better refinement. It was conducted 180 simulations for the single pit case and 90 simulations for double pit.

5 ANALYSIS AND RESULTS

In this section results are presented for both cases simulated: single pit corrosion defect and double pit corrosion.

5.1 MAXIMUM STRESS INSIDE SINGLE PIT

Results of maximum stress σ_{max} inside the pit on the external curved surface of the pipe for internal pressures ranging from 5 to 25 MPa with 5 MPa intervals are presented on Table 14 and Table 15, and graphically on Figure 37 (small bullet for 300 mm diameter pipe, medium bullet for 400 mm and large bullet for 500 mm). It is possible to observe that maximum stress inside the pit corrosion increases with the increase of pipe diameter and increase of the aspect ratio.

Table 14 – Maximum Stress as a function of *a*/2*c* for pipe diameters of 300 and 400 mm

a/2c	Pipe diameter (mm)					Pipe diameter (mm)				
	300					400				
	Internal pressure (MPa)					Internal pressure (MPa)				
	5	10	15	20	25	5	10	15	20	25
No defect	**50.00**	**100.00**	**150.00**	**200.00**	**250.00**	**66.67**	**133.33**	**200.00**	**266.67**	**333.33**
0.10	60.12	120.27	180.46	240.68	300.93	83.36	166.78	250.26	333.80	417.41
0.20	71.72	143.46	215.24	287.05	358.89	97.48	195.01	292.59	390.24	487.93
0.30	77.09	154.20	231.35	308.54	385.75	106.91	213.89	320.92	428.01	535.15
0.40	84.08	168.20	252.35	336.54	420.76	116.60	233.26	349.99	466.77	567.20
0.50	89.46	178.96	268.49	358.05	447.65	124.05	248.17	372.35	496.59	579.53
1.00	105.16	210.35	315.59	420.86	526.17	145.74	291.55	437.42	583.40	597.70
1.50	110.23	220.50	330.80	441.13	551.50	152.90	305.86	458.89	*583.67*	*626.26*
2.00	113.13	226.30	339.49	452.73	566.00	154.23	308.51	462.85	*583.14*	*619.57*
2.50	112.77	225.58	338.44	451.33	564.28	156.33	312.70	469.11	*582.35*	*618.93*
3.00	114.53	229.09	343.68	458.30	572.64	158.42	316.90	475.41	*623.05*	*628.52*
3.50	115.12	230.26	345.43	460.63	570.21	159.62	319.29	478.99	*563.91*	*605.66*
4.00	117.65	235.33	353.05	470.80	588.64	162.21	324.68	487.10	*566.48*	*609.28*

SOURCE: Bertin, 2015

Table 15 – Maximum Stress as a function of *a*/2*c* for pipe diameter of 500 mm

a/2*c*	Pipe diameter (mm)				
	500				
	Internal pressure (MPa)				
	5	10	15	20	25
No defect	**83.33**	**166.67**	**250.00**	**333.33**	**416.67**
0.10	101.93	203.95	306.07	408.29	510.60
0.20	125.44	250.97	376.59	502.31	568.06
0.30	137.16	274.10	411.75	549.18	593.23
0.40	149.10	298.30	447.59	572.57	*617.90*
0.50	159.30	318.70	478.20	588.24	*626.25*
1.00	186.35	372.81	559.39	*606.16*	*670.67*
1.50	196.71	393.51	573.88	*627.63*	*671.75*
2.00	196.26	392.61	578.53	*628.50*	*671.47*
2.50	201.09	402.27	578.87	*625.72*	*654.80*
3.00	201.98	404.03	592.12	*636.53*	*704.62*
3.50	204.68	409.42	*574.54*	*612.17*	*679.13*
4.00	206.40	412.89	*551.93*	*606.87*	*665.13*

SOURCE: Bertin, 2015

On any given pipe subjected to internal pressure there are three stress components (Figure 36) namely: hoop stress, σ_{hoop}, longitudinal stress, σ_{long}, and radial stress, σ_{radial}. To emphasize the stress concentration nature of the pit, the first line of the aforementioned tables presents (in bold face numbers) hoop stress for a pipe without defects. It is labeled 'No defect' and values are calculated by Equation (107). Cells with numbers in italic, bellow the thick black line, contain values that are above the threshold of the ultimate tensile strength or bellow a value that would be expected and might account for the rather erratic "ondulatory" nature of the curves in Figure 37 above the value of 550 MPa.

Figure 36 – Portion of a pipe displaying three stress components

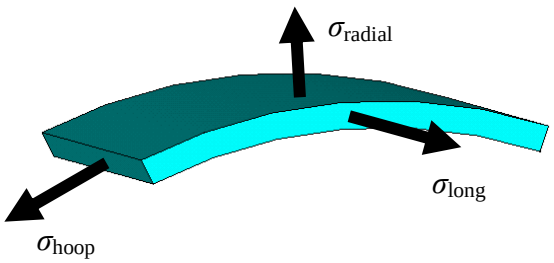

SOURCE Bertin, 2015

Figure 37 – Maximum stress versus aspect ratio ($a/2c$)

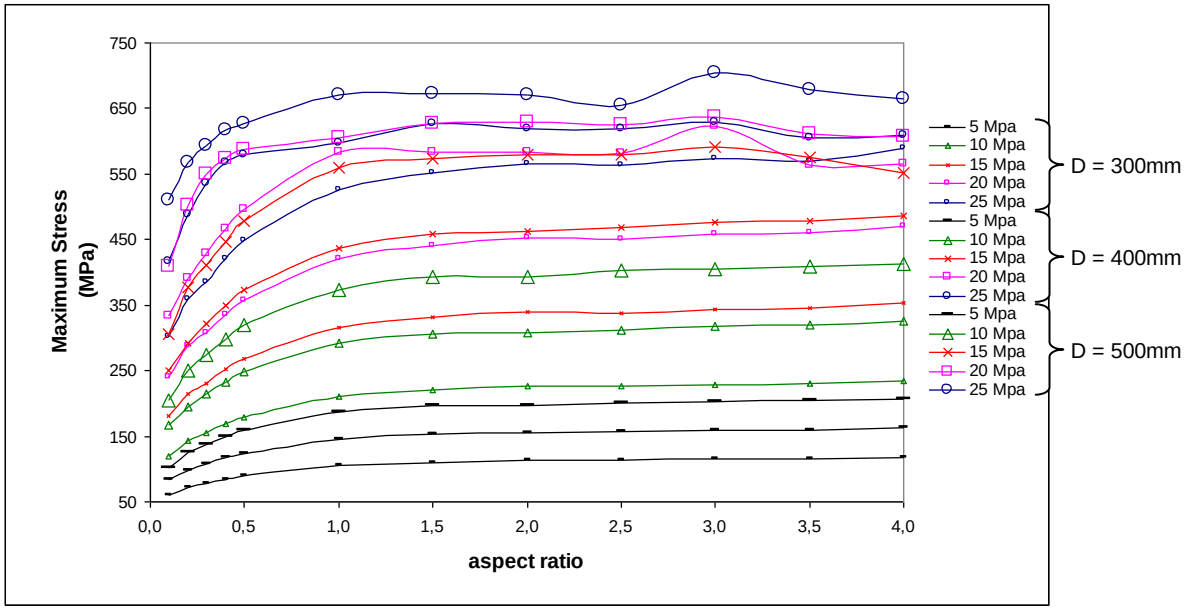

SOURCE: Bertin, 2015

5.1.1 Stress concentration factor

Stress concentration factor or SCF is the ratio of maximum stress by average or nominal stress. If it is assumed that the average stress that the pipe is subjected is the stress in the condition of no defect, in other words, not in the vicinity of the pit corrosion defect, dividing all the lines of Table 14 and Table 15 by the "No defect" line (in bold face numbers) would give as result Table 16 and Table 17.

Table 16 – SCF as a function of *a*/2*c* for pipe diameters of 300 mm and 400 mm

a/2c	Pipe diameter (mm)					Pipe diameter (mm)				
	300					400				
	Internal pressure (MPa)					Internal pressure (MPa)				
	5	10	15	20	25	5	10	15	20	25
0.10	1.20	1.20	1.20	1.20	1.20	1.25	1.25	1.25	1.25	1.25
0.20	1.43	1.43	1.43	1.44	1.44	1.46	1.46	1.46	1.46	1.46
0.30	1.54	1.54	1.54	1.54	1.54	1.60	1.60	1.60	1.61	1.61
0.40	1.68	1.68	1.68	1.68	1.68	1.75	1.75	1.75	1.75	*1.70*
0.50	1.79	1.79	1.79	1.79	1.79	1.86	1.86	1.86	1.86	*1.74*
1.00	2.10	2.10	2.10	2.10	2.10	2.19	2.19	2.19	2.19	*1.79*
1.50	2.20	2.21	2.21	2.21	2.21	2.29	2.29	2.29	*2.19*	*1.88*
2.00	2.26	2.26	2.26	2.26	2.26	2.31	2.31	2.31	*2.19*	*1.86*
2.50	2.26	2.26	2.26	2.26	2.26	2.34	2.35	2.35	*2.18*	*1.86*
3.00	2.29	2.29	2.29	2.29	2.29	2.38	2.38	2.38	*2.34*	*1.89*
3.50	2.30	2.30	2.30	2.30	2.28	2.39	2.39	2.39	*2.11*	*1.82*
4.00	2.35	2.35	2.35	2.35	2.35	2.43	2.44	2.44	*2.12*	*1.83*

SOURCE: Bertin, 2015

As already mentioned, cells containing number in italic bellow the black thick line emphasize values that appeared to be inconsistent and are related to those in Table 14 and Table 15, although not exactly the same.

Table 17 – SCF as a function of *a*/2*c* for pipe diameter of 500 mm

a/2c	Pipe diameter (mm)				
	500				
	Internal pressure (MPa)				
	5	10	15	20	25
0.10	1.22	1.22	1.22	1.22	1.23
0.20	1.51	1.51	1.51	1.51	*1.36*
0.30	1.65	1.64	1.65	1.65	*1.42*
0.40	1.79	1.79	1.79	1.72	*1.48*
0.50	1.91	1.91	1.91	*1.76*	*1.50*
1.00	2.24	2.24	2.24	*1.82*	*1.61*
1.50	2.36	2.36	2.30	*1.88*	*1.61*
2.00	2.36	2.36	2.31	*1.89*	*1.61*
2.50	2.41	2.41	*2.32*	*1.88*	*1.57*
3.00	2.42	2.42	*2.37*	*1.91*	*1.69*
3.50	2.46	2.46	*2.30*	*1.84*	*1.63*
4.00	2.48	2.48	*2.21*	*1.82*	*1.60*

SOURCE: Bertin, 2015

It is possible to conclude from the previous two tables that regardless of the internal pressure applied, the SCF is similar for the same pipe diameter and same pit corrosion aspect ratio, allowing to corroborate the findings of Cerit, Eski and Genel (2009, p. 2470) that "pit aspect ratio (*a/2c*) is a main parameter affecting the value of SCF". The percent increase in stress for pipeline without any defect to pipeline with pit corrosion defects range from 20%, for a pipe of 300 mm diameter and pit corrosion of *a/2c* = 0.1, to 148%, for a 500 mm diameter pipe with a pit of 4.0 aspect ratio, thus emphasizing the stress concentrator nature of the pit corrosion, even for shallow ones

5.1.2 Linearizing maximum stress

Comparing finite element models of elliptical pit corrosion with burst tests on machined defects, Choi et al. (2003) obtained best prediction using 90% of ultimate strength as reference stress. As can be seen on Figure 37, values of maximum stress fluctuates above 550 MPa, suggesting unreliability of the results near the ultimate tensile strength. Hence normalization of maximum stress σ_{max} is performed for 90% of ultimate tensile strength σ_u, and such results are presented and depicted using a logarithmic scale on x axis in . Values of σ_{max} / $0.9\sigma_u$ greater than 1.0 are discarded with the exception of the first result to allow continuity of the graph.

Table 18 – σ_{max} / $0.9\sigma_u$ as a function of *a*/2*c* for pipe diameters of 300 mm and 400 mm

a/2c	Pipe diameter (mm)					Pipe diameter (mm)				
	300					400				
	Internal pressure (MPa)					Internal pressure (MPa)				
	5	10	15	20	25	5	10	15	20	25
0.10	0.1119	0.22384	0.33586	0.44794	0.56008	0.1551	0.3104	0.46577	0.62125	0.77687
0.20	0.1335	0.2670	0.40060	0.53425	0.66795	0.1814	0.36294	0.54456	0.7263	0.90811
0.30	0.1435	0.28699	0.43058	0.57424	0.71794	0.1990	0.39808	0.59728	0.79659	0.99600
0.40	0.1565	0.31305	0.46966	0.62635	0.78310	0.2170	0.43413	0.65139	0.86873	1.05565
0.50	0.1665	0.33307	0.49970	0.66639	0.83315	0.2309	0.46188	0.69300	0.92423	
1.00	0.1957	0.39149	0.58736	0.78329	0.97929	0.2712	0.54262	0.81411	1.08580	
1.50	0.2052	0.41039	0.61567	0.82101	1.02643	0.2846	0.56925	0.85407		
2.00	0.2106	0.42118	0.63184	0.84260		0.2870	0.57419	0.86144		
2.50	0.2099	0.41984	0.62989	0.84000		0.2910	0.58198	0.87309		
3.00	0.2132	0.42637	0.63964	0.85297		0.2948	0.58980	0.88481		
3.50	0.2143	0.42855	0.64290	0.85731		0.2971	0.59425	0.89148		
4.00	0.2190	0.43799	0.65708	0.87623		0.3019	0.60428	0.90657		

SOURCE: Bertin, 2015

Table 19 – σ_{max} / $0.9\sigma_u$ as a function of $a/2c$ for pipe diameter of 500 mm

$a/2c$	Pipe diameter (mm)				
	500				
	Internal pressure (MPa)				
	5	10	15	20	25
0.10	0.18971	0.3796	0.5696	0.75989	0.95031
0.20	0.23346	0.4671	0.7009	0.93488	1.05725
0.30	0.25528	0.5101	0.7663	1.02211	
0.40	0.27750	0.5552	0.8330		
0.50	0.29648	0.5932	0.8900		
1.00	0.34683	0.6939	1.0411		
1.50	0.36611	0.7324			
2.00	0.36527	0.7307			
2.50	0.37426	0.7487			
3.00	0.37592	0.7520			
3.50	0.38094	0.7620			
4.00	0.38414	0.7685			

SOURCE: Bertin, 2015

Figure 38 – $\sigma_{max}/0.9\sigma_u$ versus aspect ratio for various internal pressure values.

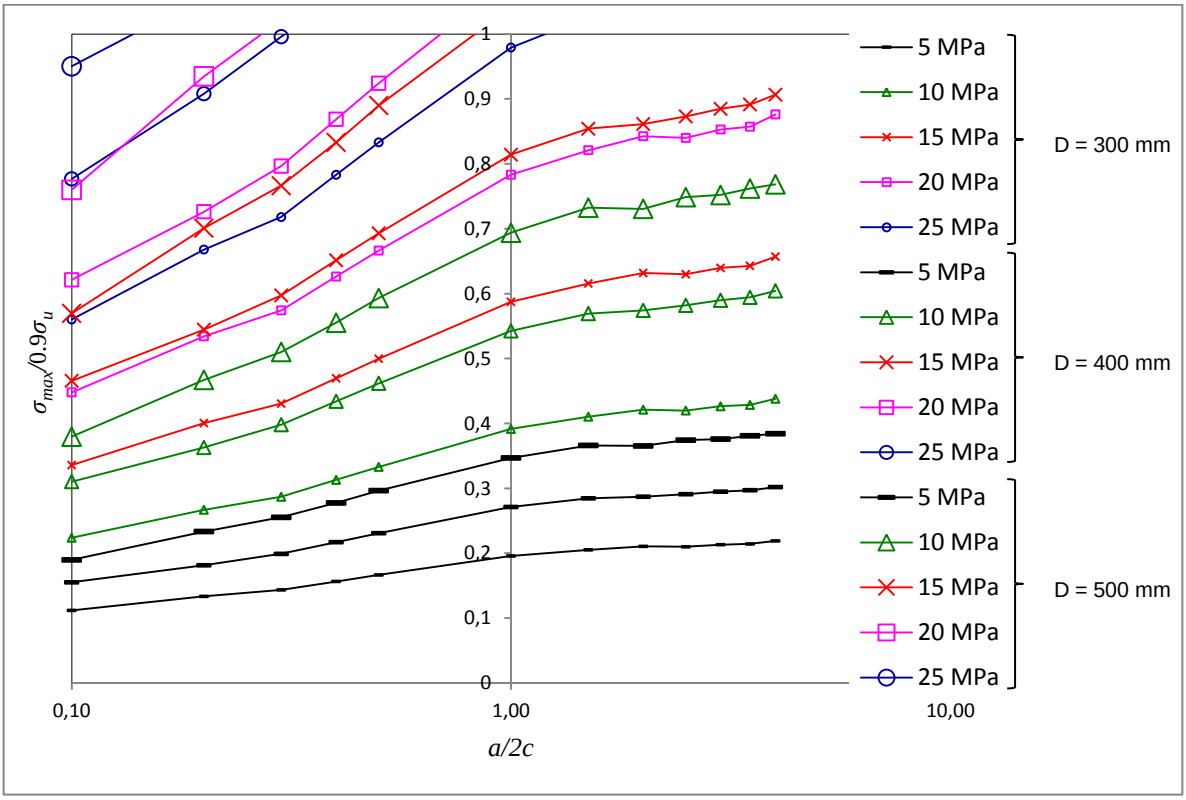

SOURCE: Bertin, 2015

For each curve of Figure 38, except the last one on the left superior corner (relative to pipe diameter of 500 mm and internal pressure of 25 MPa) that has just two points, a function

was adjusted by least squares. Several fitting curves are attempted and the best fit, using method of least squares, is obtained with the following logarithmic expression:

$$\frac{\sigma_{max}}{0.9\sigma_u} = \alpha \ln\left(\frac{a}{2c}\right) + \beta \quad (106)$$

where:

σ_{max} : is the maximum stress inside the pit;

σ_u : is the ultimate tensile strength;

$a/2c$: is the aspect ratio;

α : is the parameter that controls the steepness of the logarithmic curve;

β : is the parameter that controls the position the curve intersects the Y axis.

Table 20 summarizes the values found for each pipe diameter and for each internal pressure applied.

Table 20 – Values of parameters α and β

Internal applied pressure (MPa)	Pipe diameter (mm)	α	β
5.0	300	0.0298	0.1840
5.0	400	0.0413	0.2543
5.0	500	0.0536	0.3248
10.0	300	0.0597	0.3682
10.0	400	0.0826	0.5087
10.0	500	0.1073	0.6498
15.0	300	0.0895	0.5523
15.0	400	0.1239	0.7632
15.0	500	0.2046	1.0295
20.0	300	0.1194	0.7366
20.0	400	0.2033	1.0651
20.0	500	0.2402	1.3152
25.0	300	0.1795	0.9575
25.0	400	0.1984	1.2320

SOURCE: Bertin, 2015

5.1.3 Hoop stress as a function of the pit aspect ratio

As said before on a pipe subjected to internal pressure there are three stress components namely: hoop stress, σ_{hoop}, longitudinal stress, σ_{long}, and radial stress, σ_{radial}. Barlow's equation (1) can be used to calculate hoop stress, as follows:

$$\sigma_{hoop} = \frac{P \times D}{2t} \tag{107}$$

where:

σ_{hoop} : is the hoop stress,

P : is the internal applied pressure,

D : is the external diameter of the pipe

t : is the wall thickness.

The same internal applied pressure responsible for maximum stress inside the pit, in another part of the pipe without defects, is also responsible for hoop stress. Therefore in an attempt to correlate these two stresses under the same applied pressure parameters α and β are compared to hoop stress calculated by Equation (107). Such results are presented on Table 21 and on Figure 39 – Hoop stress versus parameters α and β.

Table 21 – Hoop stress versus parameters α and β

Internal pressure (MPa)	Diameter (mm)	σ_{hoop} (MPa)	α	β
5	300	50.00	0.0298	0.1840
5	400	66.67	0.0413	0.2543
5	500	83.33	0.0536	0.3248
10	300	100.00	0.0597	0.3682
10	400	133.33	0.0826	0.5087
15	300	150.00	0.0895	0.5523
10	500	166.67	0.1073	0.6498
20	300	200.00	0.1194	0.7366
15	400	200.00	0.1239	0.7632
25	300	250.00	0.1795	0.9575
15	500	250.00	0.2046	1.0295
20	400	266.67	0.2033	1.0651
25	400	333.33	0.1984	1.2320
20	500	333.33	0.2402	1.3152

SOURCE: Bertin, 2015

Figure 39 – Hoop stress versus parameters α and β

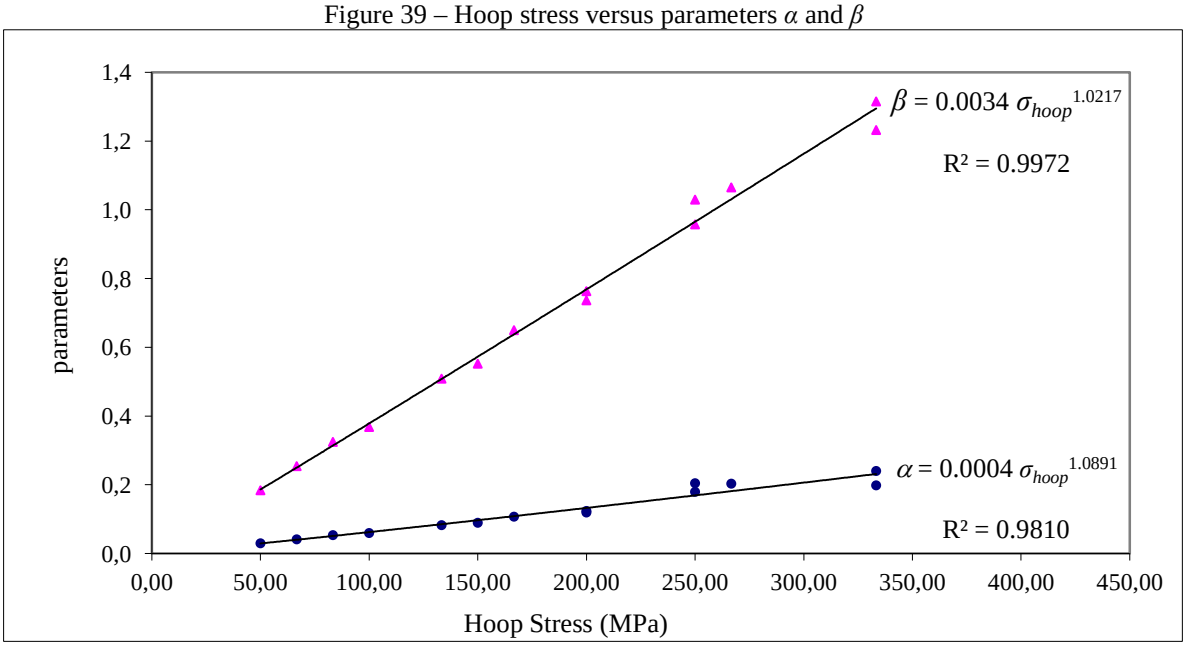

SOURCE: Bertin, 2015

Best fit by least squares method is performed leading to the following power equations for each parameter:

$$\alpha = 0.0004\sigma_{hoop}{}^{1.0891} \quad (R^2 = 98.1\%) \tag{108}$$

$$\beta = 0.0034\sigma_{hoop}{}^{1.0217} \quad (R^2 = 99.7\%) \tag{109}$$

where σ_{hoop} is the applied hoop stress. Parentheses contain the correlation parameter. Substituting (108) and (109) on (106) leads to:

$$\frac{\sigma_{\max}}{0.9\sigma_u} = 0.0004\sigma_{hoop}{}^{1.0891} \ln\left(\frac{a}{2c}\right) + 0.0034\sigma_{hoop}{}^{1.0217} \tag{110}$$

The defined critical condition, or the condition for the progression of the pit corrosion, is when maximum stress inside the pit is equal to 90% of the ultimate tensile strength, or:

$$\sigma_{\max} = 0.9\sigma_u \Rightarrow \frac{\sigma_{\max}}{0.9\sigma_u} = 1 \tag{111}$$

allowing:

$$1 = 0.0004{\sigma_{hoop}}^{1.0891} \ln\left(\frac{a}{2c}\right) + 0.0034{\sigma_{hoop}}^{1.0217} \quad (112)$$

Hoop stress as a function of the aspect ratio can be calculated, if needed, by a convenient method of solution. For instance, values in Table 23 are obtained using Microsoft Excel Solver App. Although the objective here is not to explain the theory behind Excel Solver, it is relevant to say that, according to Fylstra et al. (1998) first version of Solver uses simplex method to solve linear problems and generalized reduced gradient method to solve nonlinear problems.

Table 22 – Hoop stress as a function of the pit aspect ratio

a/2*c*	σ_{hoop} (MPa)
0.1	435.20
0.2	360.29
0.3	328.25
0.4	308.68
0.5	295.30
1.0	260.67
2.0	233.76
3.0	220.78
4.0	212.27

SOURCE: Bertin, 2015

The following figure presents the values of hoop stress from the previous table in a graphic format as a function of the pit aspect ratio. The curve has an asymptotic shape since, for the critical condition stipulated, hoop stress decreases with the increase of the aspect ratio according to the logarithmic function of Equation (112).

Figure 40 – Hoop stress as a function of the pit aspect ratio

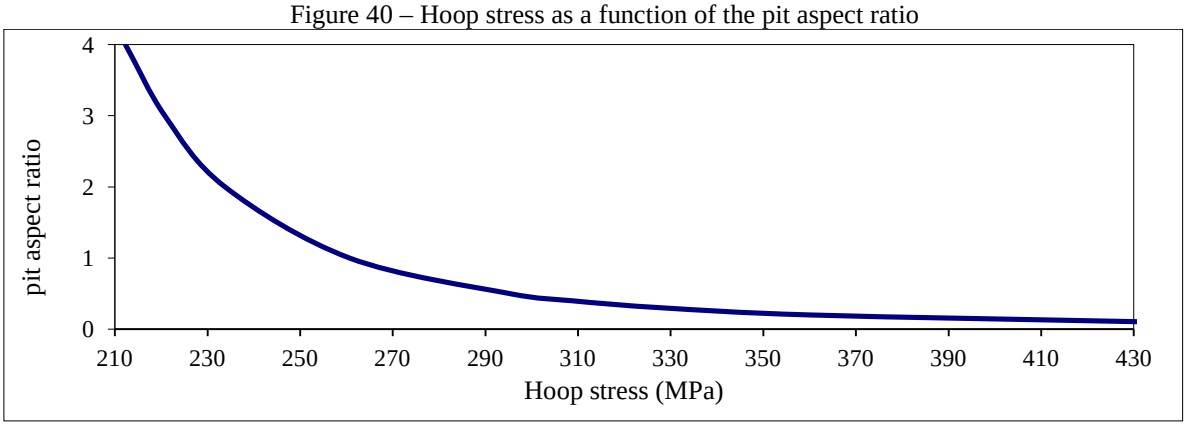

SOURCE: Bertin, 2015

5.1.4 Internal failure pressure formulation for a single pit corrosion

Internal failure pressure is normally defined as the pressure inside a pipeline that will lead to failure of the system, generally speaking, cracking, leaking and burst. Failure pressure is here understood as internal applied pressure in the pipe that causes the pit corrosion defect to progress, in other words, the passive film to break or the appearance of a crack. In this context, if on Equation (107) pressure P is substituted by failure pressure, P_f, it is possible to obtain:

$$\sigma_{\text{hoop}} = \frac{P_f \times D}{2t} \tag{113}$$

and substituting (113) on (112) allows:

$$1 = 0.0004 \left\{ \left[\frac{P_f \times D}{2t} \right]^{1.0891} \right\} \ln\left(\frac{a}{2c}\right) + 0.0034 \left[\frac{P_f \times D}{2t} \right]^{1.0217} \tag{114}$$

where:

P_f : failure pressure, MPa

D : pipe external diameter, mm

t : wall thickness, mm

$a/2c$: pit corrosion aspect ratio

Equation (114), in turn, can be used to calculate the internal applied pressure that will lead to failure (progression of the pit corrosion) for any given pipe containing a single pit corrosion of aspect ratio *a/2c*, diameter *D* and wall thickness *t*, using the same method used to calculate hoop stress. Results are presented in Table 23.

Table 23 – Failure pressure (MPa) as a function of the pipe diameter and the pit corrosion aspect ratio for pipes 15 mm of wall thickness

a/2*c*	diameter (mm)		
	300	400	500
No defect	59.7	44.78	35.82
0.1	43.543	32.658	26.121
0.2	35.998	27.018	21.617
0.3	32.813	24.602	19.694
0.4	30.887	23.151	18.521
0.5	29.548	22.147	17.718
1.0	26.071	19.550	15.640
1.5	24.415	18.312	14.650
2.0	23.374	17.531	14.025
2.5	22.630	16.973	13.588
3.0	22.058	16.545	13.242
3.5	21.599	16.200	12.963
4.0	21.217	15.913	12.731

SOURCE: Bertin, 2015

5.2 MAXIMUM STRESS INSIDE DOUBLE PIT

Results of maximum stress σ_{max} on the external curved surface of a pipe in the vicinity of two adjacent pit corrosion defects, considering an internal pressure of 25 MPa, are presented on Table 24 and Figure 41. The maximum stress for a isolated pit corrosion of 1.0 mm in diameter and depth of 1.0 mm on a pipe with diameter of 300 mm subjected to internal pressure of 25 MPa is 526,17 MPa (Table 14). Therefore, values above 526,17 MPa would indicate the influence of the second pit on the global state of stress in the vicinity of the pits. Results indicate that for a shallow second pit (aspect ratio 0.1) the effects on the first pit cease at short distance of 0.3 mm. For a narrow second pit (aspect ratio 4.0) the increase in stress is sensed even when pits are 5.0 mm apart. Some inconsistencies in the results perhaps do to the proximity to the ultimate tensile strength, make it difficult to reach a final conclusion. However it appears that the dashed line in Table 14 mark the transition of the influence zone.

Table 24 – Maximum Stress (MPa) as a function of aspect ratio and spacing between pits

Aspect ratio of second pit	Spacing between borders of pits (mm)									
	0.1	0.2	0.3	0.4	0.5	1.0	2.0	3.0	4.0	5.0
0.1	*523.32*	**527.02**	*517.53*	*504.12*	*520.87*	*516.04*	*525.48*	*525.89*	**526.85**	**526.19**
0.2	**528.02**	**529.36**	**528.73**	*525.80*	**527.70**	*525.77*	*525.81*	*525.74*	*525.75*	*525.23*
0.3	**534.35**	**531.57**	**528.80**	**528.54**	**529.85**	**526.89**	*525.84*	*525.94*	*525.36*	*525.48*
0.4	**552.83**	**537.71**	**535.38**	**531.25**	**533.55**	525.01	**526.58**	**526.19**	*524.94*	*525.47*
0.5	**567.94**	**542.72**	**540.48**	**534.30**	**535.10**	**529.38**	**526.95**	**526.26**	*523.62*	*525.51*
1.0	**613.94**	**574.64**	**562.59**	**553.40**	**547.40**	**534.28**	**530.56**	**527.02**	**527.92**	*525.94*
2.0	**645.81**	**605.90**	**588.22**	**584.90**	**575.48**	**561.23**	**559.83**	**565.02**	**555.41**	**554.66**
3.0	**658.52**	**617.54**	**599.08**	**604.05**	**579.07**	**573.65**	**595.01**	**570.97**	**615.49**	**612.77**
4.0	**666.90**	**627.48**	**603.90**	**601.97**	**598.16**	**579.04**	**586.05**	**586.76**	**587.18**	**584.10**

SOURCE: Bertin, 2015

Figure 41 – Maximum Stress as a function of aspect ratio and spacing between pits

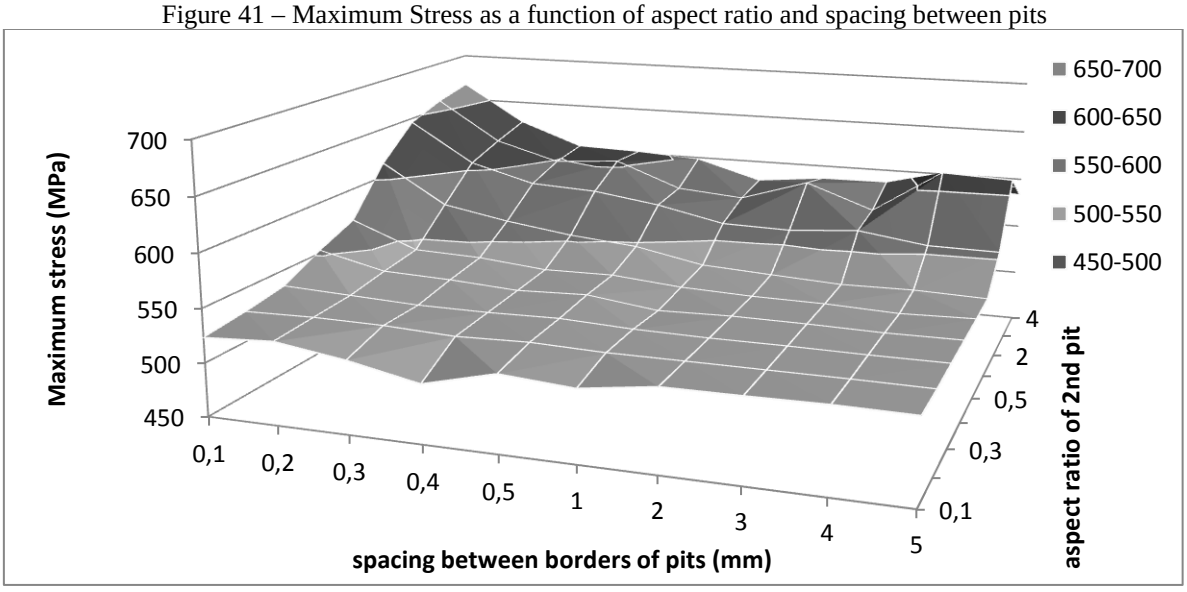

SOURCE: Bertin, 2015

5.3 SECTION SUMMARY

In this section, results were presented for both cases simulated. It was possible to derive a formulation to calculate failure pressure for pipelines with a single pit corrosion defect on the external surface. It was confirmed the influence of a second pit longitudinally aligned with the first one. However it was not possible to conclusively determine the precise location of the transition of the influence zone.

6 CONCLUSION

This section presents a summary of the work, conclusions reached and suggestions for further work. Pit corrosion is an insidious defect that may pass undetected due to its minute dimensions in early stages of formation. Under certain level of loading it acts as stress intensifier and has the potential to become a crack inducer. Moreover, most of the current methods of appraisal of corroded pipelines do not perform well for small or very shallow defects. In this context, the objective of this work was to derive a formulation to calculate internal failure pressure of pipelines with a single pit corrosion defect and to investigate the influence of a second pit longitudinally aligned with the first one.

Three API-5L-X60 steel pipes of diameters 300, 400 and 500 mm with a single pit on their external surface and a pipe 300 mm with two longitudinally aligned pits were modeled via finite element. Pit corrosion was modeled as a semi ellipsoid with opening diameter, 2*c*, equals to 1.0 mm and depth, *a*, equals to 0.1, 0.2, 0.3, 0.4, 0.5, 1.0, 1.5, 2.0, 2.5, 3.0, 3.5, and 4.0 mm. Quarter models were simulated with internal pressures from 5.0 to 25.0 MPa, in 5.0 MPa steps, in the case of the single pit and a fixed 25 MPa internal pressure was used in the case of double pit. Proper boundary conditions were applied to simulate continuity of the pipeline. Material was modeled as multilinear isotropic hardening with von Mises yield criterion and associated flow rule. Models were meshed using 10 node second order solid tetrahedron. Two volumes of refinement were used around the pit corrosion. Simulation was conducted by means of a parametric script written in APDL, the programming language of ANSYS®. Results of maximum principal stress, σ_{max}, from 180 simulations were graphically plotted as a function of the aspect ratio, *a/2c*. An erratic behavior of the curves σ_{max} - *a/2c* close to the ultimate tensile strength threshold was observed; therefore values of maximum stress were linearised, dividing them by 90% of the ultimate tensile strength. Results were graphically plotted as a function of the aspect ratio, as previously, but this time, aspect ratio is presented on logarithmic scale. For each curve, corresponding to a particular pipe diameter, internal pressure and aspect ratio, a logarithmic function was adjusted by least squares correlating the pit corrosion aspect ratio and the ratio of maximum stress and 90% of the ultimate strength, defined as the critical condition. Parameters controlling slope and position of each curve were related to the hoop stress, σ_{hoop}, calculated for the same internal pressure and pipe diameter and wall thickness as if no defect were present. For each parameter a power function, correlating parameter values and hoop stress was adjusted by least squares and

substituted in the previous logarithmic equation. Hoop stress was substituted by Barlow's equation. Stress concentration factor – SCF was also calculated.

It has been found that:

a) A formulation to calculate failure pressure was derived as a function of the pipe diameter, wall thickness, and the pit aspect ratio, considering plastic deformation. This formulation is based on Barlow's equation also used by most of the methods and procedures for appraisal of corroded pipelines. The formulation also includes indirectly material properties of ultimate tensile strength, yield stress, Young's elastic modulus and Poisson's ratio, since these parameters were intrinsically related to the simulations.
b) The formulation gives more conservative values for internal failure pressure than formulations of various corrosion assessment methods.
c) Maximum stress inside a single pit corrosion on external surface of a oil or gas pipeline increases with the increase of pipe diameter and with the pit depth. Therefore internal failure pressure decreases with the same parameters.
d) Inconsistent values of maximum stress inside the pit occur when these values approach ultimate tensile strength threshold. Hence, results best fit if failure is considered to occur for a stress level equal to 90% of the material´s ultimate strength.
e) The nature of stress concentrator of the pit, even for shallow ones, was corroborated. The percent increase in stress for pipeline without any defect to pipeline with pit corrosion defects ranges from 20% to 148% for the pipe diameters and internal pressures used.
f) For any given aspect ratio and applied internal pressure for the same pipe diameter the same value of SCF was obtained, also corroborating that values of SCF are directly related to pit corrosion aspect ratio.
g) It was confirmed the influence of a second pit longitudinally aligned with the first one. However it was not possible to conclusively determine the precise location of the transition of the influence zone.
h) APDL script allowed great control of parameters in preprocessing, solving and post processing phases of the simulation. By working each processing phase

separately with its own script, debugging was easy and stopping by error was minimized.

It is suggested that further research should be carried on as follows:

a) Analysis should be conducted to other pipe diameters and wall thicknesses, such as commercial ones, to validate the formulation for single pit corrosion, as well as better calibrate the parameters α and β.
b) A nonlinear isotropic hardening model could be used instead of the multilinear isotropic hardening. Results should be compared with those from the present work.
c) Other types of load apart from internal pressure should be investigated. For example, bending, torsion and buckling could be incorporated.
d) Simulations should incorporate cracks emanating from the pit corrosion, particularly on the pit mouth.
e) Colonies of pits should be investigated by means of three dimensional laser scanning of a actual corrosion defect on pipes and incorporated on FEM analysis.
f) Influence of longitudinal stress.
g) Modeling of crack propagation from points of maximum stress inside the pit.
h) Simulation over time of pit evolution.
i) Modeling and simulation of other types of pit.

REFERENCES

ABDALLA FILHO, J., MACHADO, R., BERTIN, R. & VALENTINI, M., 2014. On the failure pressure of pipelines containing wall reduction and isolated pit corrosion defects. *Computers & Structures*, Volume 132, pp. 22-33.

ADIB-RAMEZANI, H. et al., 2007. Evaluation of the effect of corrosion defects on the structural integrity of X52 gas pipelines using SINTAP procedure and notch theory. *International Journal of Pressure Vessels and Piping*, Volume 84, pp. 123-131.

ADIB-RAMEZANI, H., SCHMITT, C. & PLUVINAGE, G., 2006a. Application of volumetric method to the assessment of damage induced by action of foreign object on gas pipes. *Strength of materials*, 38(4), pp. 409-416.

ADIB-RAMEZANI, H., JEONG, J. & PLUVINAGE, G., 2006b. Structural integrity evaluation of X52 gas pipes subjected to external corrosion defects using the SINTAP procedure. *International journal of Pressure Vessels and Piping*, Issue 83, pp. 420-432.

AHAMMED, M., 1997. Prediction of remaining strength of corroded pressurised pipelines. *International Journal of Pressure Vessel and Piping*, Volume 71, pp. 213-217.

AHAMMED, M., 1998. Probabilistic estimation of remaining life of a pipeline in the presence of active corrosion defects. *International Journal of Pressure Vessels and Piping*, Volume 75, pp. 321-329.

ALVES, J. L., 2002. *Avaliação Numérica da Capacidade de Carga de Dutos Corroídos*, Rio de Janeiro: PUCRJ.

ALVES, J. L., 2002. *Avaliação numérica da capcidade de carga de dutos corroídos (Tese de Doutorado).* Rio de Janeiro: s.n.

AMERICAN PETROLEUM INSTITUTE, 2004. *API Specification 5L*. 43 ed. Washington: American Petroleum Institute.

AMERICAN PETROLEUM INSTITUTE, 2008. *API Specification 5L*. 44 ed. Washington: American Petroleum Institute.

ANSYS Academic Research, r. 1. h. s., 2012. *Structural Analysis Guide*, s.l.: ANSYS, Inc..

ARGENT, C. et al., 2003. *Macaw's pipeline defects.* Basingstoke(Hampshire): Yellow Pencil Marketing Co. Ltda.

ASME, 1991. *ASME-B31 - Manual for Determining the remaining Strength of Corroded Pipelines - a supplement to ASME B31 Code for Pressure Piping.* New York: American Society of Mechanical Engineers.

BARLOW, P., 1837. *A Treatise on the Strength of Timber, Cast Iron, Malleable Iron, and Other Materials, with rules for application in Architecture, Construction of Suspension Bridges, Railways, etc., with an Appendix on the power of locomotive engines, and the effect of in.* London, John Weale, Architectural Library.

BENJAMIN, A. C. & ANDRADE, E. Q., 2003. *Modified method for the assessment of the remmaining strength of corroded pipelines.* Rio de Janeiro: Rio Pipeline, IBP - Instituto Brasileiro de Petróleo e Gás.

BENNETT, L. et al., 1978. *Economic Effects of Metallic Corrosion in the United States - a report to the Congress by the National Bureau of Standards,* Washingtin, D.C.: National Bureau of Standards.

BERTIN, R. J., ABDALLA FILHO, J. E. & MACHADO, R. D., 2010. *Stress analysis of corrosion pits present on curved and plane surfaces considering plasticity.* Buenos Aires, s.n.

BJØRNØY, O. H. & MARLEY, M., 2001. *Assessment of Corroded Pipelines: Past, Present and Future.* Stavanger, Norway, The International Society of Offshore and Polar Engineers.

BJØRNØY, O., SIGURDSSON, G. & MARLEY, M., 2001. *Background and development of DNV-RP-F101 "corroded pipelines".* Stavanger, The International Society of Offshore and Polar Enginners.

CALEYO, F., GONZÁLES, J. & HALLEN, J., 2002. A study on the relaiability ssessment methodology for pipelines with active corrosion defects. *International Journal of Pressure Vessels and Piping*, Volume 79, pp. 77-86.

CALLISTER, W. D., 2001. *Fundamentals of Material Science and Engineering.* 5th ed. New York: John Wiley.

CERIT, M., 2013. Numerical investigation on torsional stress concetration factor at the semi elliptical corrosion pit. *Corrosion Science,* Volume 67, pp. 225-232.

CERIT, M., GENEL, K. & EKSI, S., 2009. Numerical investigation on stress concentration of corrosion pit. *Engineering Failure Analysis,* Volume 16, pp. 2467-2472.

CHEN, Y. et al., 2015. Failure assessment of X80 pipeline with interacting corrosion defects. *Engineering Failure analysis*, Volume 47, pp. 67-76.

CHEN, Y. et al., 2015. Failure analysis of high strength pipeline with single and multiple corrosions. *Materials and Design*, Volume 67, pp. 552-557.

CHOI, J. et al., 2003. Development of limit load solutions for corroded gas pipelines. *Pressure Vessels and Piping*, Volume 80, pp. 121-128.

CHOUCHAOUI, B. A. & PICK, R. J., 1996. Behaviour of longitudinally aligned corrosion pits. *International Journal of Pressure Vessel & Piping*, Issue 67, pp. 17-35.

COOKE, R. & JAGER, E., 1998. A Probabilistic Model for the Failure Frequency of Underground Gas Pipelines. , vol.18, nº 4. *Risk Analysis*, 18(4), pp. 511-527.

COSHAM, A. & HOPKINS, P., 2004. *The Assessment of Corrosion in Pipelines - guidance in the pipeline defect assessment manual (PDAM).* Amsterdam, Pipeline Piggiing and Integrity Management Conference.

COSHAM, A., HOPKINS, P. & MACDONALD, K. A., 2007. Best practice for the assessment of defects in pipelines - corrosion. *Engineering Failure Analysis*, pp. 1245-1265.

COSHAM, A. & KIRKWOOD, M., 2000. *Best practice in pipeline defect assessment.* Calgary, International Pipeline Conference.

CRONIN, D. S. & PICK, R. J., 2002. Prediction of the failure pressure for complex corrosion defects. *International Journal of Pressure Vessels and Piping*, Volume 79, pp. 279-287.

DET NORSKE VERITAS, 2010. *RECOMMENDED PRACTICE DNV-RP-F101 - corroded pipelines.* [Online]
Available at: http://exchange.dnv.com/publishing/Codes/ToC_edition.asp [Acesso em 10 September 2012].

DOLLEY, E. J., LEE, B. & WEI, R. P., 2000. The effect of pitting corrosion on fatigue life. *Fatigue and Fracture of Engineering Materials & Structures*, Issue 23, pp. 555-560.

DOTTA, F. & RUGGIERI, C., 2004. Structural integrity assessments of hogh pressure pipelines with axial flaes using a micromechanics model. *International Journal of Pressure Vessels and Piping*, Volume 81, pp. 761-770.

ESCOE, A. K., 2006. *Piping and pipeline assessment guide.* Oxford: Elsevier.

FAN, Y., HU, Z. & ZHOU, J., 2007. *Study on Mechanical Property of Corroded Piipeline.* Puerto de La Cruz, Canary Islands, Spain, WSEAS - World Scientific and Engineering Academy and Society, pp. 1-9.

FAZZINI, P. G. & OTEGUI, J. L., 2007. Experimental determination of stress corrosion crack rates and service lives in a buried ERW pipeline. *International Journal of Pressure Vessels and Piping,* Issue 84, p. 739–748.

FERRAZ, U. S., 2007. *Resistência Estrutural de Dutos Corroídos sobre Pressão Interna e Externa,* Rio de Janeiro: UFRJ.

FU, B., STEPHENS, D., RITCHIE, D. & JONES, C., 2001. *Methods for assessing corroded pipeline - review, validation and recomendations.* New Orleans, 13th Ppipeline Research Council International - PRCI/European Pipeline Research Group - ERPG Joint Technical Meeting on Linepipe Research.

FYLSTRA, D., LASDON, L., WATSON, J. & WAREN, A., 1998. *Design and Use of the Microsoft Excel Solver.* [Online] Available at: http://www.utexas.edu/courses/lasdon/design3.htm [Acesso em 01 09 2013].

GENTIL, V., 2012. *Corrosão.* 6th ed. Rio de Janeiro: LTC.

HIBBELER, R., 2010. *Resistência dos Materiais,* s.l.: Pearson.

HIPPERT JR., E., 2004. *Investigação Experimental do Comportamento Dúctil de Aços API-X70 e aplicação de Curvas de Resistência J-delta a para Previsão de Colapso em Dutos.* São Paulo: Tese de Doutorado - USP.

HOEPPNER, D. W., March, 2011. Chapter 5 – Pitting Corrosion: morphology and characterization. In: *Corrison Fatigue and Environmentally Assisted Cracking in Aging Military Vehicles.* s.l.:NATO - Research and Technology Organization Report Number: RTO-AG-AVT-140, (AC/323(AVT-140) TP/346), pp. 5-1 to 5-16.

HOOKE, R., 1676. *A description of helioscopes and some ohter instruments.* London: T.R..

HOOKE, R., 1678. *De Potentia Restitutiva or of Spring – explaining the power of springing bodies.* London: John Martin.

HORNER, D. et al., 2011. Novel images ot the evolution of stress corrosion cracks from corrosion pits. *Corrosion Science,* Volume 53, pp. 3466-3485.

HUGHES, T. J., 2000. *The Finite Element Method: linear static and dynamic finite element analysis.* Englewood Cliffs, N.J.: Prentice-Hall.

HU, H., 1999. Stochastic theory of fatigue corrosion. *Physics Letters A,* Issue 261, pp. 217-225.

JANELLE, J. L., 2005. *An overview and validation of the fitness-for-service assessment procedure for local thin areas.* Akron: Master of Science dissertation - Mechanical Engineering - University of Akron.

JI, J., ZHANG, C., KODIKARA, J. & YANG, S.-Q., 2015. Prediction of stress concentration factor of corrosion pits on buried pipes by least squares support vector machine. *Engineering Failure Analysis*, Volume 55, pp. 131-138.

JIVKOV, A. P., 2004. Strain-induced passivity breakdown in corrosopn crack initiation. *Theoretical and Applied Fracture Mechanics,* Issue 42, pp. 43-52.

KONDO, Y., 1989. Prediction of Fatigue Crack Initiation Life Based on Pit Growth. *Corrosion*, Volume 45, pp. 7-11.

LAMÉ, G., 1852. *Leçons sur la Théorie Mathématique de l'Élasticité des Corps Solides.* Paris: Imprimerie de Bachelier.

LEE, O. S. & KIM, H. J., 2000. *Effect of External Corrosion in Pipeline on Failure Prediction.* International journal of the Korean Society of Precision Engineering, Dezembro, 1(2), pp. 48-54.

Liu, G. & Quek, S., 2003. *The Finite Element Method - a pratical course.* Boston: Butterworth-Heinemann.

LUBLINER, J., 2008. *Plasticity Theory.* New York: Dover Publications, Inc..

MA, F.-Y., 2012. *Corrosive Effects of Chlorides on Metals, Pitting Corrosion.* [Online] Available at: Fong-Yuan Ma (2012). Corrosive Effects of Chlorides on Metals, Pitting Corrosion, Prof. Nasr Bensalah (Ed.), ISBN: 978-953-51-0275-5, InTech, DOI: 10.5772/32333. Available from: http://www.intechopen.com/books/pitting-corrosion/corrosive-effects-of-chlori
[Acesso em 29 08 2013].

MARCINIAK, Z., DUNCAN, J. & HU, S., 2002. *Mechanics of Sheet Metal Forming.* Oxford: Butterworth-Heinemann.

MOHD, M. H. & PAIK, J. K., 2013. Investigation of the corrosion progress characteristics of offshore subsea oil well tubes. *Corrosion Science*, Volume 67, pp. 130-141.

OK, D., PU, Y. & INCECIK, A., 2007. Artificial neural networks and their application to assessment of ultimate strength of plates with pitting corrosion. *Ocean Engineering,* Issue 34, pp. 2222-2230.

PAIK, J. K., LEE, J. M. & KO, M. J., 2004. Ultimate shear strength of plate elements with pit corrosion wastage. *Thin-walled Structures,* Volume 42, pp. 1161-1176.

PIDAPARTI, R. M. & PATEL, R. K., 2010. Investigation of a single pit/defect evolution during the corrosion process. *Corrosion Science,* Volume 52, pp. 3150-3153.

PIDAPARTI, R. M. & RAO, A. S., 2008. Analysis of pits induced stresses due to metal corrosion. *Corrosion Science,* Issue 50, p. 1932–1938.

Process Performance Improvement Consultants, LLC, 2007. *Comparison of Integrity Management Assessment Techniques for Natural Gas Transmission Pipelines,* Houston, TX, USA: s.n.

QUALES, B., 1970. Battelle Line Pipe Research program helps solve industry problems. *Pipeline News,* 01 Feb, Volume 42, pp. 23-28.

RAJABIPOUR, A. & MELCHERS, R. E., 2013. A numerical study of damage caused by combined pitting corrosion and axial stress in steel pipes. *Corrosion Science*, Volume 76, pp. 292-301.

REES, D. W., 2006. *Basic Engineering Plasticity.* Oxford: Butterworth-Heineman.

REVIE (Ed.), R. W., 2011. *Uhlig's Corrosion Handbook.* 3rd ed. Hoboken: John Wiley & Sons.

SCHWEITZER, P. A., 2010. *Fundamentals of corrosion: mechanisms, causes, and preventative methods.* Boca Raton: CRC Press.

SOUZA, R. D. d., 2003. *Avaliação estrutural de dutos com defeitos de corrosão reais.* Rio de Janeiro: Dissertação de Mestrado, PUC - Rio.

SQUARCIO, R. M. F., 2009. *Análise da confiabilidade de oleodutos corroídos utilizando o método Monte Carlo:um estudo de caso.* Curitiba: Masters dissertation - Computational Mechanics - UFPR.

SZKLARSKA-SMIALOWSKA, Z., 1999. Pitting corrosion of aluminum. *Corrosion Science*, Volume 41, pp. 1743-1767.

TIMOSHENKO, S. P., 1983. *History of Stregth of Materials.* New York: Dover Publishing, Inc..

TURNBULL, A., HORNER, D. A. & CONNOLLY, B. J., 2008. Challenges in modelling the evolution of stress corrosion cracks from pits. *Engineering Fracture Mechanics.*

TURNBULL, A., McCARTNEY, L. & ZHOU, S., 2006. Modelling of the evolution of stress corrosion cracks from corrosion pits. *Scripta materialia,* Volume 54, pp. 575-578.

TURNBULL, A., WRIGHT, L. & CROCKER, L., 2010. New insight into the pit-to-crack transition from finite element analysis of the stress and strain distribution around a corrosion pit. *Corrosion Science*, Volume 52, pp. 1492-1498.

TURNBULL, A. & ZHOU, S., 2004. Pit to crack transition in stress corrosion cracking of a steam turbine disc steel. *Corrosion Science*, Volume 46, pp. 1239-1264.

TURNBULL, A. & ZHOU, S., 2012. Electrochemical short crack effect in environmentally assisted cracking of a steam blade steel. *Corrosion Science*, Volume 58, pp. 33-40.

U.S. Department of Transportation, Pipeline & Hazardous Materials Safety Administration, 2013. *Pipeline Safety Stakeholder Communications - All Reported Pipeline Incidents By Cause.* [Online]
Available at: http://primis.phmsa.dot.gov/comm/reports/safety/AllPSIDet_1993_2012_US.html?nocache=2884
[Acesso em 22 August 2013].

WATKINS, R. K. & ANDERSON, L. R., 1999. *Strucutral Mechanics of Buried Pipes.* Boca Raton(Flórica): CRC Press.

WESSELS, J. & HOOGEVEEN, R., 2002. *Renovation of Qanats in Syria.* s.l.:UNU/UNESCO/ICARDA.

WRIGHT, P. H. & ASHFORD, N. J., 1989. *Transportation Engineering - planning and design.* 3ª ed. New York: John Wiley & Sons.

YOUNG, T., 1807. *A course of lectures on natural philosophy and the mechanical arts.* London: Joseph Johnson.

APPENDICES

APPENDIX A – ANSYS script for pre processing

Single pit

```
!ANSYS - Análise não linear de pites elipsoidais de corrosão
!arquivo de comandos para análise de pite elipsoidal em modelo de 1/4 de tubo

!Pontifícia Universidade Católica do Paraná
!Programa de Pós-Graduação em Engenharia Mecânica
!Mecânica dos Sólidos Computacional
!Orientador: Dr. João Elias Abdalla Filho
!Doutorando: Ricardo J. Bertin
!ricardo.bertin@pucpr.br

!*****************************************************************
/CLEAR                                          !limpa e reinicia
/UIS,msgpop,3                                   !desabilita mensagens de erros


*ASK,DIRECTORY,'diretório - digitar nome entre 'aspas simples'','A187'
MULTIPRO,'start',3
*CSET,1,3,DIAMETER,'diâmetro externo do duto em mm',300
*CSET,4,6,THICK,'espessura - parede do duto em mm',15
*CSET,7,9,COMP,'comprimento do tubo em m',0.3
*CSET,10,12,BOCA_PITE,'diâmetro do pite em mm',1
MULTIPRO,'end'

/MKDIR,c:\ansys\%DIRECTORY%\pre\%DIAMETER%\%THICK%          !cria diretório padrão
/CWD,c:\ansys\%DIRECTORY%\pre\%DIAMETER%\%THICK%            !muda para diretório padrão
PARSAV,all,c:\ansys\parametros,

!*********define o título da análise e o nome do arquivo**********


*DO,i,1,12,1

!************************entrada de dados************************
!define parâmetros
        raio_ext=DIAMETER/2000
        raio_int=raio_ext-(THICK/1000)
        PP1=0.1
        PP2=0.2
        PP3=0.3
        PP4=0.4
        PP5=0.5
        PP6=1
        PP7=1.5
        PP8=2
        PP9=2.5
        PP10=3
        PP11=3.5
        PP12=4
        raio_pite=BOCA_PITE/2000
        c_2=BOCA_PITE
        faixa_ref=14*raio_pite          !largura da faixa de refino
        ref1=raio_pite/7
        ref2=raio_pite
        ref3=THICK/4000                 !lado do elemento de refino 3
!*****************************************************************
        a=PP%i%
        /TITLE,**pit mouth=%c_2%mm depth=%a%mm**
        /FILENAME,RJB_%DIAMETER%_%THICK%_%i%
!*****************************************************************

!**********calcula parâmetros do pite*****************************
        prof_pite=(PP%i%)/1000
        ligament_1=raio_ext-prof_pite
        ligament_2=raio_ext-(prof_pite+raio_pite)
        ligament_3=raio_ext-(prof_pite+3*raio_pite)
        razao_1=(2*prof_pite)/(boca_pite/1000)
        razao_2=(2*(prof_pite+raio_pite))/(2*boca_pite/1000)
        razao_3=(2*(prof_pite+3*raio_pite))/(4*boca_pite/1000)
!*****************************************************************

        /PREP7   !fase de preprocessamento
```

```
!**********carrega elemento e material**************************
        ET,1,solid187                   !elemento tetraédrico de 10 nós
        /COM,Internal UNITS set at file creation time = SI   (MKS)
        TBDEL,ALL,_MATL
        MPDEL,ALL,_MATL
        MPTEMP,R5.0, 1, 1,  25.0000000    ,
        MPDATA,R5.0, 1,EX  ,_MATL   , 1,  210000.000    ,
        MPTEMP,R5.0, 1, 1,  25.0000000    ,
        MPDATA,R5.0, 1,PRXY,_MATL   , 1, 0.300000000    ,
        TB,MISO,_MATL   ,   1,   8
        TBTEMP,  20.0000000    ,   1
        TBPT,,0.0023,483
        TBPT,,0.0100,483
        TBPT,,0.0500,536
        TBPT,,0.1000,559
        TBPT,,0.1500,573
        TBPT,,0.2000,584
        TBPT,,0.2500,592
        TBPT,,0.2900,597
!*****************************************************************

!**********modelagem*********************************************

!geração dos keypoints

        K,1,-raio_ext,0,0
        K,2,-raio_int,0,0
        K,3,0,raio_int,0
        K,4,0,raio_ext,0
        K,5,-raio_ext,0,-COMP
        K,6,-raio_int,0,-COMP
        K,7,0,raio_int,-COMP
        K,8,0,raio_ext,-COMP
        K,9,0,ligament_1,0
        K,10,-raio_pite,raio_ext,0
        K,11,0,ligament_2,0
        K,12,-2*raio_pite,raio_ext,0
        K,13,0,ligament_3,0
        K,14,-4*raio_pite,raio_ext,0
        K,15,0,0,0
        K,16,0,0,-COMP
        K,40,-raio_ext,0,-faixa_ref
        K,41,-raio_int,0,-faixa_ref
        K,42,0,raio_int,-faixa_ref
        K,43,0,raio_ext,-faixa_ref
        K,45,0,0,-faixa_ref

!mudança do plano de trabalho
        WPLANE,,0,raio_ext,0,-0.1,raio_ext,0,0,0,0

        CSWPLA,11,1,razao_1,1       !coordenadas cilíndricas
        L,10,9                      !linha 1
        CSWPLA,11,1,razao_2,1       !coordenadas cilíndricas
        L,12,11                     !linha 2
        CSWPLA,11,1,razao_3,1       !coordenadas cilíndricas
        L,14,13                     !linha 3
        WPLANE,,0,0,0,0.1,0,0,0,raio_ext,0      !plano de trabalho default
        CSYS,0                      !coordenadas cartesianas
        AROTAT,1,,,,,,4,3,90,1      !linhas 4 e 5 área 1 - superfície do pite
        AROTAT,2,,,,,,4,3,90,1      !linhas 6 e 7 área 2 - interface entre V1 e V2
        AROTAT,3,,,,,,4,3,90,1      !linhas 8 e 9 área 3 - interface entre V2 e V3

!geração das linhas
        L,1,2                       !linha 10
        L,5,6                       !linha 11
        L,7,8                       !linha 12
        L,3,13                      !linha 13
        L,13,11                     !linha 14
        L,11,9                      !linha 15
        L,1,40                      !linha 16
        L,2,41                      !linha 17
        L,3,42                      !linha 18
        LARC,1,14,15,raio_ext       !linha 19
```

```
            LARC,14,12,15,raio_ext      !linha 20
            LARC,12,10,15,raio_ext      !linha 21
            LARC,2,3,15,raio_int        !linha 22
            LARC,5,8,16,raio_ext        !linha 23
            LARC,6,7,16,raio_int        !linha 24
            L,17,18                     !linha 25
            L,18,19                     !linha 26
            L,19,43                     !linha 27
            L,40,41                     !linha 28
            LARC,41,42,45,raio_int      !linha 29
            L,42,43                     !linha 30
            LARC,40,43,45,raio_ext      !linha 31
            L,40,5                      !linha 32
            L,41,6                      !linha 33
            L,42,7                      !linha 34
            L,43,8                      !linha 35

!geração das áreas
            AL,1,15,2,21                !área 4     - sofrerá restrição em Z
            AL,2,14,3,20                !área 5 - sofrerá restrição em Z
            AL,3,13,22,10,19            !área 6 - sofrerá restrição em Z
            AL,12,24,11,23              !área 7 - sofrerá restrição em Z
            AL,10,17,28,16              !área 8 - sofrerá restrição em Y
            AL,13,18,30,27,8            !área 9 - sofrerá restrição em X
            AL,14,6,26,8                !área 10 - sofrerá restrição em X
            AL,6,15,4,25                !área 11 - sofrerá restrição em X
            AL,22,18,29,17              !área 12 - face interna do tubo - vol 3 - carregamento
            AL,5,25,7,21                !área 13 - face externa no volume do refino
            AL,7,26,9,20                !área 14 - face externa no volume do refino
            CSWPLA,12,1                 !coordenadas cilíndricas
            AL,9,31,27,19,16            !área 15 - superfície externa do tubo - vol 3
            CSYS,0                      !coordenadas cartesianas
            AL,28,33,11,32              !área 16 - sofrerá restrição em Y
            AL,30,34,12,35              !área 17 - sofrerá restrição em X
            AL,28,29,30,31              !área 18 - interface interna entre vol 3 e vol 4
            AL,29,34,24,33              !área 19 - face interna do tubo - vol 4 - carregamento
            AL,31,35,23,32              !área 20 - superfície externa do tubo - vol 4

!geração do volume
            VA,1,2,4,11,13
            VA,2,3,5,10,14
            VA,3,6,18,8,9,12,15
            VA,16,17,18,19,20,7

!geração da malha
!malha volume 1
            ESIZE,ref1
            VMESH,1
!malha volume 2
            ESIZE,ref2
            VMESH,2
!malha volume 3
            ESIZE,ref3
            VMESH,3
!malha volume 4
            SMRTSIZE,10
            VMESH,4

            FINISH                      !fim da fase de pré-processamento
!*****************************************************************

            SAVE
            /CLEAR
            PARRES,NEW,c:\ansys\parametros,
*ENDDO
```

Double pit

```
!ANSYS - Análise não linear de pites elipsoidais de corrosão
!arquivo de comandos para análise de pite elipsoidal duplo em modelo de 1/4 de tubo

!Pontifícia Universidade Católica do Paraná
!Programa de Pós-Graduação em Engenharia Mecânica
!Mecânica dos Sólidos Computacional
!Orientador: Dr. João Elias Abdalla Filho
!Doutorando: Ricardo J. Bertin
!ricardo.bertin@pucpr.br

!*****************************************************************
/CLEAR                                          !limpa e reinicia
/UIS,msgpop,3                                   !desabilita mensagens de erros

*ASK,DIRECTORY,'diretório - digitar nome entre 'aspas simples'',’XXIsemic'

MULTIPRO,'start',5
*CSET,1,3,DIAMETER,'diâmetro externo do duto em mm',300
*CSET,4,6,THICK,'espessura - parede do duto em mm',15
*CSET,7,9,DIST_BORDA,'dist.entre bordas pites, mm',0.1
*CSET,10,12,BOCA_PITE,'diâmetro do pite em mm',1
*CSET,13,15,prof_pite_1,'prof pite, mm',1
MULTIPRO,'end'

/MKDIR,c:\ansys\%DIRECTORY%\pre\%DIAMETER%      !cria diretório padrão
/CWD,c:\ansys\%DIRECTORY%\pre\%DIAMETER%        !muda para diretório padrão
PARSAV,all,c:\ansys\param01,

*DO,i,1,9,1
!************************entrada de dados************************
!define parâmetros
        raio_ext=DIAMETER/2000
        raio_int=raio_ext-(THICK/1000)
        comp=0.3
        PP1=0.1
        PP2=0.2
        PP3=0.3
        PP4=0.4
        PP5=0.5
        PP6=1
        PP7=2
        PP8=3
        PP9=4
        raio_pite=boca_pite/2000
        c_2=boca_pite
        dist_centros=(DIST_BORDA/1000)+2*raio_pite
        d=dist_centros*1000
!*********************************************************************
!*********define o título da análise e o nome do arquivo**********
        a=PP%i%
        /TITLE,**mouth=%c_2%mm depth=%a%mm dist=%d%mm**
        /FILENAME,pite_duplo_%DIAMETER%_%i%
!*********************************************************************

!**********calcula parâmetros do pite*******************************

        prof_pite=(PP%i%)/1000
        prof_pite01=prof_pite_1/1000
        ligament_1=raio_ext-prof_pite_1/1000
        razao_1=(2*prof_pite01)/(boca_pite/1000)
        *IF,prof_pite01,GT,prof_pite,THEN
                ligament_2=raio_ext-(prof_pite01+raio_pite)
                ligament_3=raio_ext-(prof_pite01+3*raio_pite)
                razao_2=(2*(prof_pite01+raio_pite))/(2*boca_pite/1000)
                razao_3=(2*(prof_pite01+3*raio_pite))/(4*boca_pite/1000)
        *ELSE
                ligament_2=raio_ext-(prof_pite+raio_pite)
```

```
                ligament_3=raio_ext-(prof_pite+3*raio_pite)
                razao_2=(2*(prof_pite+raio_pite))/(2*boca_pite/1000)
                razao_3=(2*(prof_pite+3*raio_pite))/(4*boca_pite/1000)
        *ENDIF
        ligament_4=raio_ext-prof_pite
        razao_4=(2*prof_pite)/(boca_pite/1000)
        raio_ext_2=raio_ext*raio_ext
        um_raio_pite_2=raio_pite*raio_pite
        dois_raio_pite_2=(2*raio_pite)*(2*raio_pite)
        quatro_raio_pite_2=(4*raio_pite)*(4*raio_pite)

!*********************************************************************

        /PREP7   !fase de preprocessamento

!**********carrega elemento e material**************************
        ET,1,solid187                           !elemento tetraédrico de 10 nós
        /COM,Internal UNITS set at file creation time = SI   (MKS)
        TBDEL,ALL,_MATL
        MPDEL,ALL,_MATL
        MPTEMP,R5.0, 1, 1,  25.0000000    ,
        MPDATA,R5.0, 1,EX  ,_MATL   , 1,  210000.000    ,
        MPTEMP,R5.0, 1, 1,  25.0000000    ,
        MPDATA,R5.0, 1,PRXY,_MATL   , 1, 0.300000000    ,
        TB,MISO,_MATL   ,   1,   8
        TBTEMP,  25.0000000    ,   1
        TBPT,,0.0023,483
        TBPT,,0.0100,483
        TBPT,,0.0500,536
        TBPT,,0.1000,559
        TBPT,,0.1500,573
        TBPT,,0.2000,584
        TBPT,,0.2500,592
        TBPT,,0.2900,597

!**********modelagem**********************************************

!REFINO 1 ------------------------------------------------------------------
        K,1,0,raio_int,0
        K,2,0,raio_ext,0
        K,3,0,ligament_1,0
        K,4,-raio_pite,(sqrt(raio_ext_2-um_raio_pite_2)),0
        K,5,0,ligament_2,0
        K,6,-2*raio_pite,(sqrt(raio_ext_2-dois_raio_pite_2)),0
        K,7,0,0,0
        K,8,0,0,-comp
        K,9,0,raio_ext,-dist_centros
        K,10,0,raio_ext,-(dist_centros+2*raio_pite)
        K,11,0,ligament_2,-(dist_centros+2*raio_pite)
        K,12,-2*raio_pite,(sqrt(raio_ext_2-dois_raio_pite_2)),-(dist_centros+2*raio_pite)
        K,13,0,raio_ext,-(dist_centros-raio_pite)
        K,14,0,ligament_4,-dist_centros
        WPLANE,,0,raio_ext,0,  -0.1,raio_ext,0,  0,0,0      !mudança de plano de trabalho
        CSWPLA,11,1,razao_1,1                                   !coordenadas cilíndricas
        L,3,4                                                   !linha 1 - pite 1
        CSWPLA,11,1,razao_2,1                                   !coordenadas cilíndricas
        L,5,6                                                   !linha 2
        L,11,12                                                 !linha 3
        WPLANE,,0,raio_ext,-dist_centros,0,raio_ext,0,0,0,-dist_centros        !mudança de plano de trabalho
        CSWPLA,11,1,razao_4,1                           !coordenadas cilíndricas
        L,13,14                                         !linha 4 - pite 2
        WPLANE,,0,0,0,0.1,0,0,0,raio_ext,0      !plano de trabalho default
        CSYS,0                                          !coordenadas cartesianas
        AROTAT,1,,,,,,3,1,90,1                          !linhas 5 e 6 e superfície 1
        AROTAT,4,,,,,,9,14,180,1                !linhas 7 e 8 e superfície 2
        L,3,5                                           !linha 9
        L,4,6                                           !linha 10
        L,5,11                                          !linha 11
        L,6,12                                          !linha 12
        L,10,11                                         !linha 13
        L,10,12                                         !linha 14
        L,13,15                                         !linha 15
        L,10,16                                         !linha 16
        AL,1,9,2,10                                     !área 3
```

```
AL,6,10,12,14,16,8,15                          !área 4
AL,5,9,11,13,16,7,4,15                         !área 5
AL,2,12,3,11                                   !área 6
AL,13,3,14                                     !área 7
VA,1,2,3,4,5,6,7                    !volume 1
!-------------------------------------------------------------------------------

!REFINO 2A ------------------------------------------------------------
K,17,0,ligament_3,0
K,18,-4*raio_pite,(sqrt(raio_ext_2-quatro_raio_pite_2)),0
K,19,0,ligament_3,-(dist_centros+2*raio_pite)
K,20,-4*raio_pite,(sqrt(raio_ext_2-quatro_raio_pite_2)),-(dist_centros+2*raio_pite)
WPLANE,,0,raio_ext,0,-0.1,raio_ext,0,0,0,0     !mudança do plano de trabalho
CSWPLA,11,1,razao_3,1                          !coordenadas cilíndricas
L,17,18                                        !linha 17
L,19,20                                        !linha 18
WPLANE,,0,0,0,0.1,0,0,0,raio_ext,0             !plano de trabalho default
CSYS,0                                         !coordenadas cartesianas
L,17,19                                        !linha 19
L,18,20                                        !linha 20
L,5,17                                         !linha 21
L,6,18                                         !linha 22
L,11,19                                        !linha 23
L,12,20                                        !linha 24
AL,21,17,22,2                                  !área 8
AL,21,19,23,11                                 !área 9
AL,22,12,24,20                                 !área 10
AL,23,18,24,3                                  !área 11
AL,19,17,20,18                                 !área 12
VA,6,8,9,10,11,12                              !volume 2
!-------------------------------------------------------------------------------

!REFINO 2B ------------------------------------------------------------
K,21,-4*raio_pite,(sqrt(raio_ext_2-quatro_raio_pite_2)),-(dist_centros+4*raio_pite)
K,22,0,ligament_3,-(dist_centros+4*raio_pite)
K,23,-2*raio_pite,(sqrt(raio_ext_2-dois_raio_pite_2)),-(dist_centros+4*raio_pite)
K,24,0,ligament_2,-(dist_centros+4*raio_pite)
k,25,0,raio_ext,-(dist_centros+4*raio_pite)
WPLANE,,0,raio_ext,0,-0.1,raio_ext,0,0,0,0     !mudança do plano de trabalho
CSWPLA,11,1,razao_3,1                          !coordenadas cilíndricas
L,21,22                                        !linha 25
WPLANE,,0,0,0,0.1,0,0,0,raio_ext,0             !plano de trabalho default
CSYS,0                                         !coordenadas cartesianas
L,20,21                                        !linha 26
L,19,22                                        !linha 27
L,10,25                                        !linha 28
L,25,23                                        !linha 29
L,23,21                                        !linha 30
L,25,24                                        !linha 31
L,24,22                                        !linha 32
L,12,23                                        !linha 33
L,11,24                                        !linha 34
AL,14,33,29,28                                 !área 13
AL,33,24,26,30                                 !área 14
AL,13,34,31,28                                 !área 15
AL,23,27,32,34                                 !área 16
AL,27,25,26,18                                 !área 17
AL,29,30,25,32,31                              !área 18
VA,7,11,13,14,15,16,17,18                      !volume 3
!---------------------------------------------------------------

!REFINO 3 ------------------------------------------------------------
K,26,-raio_ext,0,0
K,27,-raio_int,0,0
K,28,-raio_ext,0,-comp
K,29,-raio_int,0,-comp
K,30,0,raio_int,-comp
K,31,0,raio_ext,-comp
LARC,26,18,7,raio_ext                          !linha 35
LARC,27,1,7,raio_int                           !linha 36
LARC,28,31,8,raio_ext                          !linha 37
LARC,29,30,8,raio_int                          !linha 38
L,26,27                                        !linha 39
L,27,29                                        !linha 40
```

```
        L,29,28                                 !linha 41
        L,28,26                                 !linha 42
        L,17,1                                  !linha 43
        L,1,30                                  !linha 44
        L,30,31                                 !linha 45
        L,31,25                                 !linha 46
        AL,39,40,41,42                          !área 19
        AL,43,44,45,46,31,32,27,19              !área 20
        AL,36,39,35,17,43                       !área 21
        AL,38,41,37,45                          !área 22
        AL,36,40,38,44                          !área 23
        CSWPLA,12,1                             !coordenadas cilíndricas
        AL,35,42,37,46,29,30,26,20              !área 24
        CSYS,0                                  !coordenadas cartesianas
        VA,19,20,21,22,23,24,12,17,18           !volume 4
!-----------------------------------------------------------------

        VADD,2,3                                !soma volumes 2 e 3 = 5

!geração da malha
!malha volume 1
        ESIZE,0.00015                           !tamanho do elemento no refino 1
        VMESH,1                                 !geração da malha 1
!malha volume 5
        ESIZE,0.0005                            !tamanho do elemento no refino 2
        VMESH,5                                 !geração da malha 2
!malha volume 4
        ESIZE,0.005                             !tamanho do elemento no refino 3
        VMESH,4                                 !geração da malha 3

        FINISH                                  !fim da fase de pré-processamento
!*****************************************************************

        SAVE
/CLEAR
PARRES,NEW,c:\ansys\param01,
*ENDDO
```

APPENDIX B – ANSYS script for solver

Single pit

```
!ANSYS - Análise não linear de pites elipsoidais de corrosão
!arquivo de comandos para análise de pite elipsoidal em modelo de 1/4 de tubo

!Pontifícia Universidade Católica do Paraná
!Programa de Pós-Graduação em Engenharia Mecânica
!Mecânica dos Sólidos Computacional
!Orientador: Dr. João Elias Abdalla Filho
!Doutorando: Ricardo J. Bertin
!ricardo.bertin@pucpr.br

!*****************************************************************
/CLEAR                  !limpa e reinicia
/UIS,msgpop,3           !desabilita mensagens de erros
finish

*ASK,DIRECTORY,'diretório - digitar nome entre 'aspas simples'','A187'
MULTIPRO,'start',2
*CSET,1,3,DIAMETER,'diâmetro externo do duto em mm',323.8
*CSET,4,6,THICK,'espessura - parede do duto em mm',12.7
MULTIPRO,'end'

/MKDIR,d:\ansys\%DIRECTORY%\solve\%DIAMETER%\%THICK%\auxiliar\          !cria diretório auxiliar

!*****************************************************************

*DO,i,1,12,1

    /CWD,d:\ansys\%DIRECTORY%\pre\%DIAMETER%\%THICK%\      !troca diretório para ler arq preprocessamento
    resume,RJB_%DIAMETER%_%THICK%_%i%,db                  !lê arq preprocessamento

    *DO,PI,5,25,5
        /CWD,d:\ansys\%DIRECTORY%\solve\%DIAMETER%\%THICK%\auxiliar\      !troca diretório para gravar arqs solução
        /FILENAME,RJB_%DIAMETER%_%THICK%_%i%                             !nome do arquivo

        !fase de solução
        /solution
        antype,static,new   !nova solução estática

        solcontrol,on       !ativa controle de solução
        autots,on
        nsubst,20,1000,1    !20 passos de carga, 1000 iterações max, 1 iteração min
        outres,all,all      !grava todos os passos de carga
        nlgeom,on           !ativa grandes deformações
        lnsrch,on
        neqit,1000

        da,4,uz             !restrição translação em z na área 4
        da,5,uz             !restrição translação em z na área 5
        da,6,uz             !restrição translação em z na área 6
        da,7,uz             !restrição translação em z na área 7
        da,8,uy             !restrição translação em Y na área 8
        da,16,uy            !restrição translação em Y na área 16
        da,9,ux             !restrição translação em x na área 9
        da,10,ux            !restrição translação em x na área 10
        da,11,ux            !restrição translação em x na área 11
        da,17,ux            !restrição translação em x na área 17
        sfa,12,1,pres,PI    !pressão aplicada na área 12
        sfa,19,1,pres,PI    !pressão aplicada na área 19

        solve               !solucionar

        finish              !finaliza fase de solução

        /MKDIR,d:\ansys\%DIRECTORY%\solve\%DIAMETER%\%THICK%\%PI%\      !cria diretório para cada pressão
        /CWD,d:\ansys\%DIRECTORY%\solve\%DIAMETER%\%THICK%\%PI%\        !troca diretório para gravar resultado
        SAVE                                                           !grava resultado
    *ENDDO
*ENDDO
```

Double pit

```
!ANSYS - Análise não linear de pites elipsoidais de corrosão
!arquivo de comandos para análise de pite elipsoidal duplo em modelo de 1/4 de tubo

!Pontifícia Universidade Católica do Paraná
!Programa de Pós-Graduação em Engenharia Mecânica
!Mecânica dos Sólidos Computacional
!Orientador: Dr. João Elias Abdalla Filho
!Doutorando: Ricardo J. Bertin
!ricardo.bertin@pucpr.br

!*****************************************************************
/CLEAR                  !limpa e reinicia
/UIS,msgpop,3           !desabilita mensagens de erros
finish

*ASK,DIRECTORY,'diretório - digitar nome entre 'aspas simples'','XXIsemic'
MULTIPRO,'start',2
*CSET,1,3,DIAMETER,'diâmetro externo do duto em mm',300
*CSET,4,6,THICK,'espessura - parede do duto em mm',15
MULTIPRO,'end'

/MKDIR,c:\ansys\%DIRECTORY%\solve\%DIAMETER%\auxiliar\      !cria diretório auxiliar
/MKDIR,c:\ansys\%DIRECTORY%\solve\%DIAMETER%\               !cria diretório para solução

!*********************************************************************

*DO,i,1,9,1

    /CWD,c:\ansys\%DIRECTORY%\pre\%DIAMETER%     !troca diretório para ler arq preprocessamento
    resume,pite_duplo_%DIAMETER%_%i%,db          !lê arq preprocessamento

!************************entrada de dados************************
!define parâmetros
    *IF,DIAMETER,EQ,300,THEN
        PF1=25
        PF2=25
        PF3=25
        PF4=25
        PF5=25
        PF6=25
        PF7=25
        PF8=25
        PF9=25
    *ELSEIF,DIAMETER,EQ,400,THEN
        PF1=25
        PF2=25
        PF3=25
        PF4=25
        PF5=25
        PF6=25
        PF7=25
        PF8=25
        PF9=25
    *ELSE
        PF1=25
        PF2=25
        PF3=25
        PF4=25
        PF5=25
        PF6=25
        PF7=25
        PF8=25
        PF9=25
    *ENDIF
!*********************************************************************
    PF=PF%i%
    /CWD,c:\ansys\%DIRECTORY%\solve\%DIAMETER%\auxiliar\     !troca diretório para gravar arqs solução
    /FILENAME,pite_duplo_%DIAMETER%_%i%                     !nome do arquivo

!fase de solução
    /solution
```

```
antype,static,new          !nova solução estática

solcontrol,on              !ativa controle de solução
autots,on
nsubst,20,1000,1           !20 passos de carga, 1000 iterações max, 1 iteração min
outres,all,all             !grava todos os passos de carga
nlgeom,on                  !ativa grandes deformações
lnsrch,on                  !ativa algoritmo Newton-Raphson
neqit,1000                 !número de iterações

da,3,uz                    !restrição translação em z na área 3
da,8,uz                    !restrição translação em z na área 8
da,21,uz                   !restrição translação em z na área 21
da,22,uz                   !restrição translação em z na área 22
da,19,uy                   !restrição translação em Y na área 19
da,5,ux                    !restrição translação em x na área 5
da,15,ux                   !restrição translação em x na área 15
da,9,ux                    !restrição translação em x na área 9
da,16,ux                   !restrição translação em x na área 16
da,20,ux                   !restrição translação em x na área 20
sfa,23,1,pres,PF           !pressão aplicada na área 23


solve                      !solucionar

finish                     !finaliza fase de solução

/CWD,c:\ansys\%DIRECTORY%\solve\%DIAMETER%\     !troca diretório para gravar resultado
SAVE                                           !grava resultado

*ENDDO
```

APPENDIX C – ANSYS script for post processing

Single Pit

```
!ANSYS - Análise não linear de pites elipsoidais de corrosao
!arquivo de comandos para análise de pite elipsoidal em modelo de 1/4 de tubo

!Pontifícia Universidade Católica do Paraná
!Programa de Pós-Graduação em Engenharia Mecânica
!Mecânica dos Sólidos Computacional
!Orientador: Dr. João Elias Abdalla Filho
!Doutorando: Ricardo J. Bertin
!ricardo.bertin@pucpr.br

!*****************************************************************
/CLEAR                                                  !limpa e reinicia
/UIS,msgpop,3                                           !desabilita mensagens de erros
finish

*ASK,DIRECTORY,'diretório - digitar nome entre 'aspas simples'','A187'
MULTIPRO,'start',2
*CSET,1,3,DIAMETER,'diâmetro externo do duto em mm',323.8
*CSET,4,6,THICK,'espessura - parede do duto em mm',12.7
MULTIPRO,'end'

!************************entrada de dados************************

*DO,PI,5,25,5
        /MKDIR,d:\ansys\%DIRECTORY%\pos\%DIAMETER%\%THICK%\%PI%\result\
        /MKDIR,d:\ansys\%DIRECTORY%\pos\%DIAMETER%\%THICK%\%PI%\
        *DO,i,1,12,1
                /CWD,d:\ansys\%DIRECTORY%\solve\%DIAMETER%\%THICK%\%PI%\        !troca diretório
                resume,RJB_%DIAMETER%_%THICK%_%i%,db                    !abre arquivo da fase de solução
                /FILENAME,RJB_%DIAMETER%_%THICK%_%i%                    !nome do arquivo

!****** fase de posprocessamento *********************************
                /post1

                /CWD,d:\ansys\%DIRECTORY%\pos\%DIAMETER%\%THICK%\%PI%\result\
                /output,RJB_%DIAMETER%_%THICK%_%i%,lis
                prnsol,s,prin
                /output

                finish
!*****************************************************************

                /CWD,d:\ansys\%DIRECTORY%\pos\%DIAMETER%\%THICK%\%PI%\
                SAVE
        *ENDDO
*ENDDO
```

Double pit

```
!ANSYS - Análise não linear de pites elipsoidais de corrosao
!arquivo de comandos para análise de pite elipsoidal duplo em modelo de 1/4 de tubo

!Pontifícia Universidade Católica do Paraná
!Programa de Pós-Graduação em Engenharia Mecânica
!Mecânica dos Sólidos Computacional
!Orientador: Dr. João Elias Abdalla Filho
!Doutorando: Ricardo J. Bertin
!ricardo.bertin@pucpr.br

!*****************************************************************
/CLEAR                                                  !limpa e reinicia
/UIS,msgpop,3                                           !desabilita mensagens de erros
finish

*ASK,DIRECTORY,'diretório - digitar nome entre 'aspas simples'','XXIsemic'
MULTIPRO,'start',2
*CSET,1,3,DIAMETER,'diâmetro externo do duto em mm',300
*CSET,4,6,THICK,'espessura - parede do duto em mm',15
MULTIPRO,'end'

/MKDIR,c:\ansys\%DIRECTORY%\pos\%DIAMETER%\result\      !cria diretório auxiliar
/MKDIR,c:\ansys\%DIRECTORY%\pos\%DIAMETER%\             !cria diretório para solução

!************************entrada de dados************************

*DO,i,1,9,1

        /CWD,c:\ansys\%DIRECTORY%\solve\%DIAMETER%\             !troca diretório
        resume,pite_duplo_%DIAMETER%_%i%,db                    !abre arquivo da fase de solução
        /FILENAME,pite_duplo_%DIAMETER%_%i%                    !nome do arquivo

!****** fase de posprocessamento ******************************
        /post1

        /CWD,c:\ansys\%DIRECTORY%\pos\%DIAMETER%\result\
        /output,pite_duplo_%DIAMETER%_%i%,lis
        prnsol,s,prin
        /output

        finish
!*****************************************************************

        /CWD,c:\ansys\%DIRECTORY%\pos\%DIAMETER%\
        SAVE

*ENDDO
```

APPENDIX D – intersection of two curved surfaces

An interesting problem arises when there is the intersection of two curved surfaces, a cylindrical and a spherical one, in ANSYS®.

Figure 42 – Intersection of a cylinder and a sphere

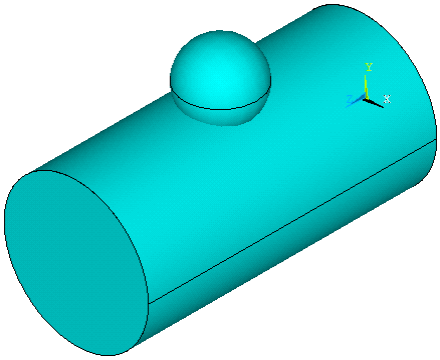

SOURCE: Bertin, 2013

The contour of the touching external surfaces of both solids would be described by the following equation:

$$x^2 + y^2 - {R_{cyl}}^2 = x^2 + y^2 + z^2 - {R_{sph}}^2 \quad (115)$$

where:

x,y,z : cartesian coordinates alogn axes X, Y and Z

R_{cyl} : radius of the cylinder

R_{sph} : radius of the sphere

In parametric terms the geometric place of the points pertaining both to the cylinder, with base on plane XY, longitudinal axis along axis Z and radius *R*, and the sphere, with center along Y axis and radius *r*, is described by the following equations:

$$x = \sqrt{{R_{cyl}}^2 - y^2}$$
$$y = \frac{2{R_{cyl}}^2 + z^2 - {R_{sph}}^2}{2R_{cyl}} \quad (116)$$
$$z = R_{sph} cos\phi$$

where:

x, y, z : are cartesian coordinates on axes X, Y and Z

R_{cyl} : radius of the cylinder

R_{sph} : radius of the sphere

ϕ : angle that describes a circumference on the face of the cylinder

If implemented this contour curve would create an area on the top of the refinement volume that would need to follow three curves, line 1 along the cylindrical surface, lines 2 and 3 described by the parametric equations and line 4, a straight line along the edge of the quarter cylinder (see Figure 28). Several attempts were made but every time a geometry error arises. Therefore, on the actual model lines 1, 2, 3 and 4 follows a horizontal plane parallel to the XZ plane (Figure 43).

Figure 43 – First volume of refinement showing the lines of top surface.

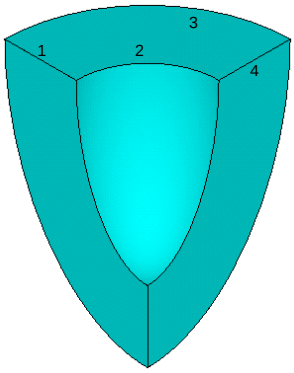

SOURCE: Bertin, 2013

The error *e* introduced by considering line 1 straight and not curved is small for a 300 mm diameter pipe. The problem can be schematically represented as on Figure 44:

Figure 44 – Error introduced when intersection of two curved surfaces is considered plane

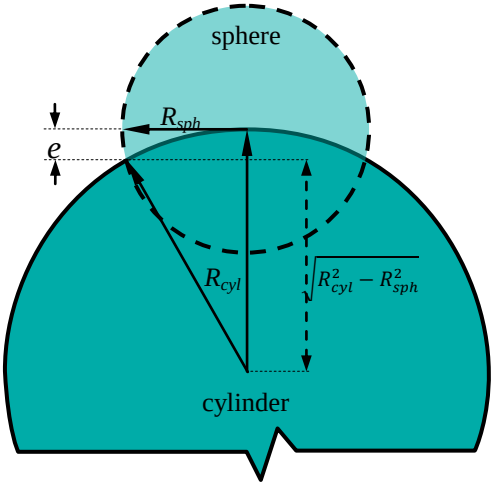

SOURCE: Bertin, 2013

The formulation for the error is:

$$e = R_{cyl} - \sqrt{{R_{cyl}}^2 - {R_{sph}}^2} \tag{117}$$

And for the smallest diameter used, 300 mm, and pit corrosion diameter of 1 mm, the error is 8.33×10^{-4} mm or 0,083%, considered negligible.

APPENDIX E – summary of the formulations of the various corrosion defects assessment methods

Table 25 – Summary of formulations of the various corrosion defects assessment methods

Method	Failure Pressure	Bulging Factor
AGA – NG 18	$P_f = \sigma_{\text{flow}} \frac{2\text{t}}{\text{D}} \left(\frac{1 - \frac{\text{d}_{\max}}{\text{t}}}{1 - \frac{\text{d}_{\max}}{\text{t}} \frac{1}{\text{M}}} \right)$	$\text{M} = \sqrt{1 + 0.6275 \left(\frac{\text{L}}{\sqrt{\text{Dt}}} \right)^2 - 0.003375 \left(\frac{\text{L}}{\sqrt{\text{Dt}}} \right)^4}$
ASME B31G	$P_f = S \times 1.1\sigma_{y_{spec}} \frac{2\text{t}}{\text{D}} \left(\frac{1 - \frac{2}{3} \frac{d_{max}}{t}}{1 - \frac{2}{3} \frac{d_{max}}{t} \frac{1}{M}} \right)$	$M = \sqrt{1 + 0.8 \left(\frac{L}{\sqrt{\text{Dt}}} \right)^2}$
Modified ASME B31G	$P_f = \sigma_{\text{flow}} \frac{2\text{t}}{\text{D}} \left(\frac{1 - 0.85 \frac{d_{max}}{t}}{1 - 0.85 \frac{d_{max}}{t} \frac{1}{M}} \right)$	$M = \sqrt{1 + 0.6275 \left(\frac{L}{\sqrt{Dt}} \right)^2 - 0.003375 \left(\frac{L}{\sqrt{Dt}} \right)^4}$
RPA Method	$P_f = \sigma_{\text{flow}} \frac{2\text{t}}{\text{D}} \left(\frac{1 - k \frac{d_{max}}{t}}{1 - k \frac{d_{max}}{t} \frac{1}{M}} \right)$	$M = 2.1 + 0.07 \frac{\text{L}^2}{\text{Dt}}$
RSTRENG	$P_f = \sigma_{\text{flow}} \frac{2\text{t}}{\text{D}} \left(\frac{1 - \frac{\text{d}_{\max}}{\text{t}}}{1 - \frac{\text{d}_{\max}}{\text{t}} \frac{1}{\text{M}}} \right)$	$\text{M} = \sqrt{1 + 0.6275 \left(\frac{\text{L}}{\sqrt{\text{Dt}}} \right)^2 - 0.003375 \left(\frac{\text{L}}{\sqrt{\text{Dt}}} \right)^4}$
DNV RP-F101	$P_f = 1.05 \times \sigma_u \frac{2t}{D - t} \left(\frac{1 - \frac{d_{max}}{\text{t}}}{1 - \frac{d_{max}}{\text{t}} \frac{1}{M}} \right)$	$M = \sqrt{1 + 0.31 \left(\frac{\text{L}}{\sqrt{\text{Dt}}} \right)^2}$
PCORR	$P_f = \sigma_{\text{u}} \frac{2t}{D} \left(1 - \left(\frac{\text{d}_{\max}}{\text{t}} \right) \left(1 - \exp \left(-0.157 \frac{\text{L}}{\sqrt{\text{R}(\text{t} - \text{d}_{\max})}} \right) \right) \right)$	
WDD	$P_{Long\ Groove} = \frac{\sigma_{\text{crit}}}{R_0 \sqrt{\frac{3}{4}}} t_{\text{L0}} \exp \left(-\sqrt{\frac{3}{4}} \varepsilon_{\text{crit}} \right)$	
Choi et al	$P_f = 0.9\sigma_u \frac{2t}{D} \left[C_2 \left(\frac{1}{\sqrt{Rt}} \right)^2 + C_1 \left(\frac{1}{\sqrt{Rt}} \right) + C_0 \right]$	

SOURCE: Bertin, 2013

APPENDIX G – Pictures of first principal stress distribution inside the pit

Figure 45 – Maximum stress inside the pit for pipe diameter of 300 mm and internal pressure of 5 MPa

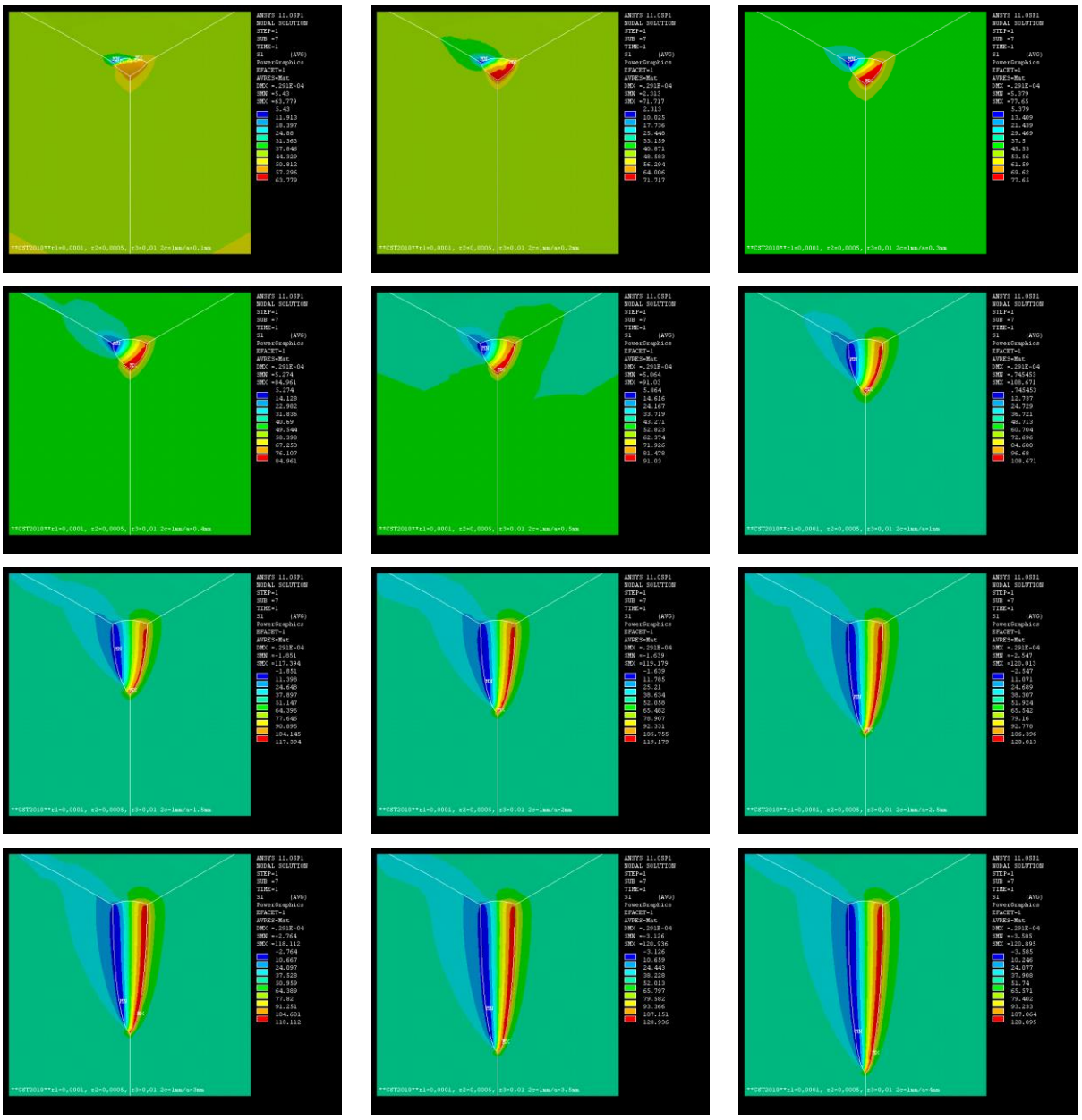

SOURCE: Bertin, 2013

From top to bottom and left to right pits with depths, respectively equal to: 0.1, 0.2, 0.3, 0.4, 0.5, 1.0, 1.5, 2.0, 2.5, 3.0, 3.5 and 4.0 mm.

Figure 46 – Maximum stress inside the pit for pipe diameter of 300 mm and internal pressure of 10 MPa

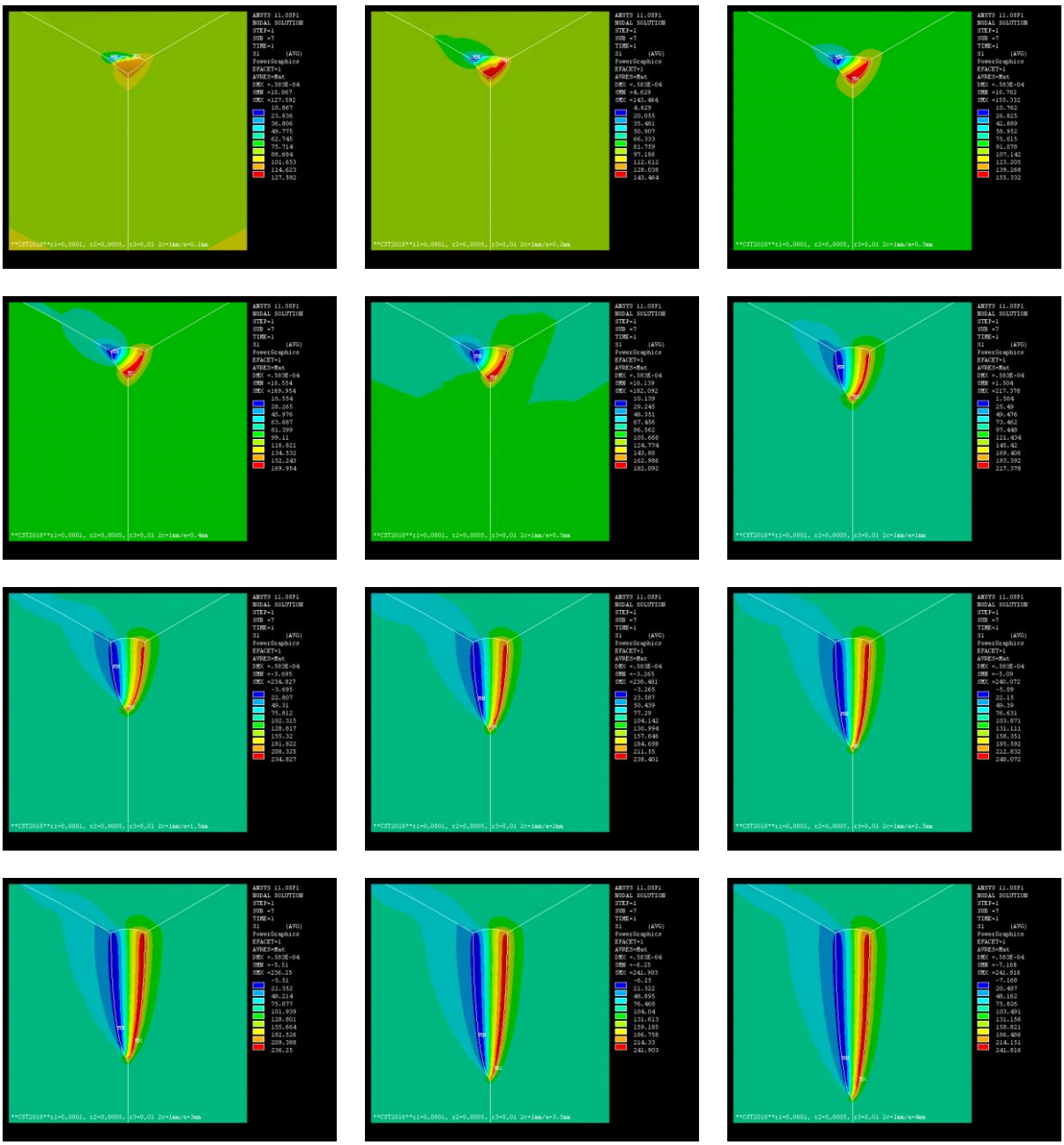

SOURCE: Bertin, 2013

From top to bottom and left to right pits with depths, respectively equal to: 0.1, 0.2, 0.3, 0.4, 0.5, 1.0, 1.5, 2.0, 2.5, 3.0, 3.5 and 4.0 mm.

Figure 47 – Maximum stress inside the pit for pipe diameter of 300 mm and internal pressure of 15 MPa

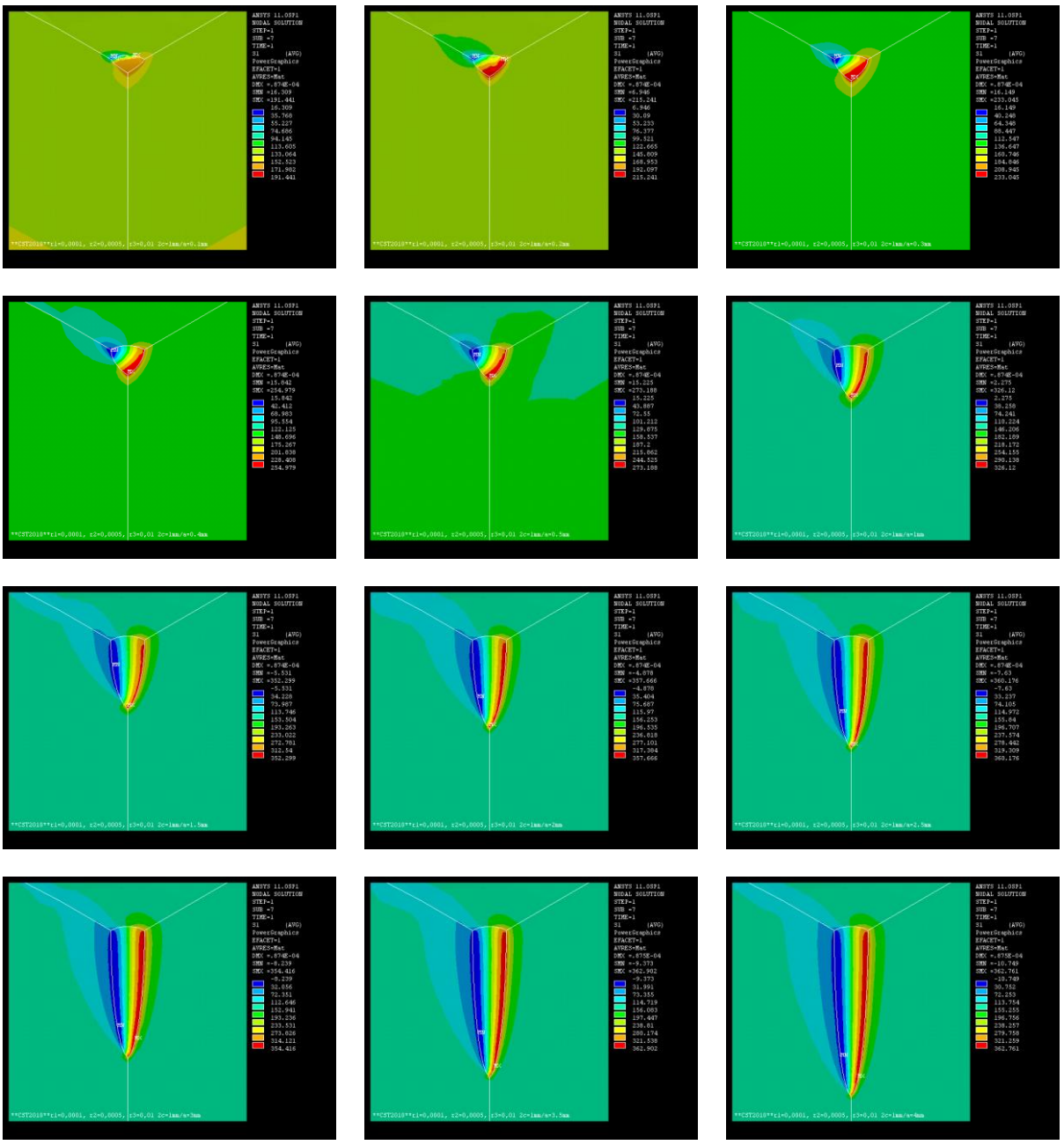

SOURCE: Bertin, 2013

From top to bottom and left to right pits with depths, respectively equal to: 0.1, 0.2, 0.3, 0.4, 0.5, 1.0, 1.5, 2.0, 2.5, 3.0, 3.5 and 4.0 mm.

Figure 48 – Maximum stress inside the pit for pipe diameter of 300 mm and internal pressure of 20 MPa

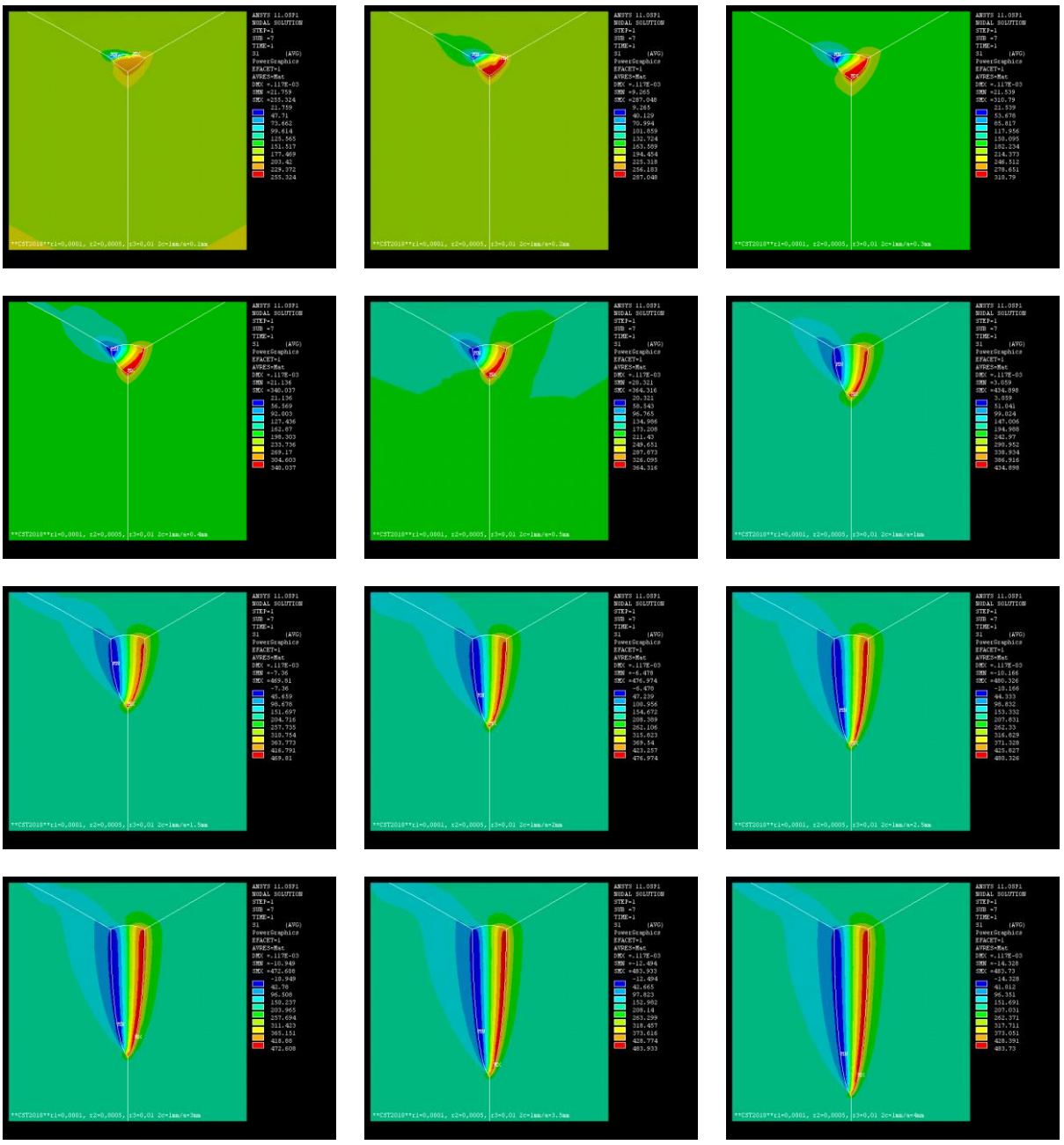

SOURCE: Bertin, 2013

From top to bottom and left to right pits with depths, respectively equal to: 0.1, 0.2, 0.3, 0.4, 0.5, 1.0, 1.5, 2.0, 2.5, 3.0, 3.5 and 4.0 mm.

Figure 49 – Maximum stress inside the pit for pipe diameter of 300 mm and internal pressure of 25 MPa

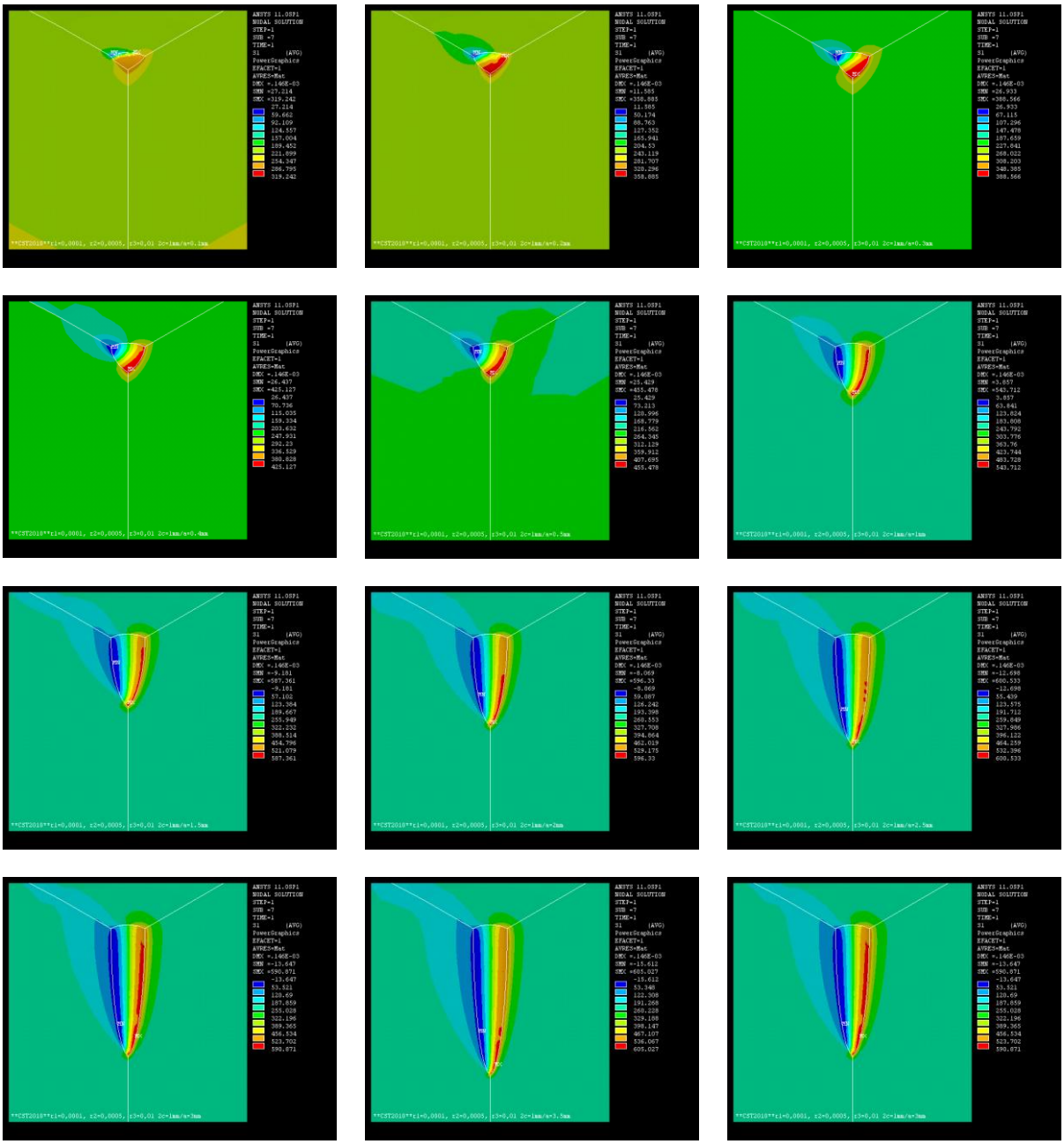

SOURCE: Bertin, 2013

From top to bottom and left to right pits with depths, respectively equal to: 0.1, 0.2, 0.3, 0.4, 0.5, 1.0, 1.5, 2.0, 2.5, 3.0, 3.5 and 4.0 mm.

Figure 50 – Maximum stress inside the pit for pipe diameter of 400 mm and internal pressure of 5 MPa

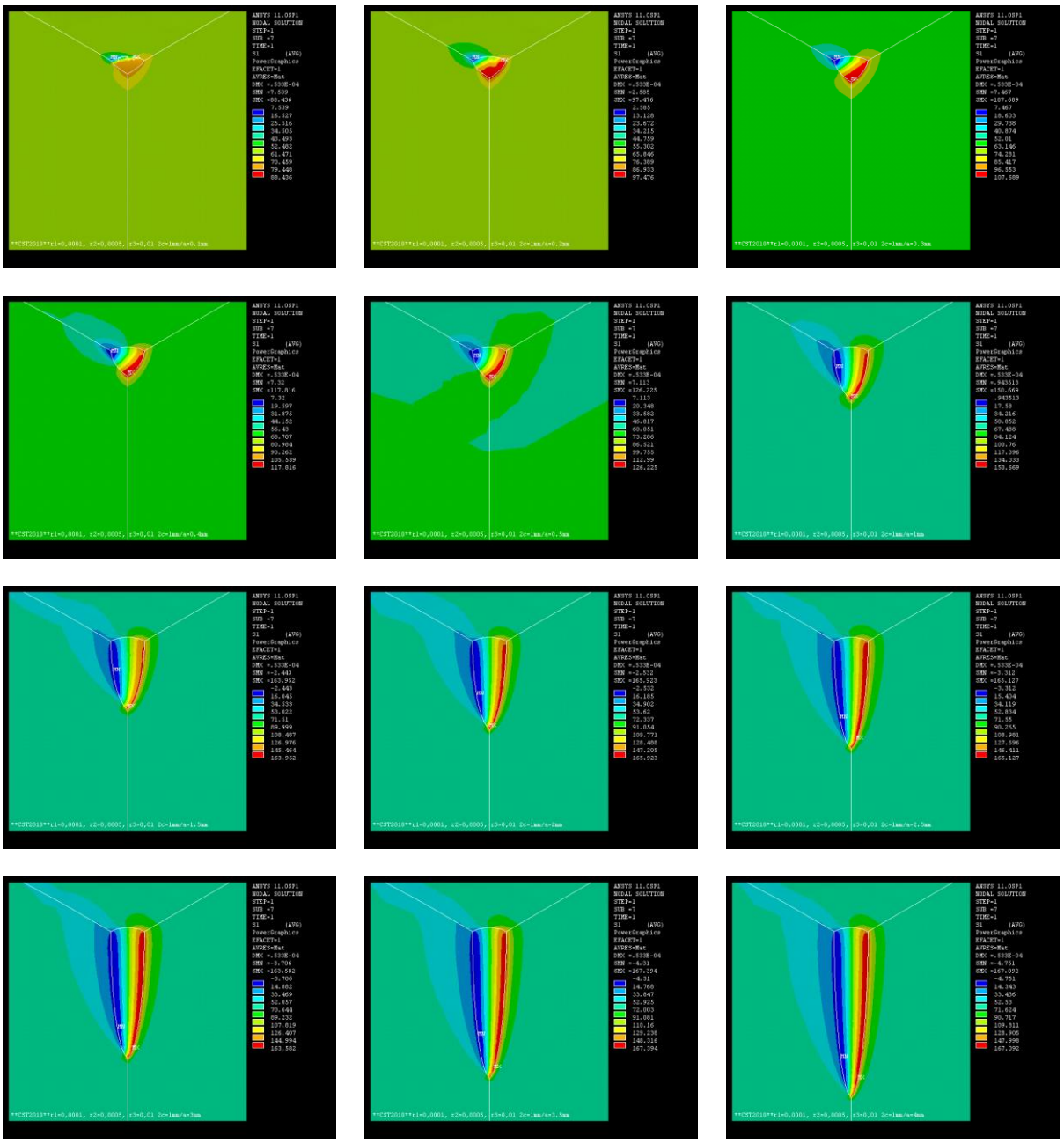

SOURCE: Bertin, 2013

From top to bottom and left to right pits with depths, respectively equal to: 0.1, 0.2, 0.3, 0.4, 0.5, 1.0, 1.5, 2.0, 2.5, 3.0, 3.5 and 4.0 mm.

Figure 51 – Maximum stress inside the pit for pipe diameter of 400 mm and internal pressure of 10 MPa

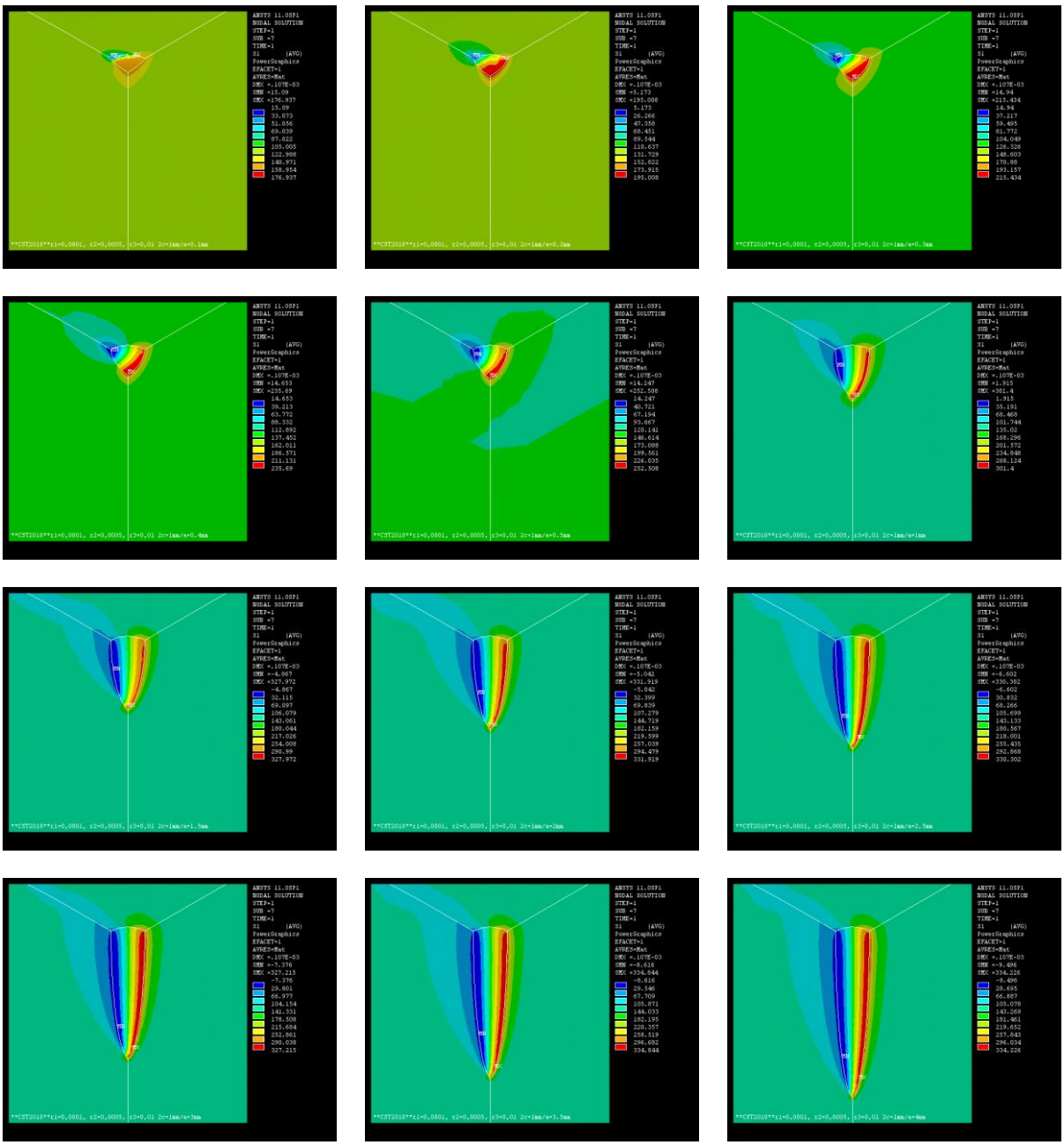

SOURCE: Bertin, 2013

From top to bottom and left to right pits with depths, respectively equal to: 0.1, 0.2, 0.3, 0.4, 0.5, 1.0, 1.5, 2.0, 2.5, 3.0, 3.5 and 4.0 mm.

Figure 52 – Maximum stress inside the pit for pipe diameter of 400 mm and internal pressure of 15 MPa

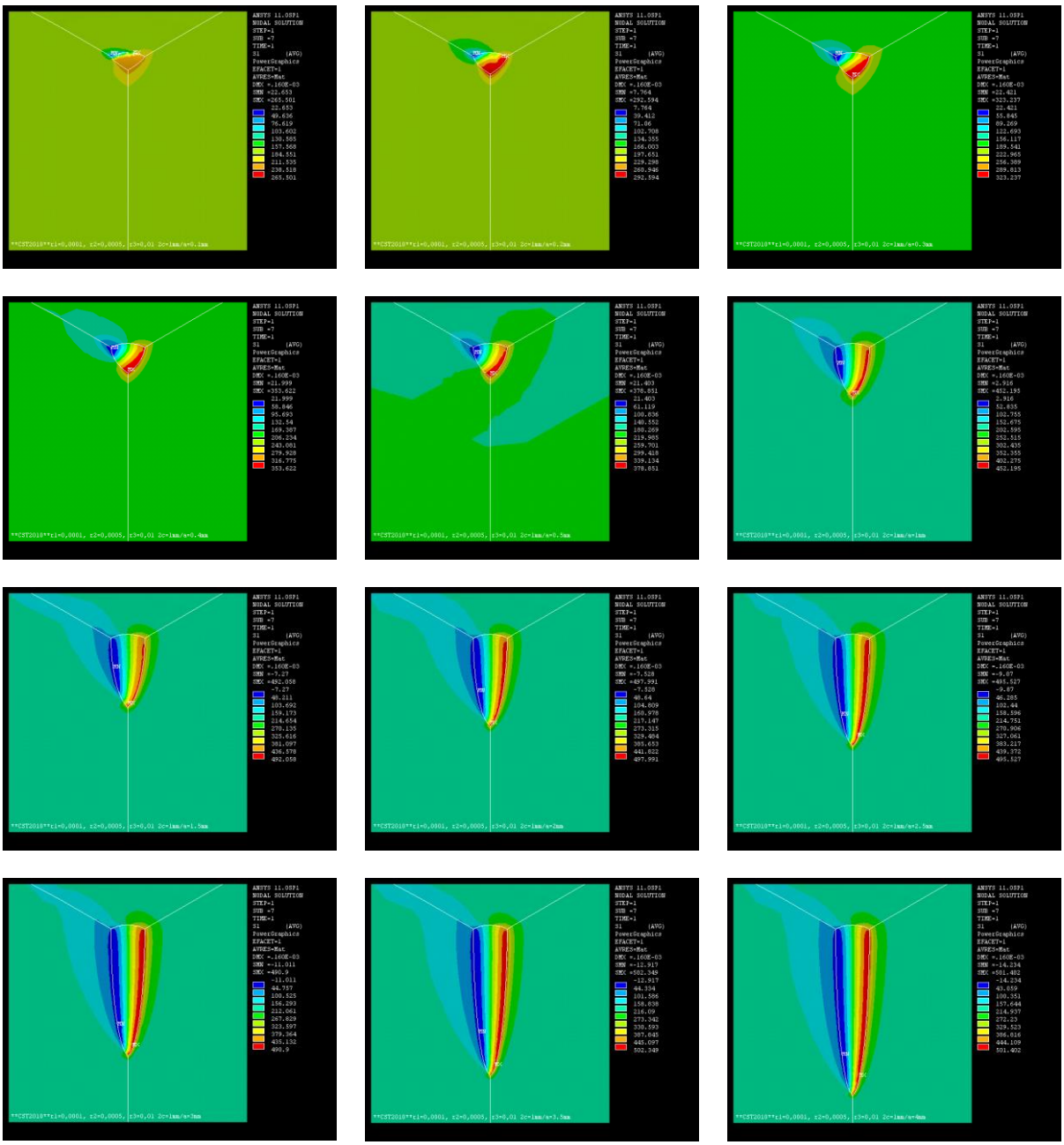

SOURCE: Bertin, 2013

From top to bottom and left to right pits with depths, respectively equal to: 0.1, 0.2, 0.3, 0.4, 0.5, 1.0, 1.5, 2.0, 2.5, 3.0, 3.5 and 4.0 mm.

Figure 53 – Maximum stress inside the pit for pipe diameter of 400 mm and internal pressure of 20 MPa

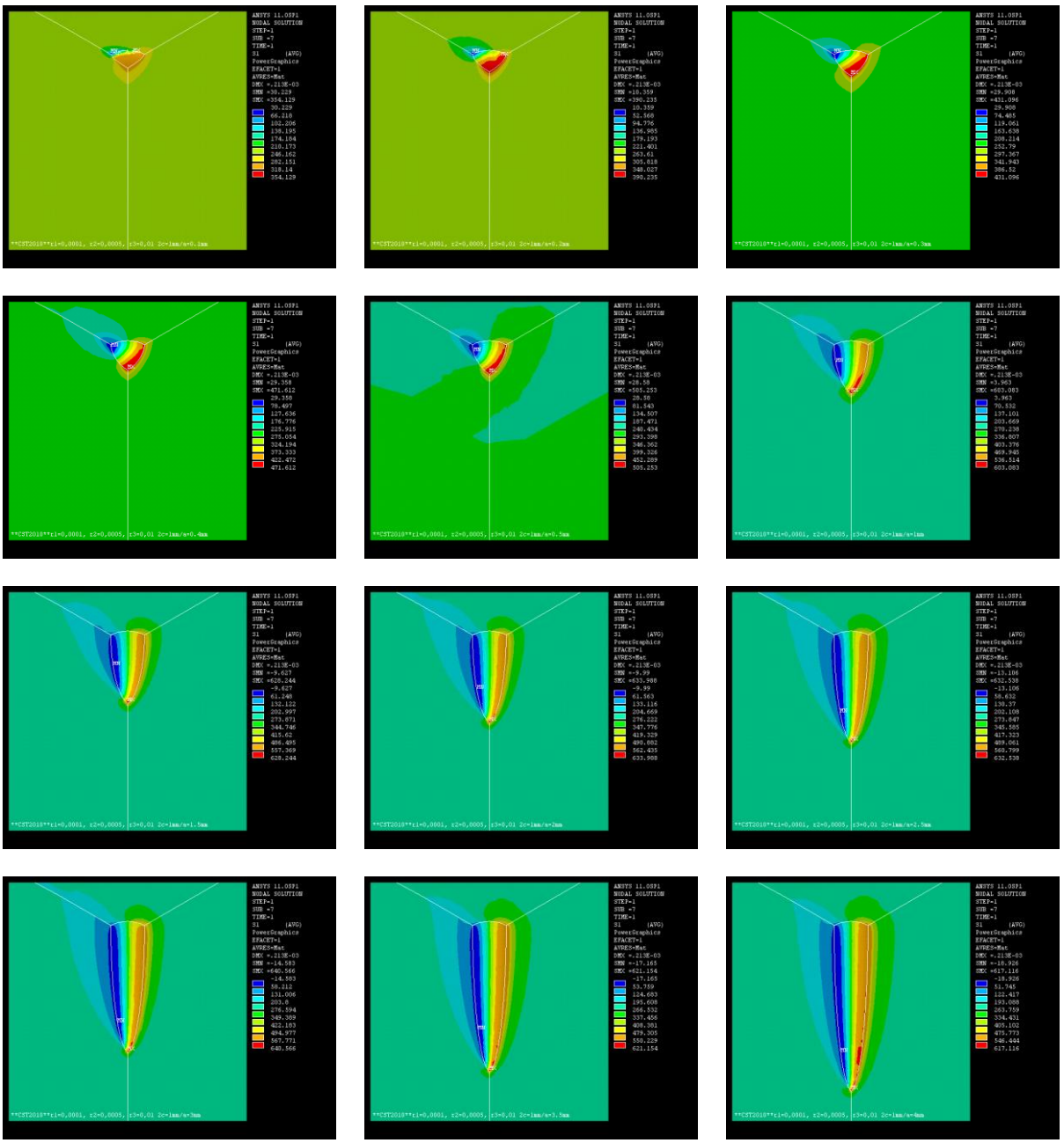

SOURCE: Bertin, 2013

From top to bottom and left to right pits with depths, respectively equal to: 0.1, 0.2, 0.3, 0.4, 0.5, 1.0, 1.5, 2.0, 2.5, 3.0, 3.5 and 4.0 mm.

Figure 54 – Maximum stress inside the pit for pipe diameter of 400 mm and internal pressure of 25 MPa

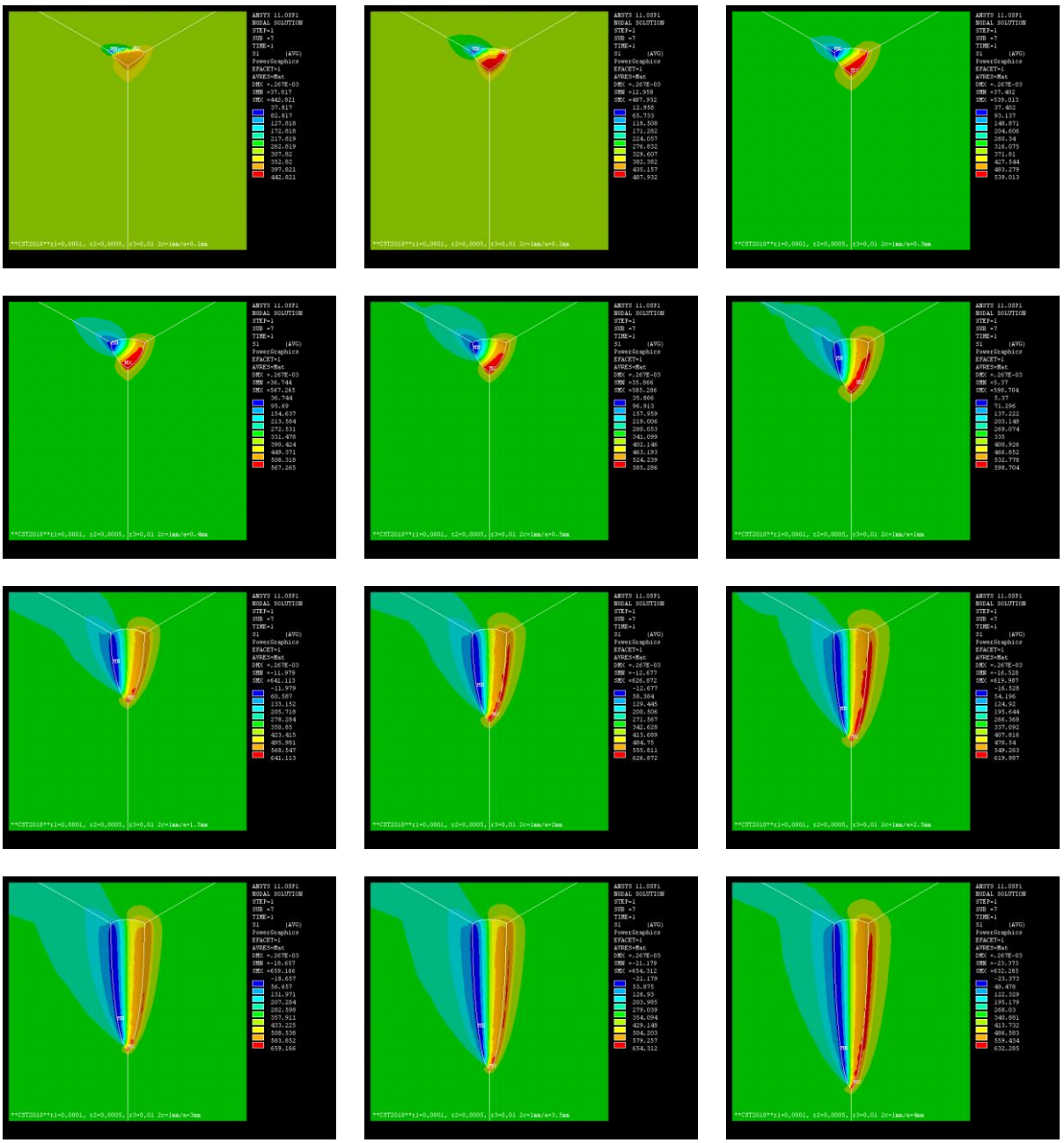

SOURCE: Bertin, 2013

From top to bottom and left to right pits with depths, respectively equal to: 0.1, 0.2, 0.3, 0.4, 0.5, 1.0, 1.5, 2.0, 2.5, 3.0, 3.5 and 4.0 mm.

Figure 55 – Maximum stress inside the pit for pipe diameter of 500 mm and internal pressure of 5 MPa

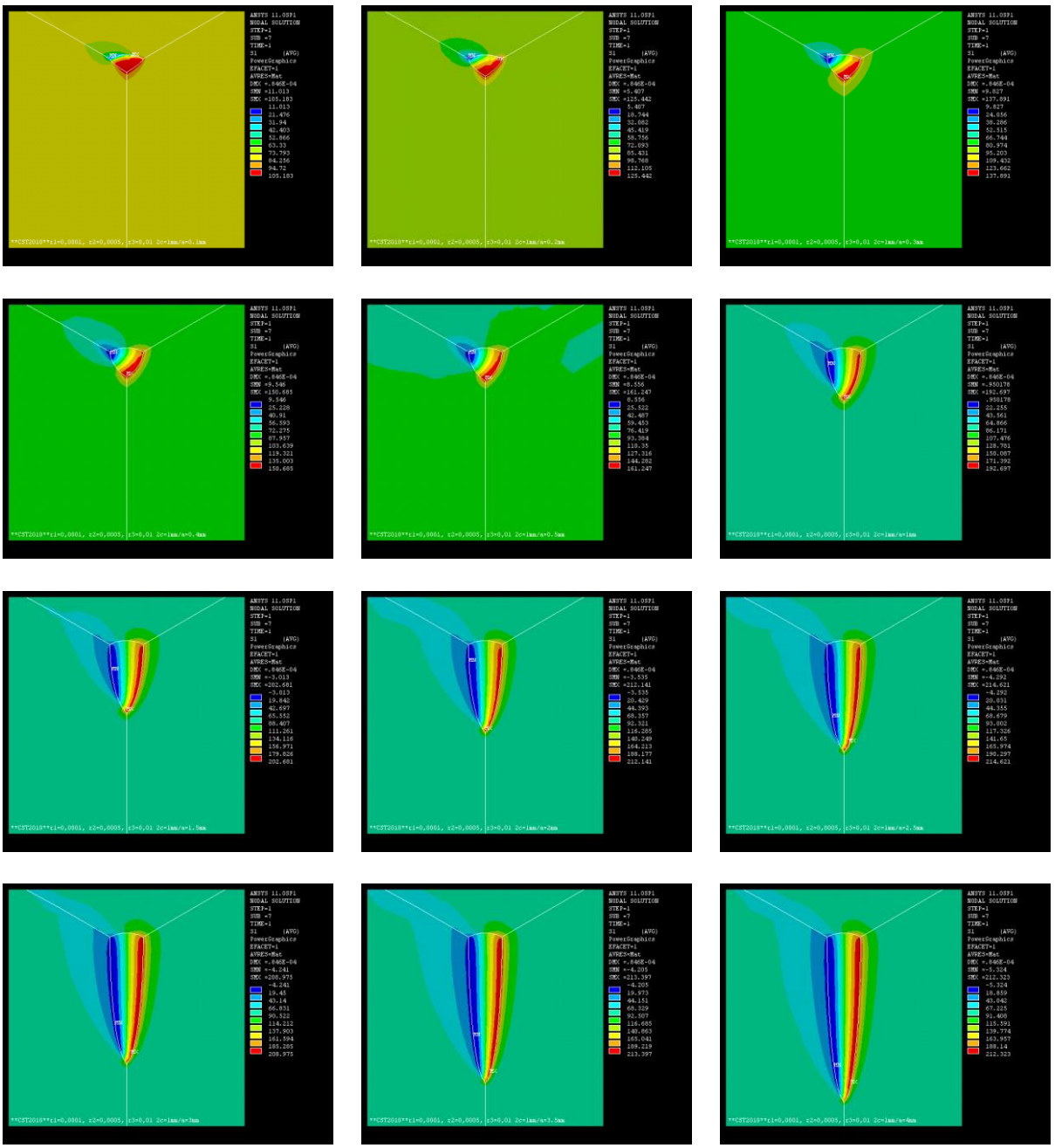

SOURCE: Bertin, 2013

From top to bottom and left to right pits with depths, respectively equal to: 0.1, 0.2, 0.3, 0.4, 0.5, 1.0, 1.5, 2.0, 2.5, 3.0, 3.5 and 4.0 mm.

Figure 56 – Maximum stress inside the pit for pipe diameter of 500 mm and internal pressure of 10 MPa

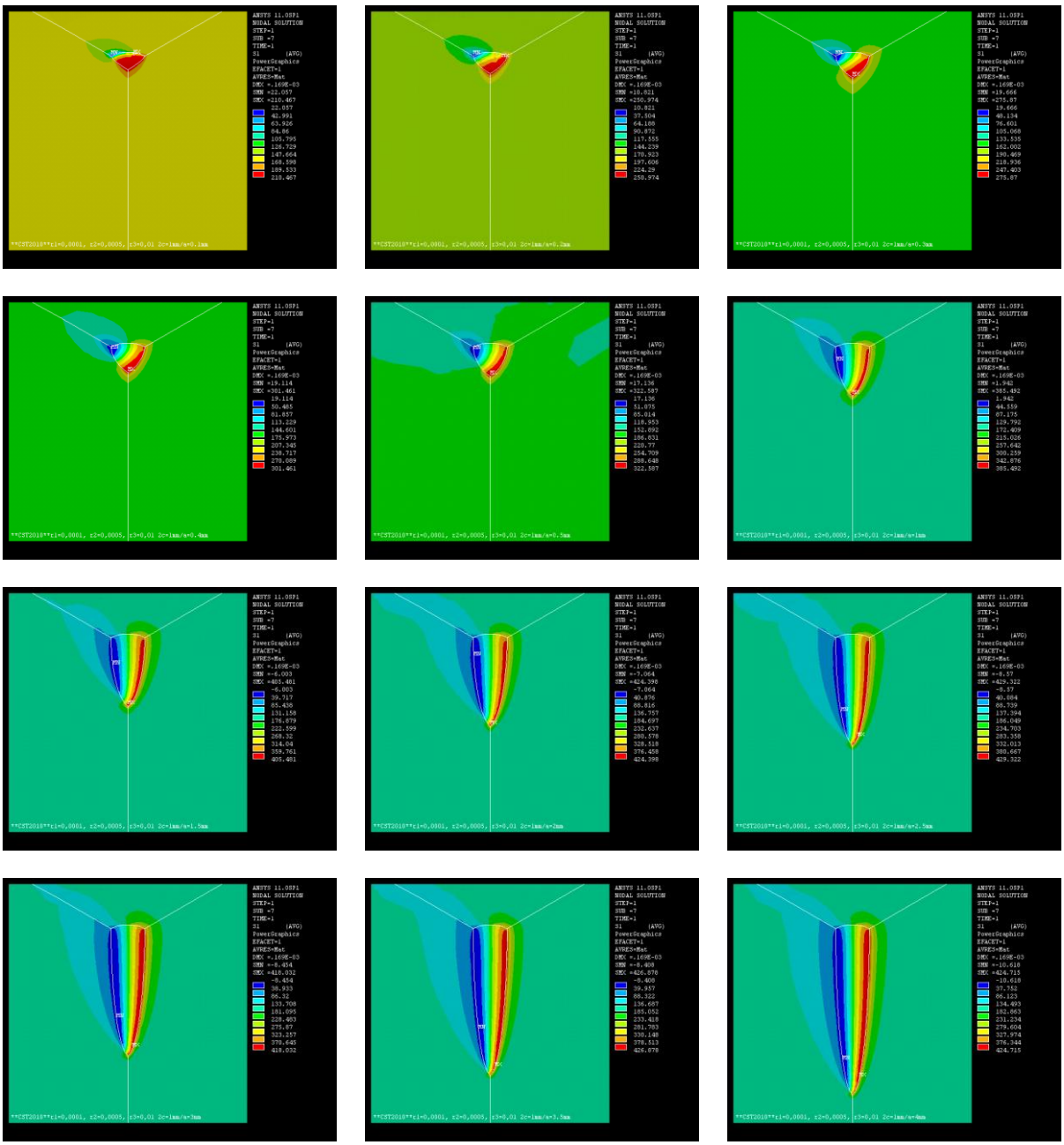

SOURCE: Bertin, 2013

From top to bottom and left to right pits with depths, respectively equal to: 0.1, 0.2, 0.3, 0.4, 0.5, 1.0, 1.5, 2.0, 2.5, 3.0, 3.5 and 4.0 mm.

Figure 57 – Maximum stress inside the pit for pipe diameter of 500 mm and internal pressure of 15 MPa

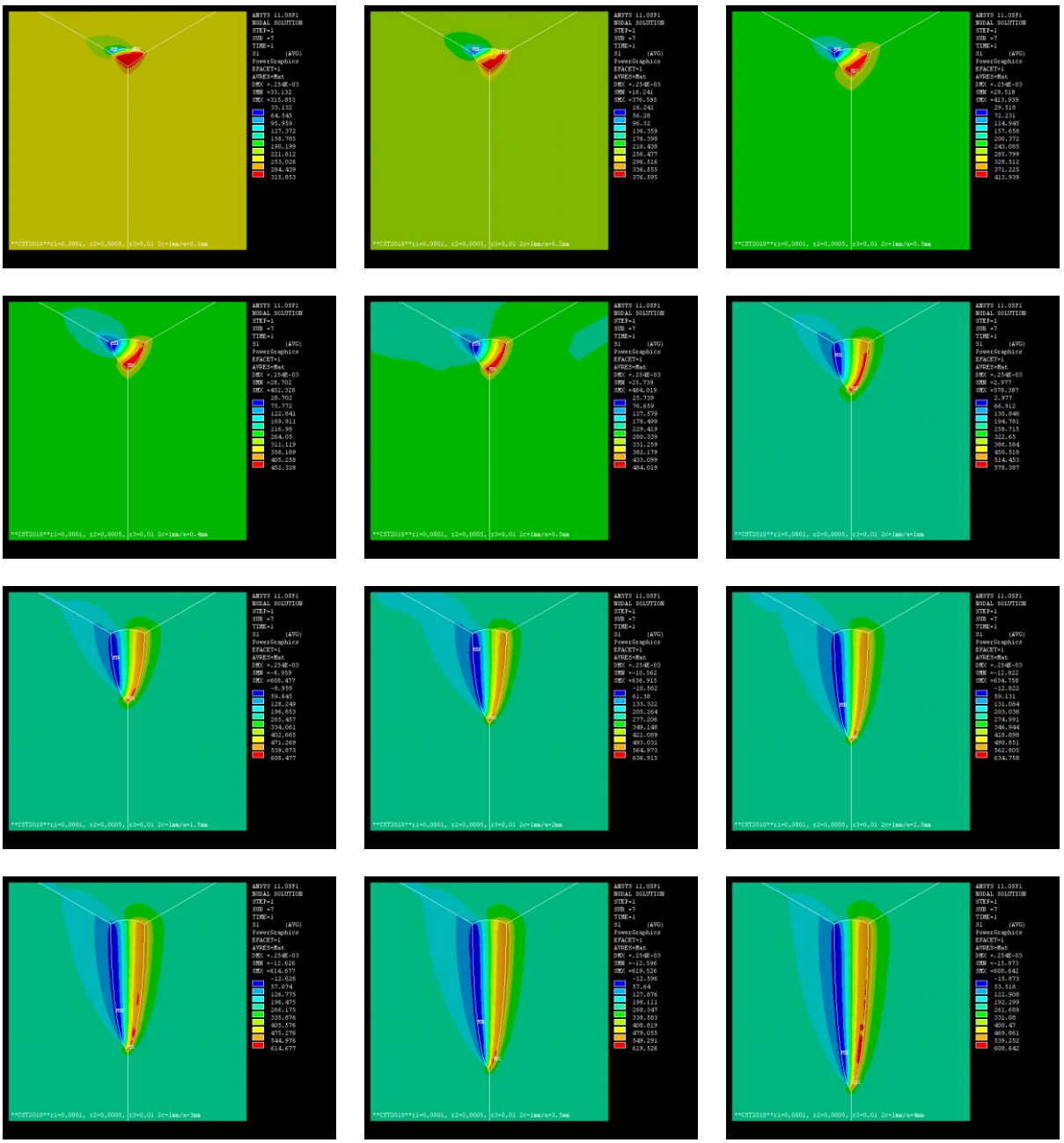

SOURCE: Bertin, 2013

From top to bottom and left to right pits with depths, respectively equal to: 0.1, 0.2, 0.3, 0.4, 0.5, 1.0, 1.5, 2.0, 2.5, 3.0, 3.5 and 4.0 mm.

Figure 58 – Maximum stress inside the pit for pipe diameter of 500 mm and internal pressure of 20 MPa

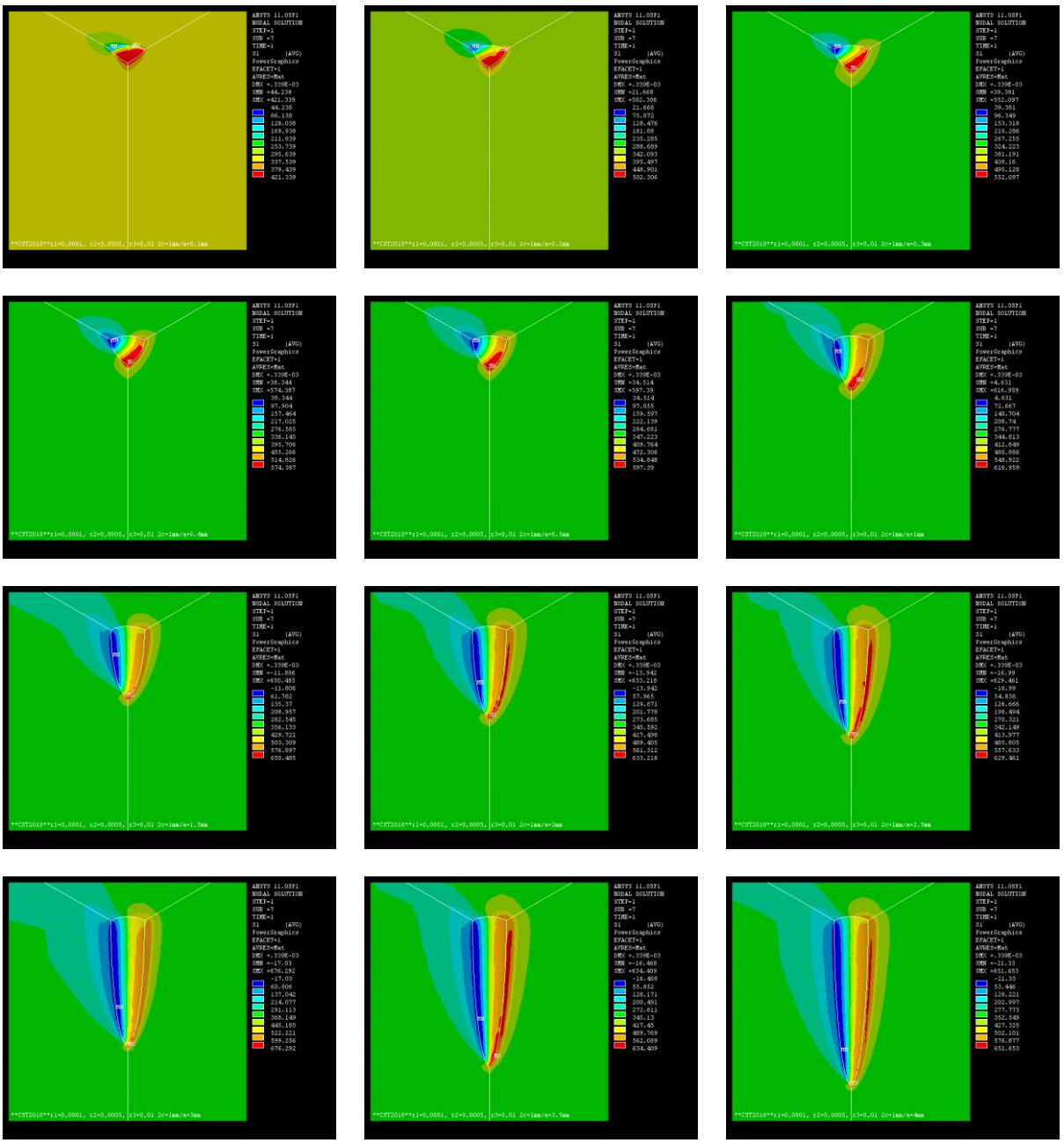

SOURCE: Bertin, 2013

From top to bottom and left to right pits with depths, respectively equal to: 0.1, 0.2, 0.3, 0.4, 0.5, 1.0, 1.5, 2.0, 2.5, 3.0, 3.5 and 4.0 mm.

Figure 59 – Maximum stress inside the pit for pipe diameter of 500 mm and internal pressure of 25 MPa

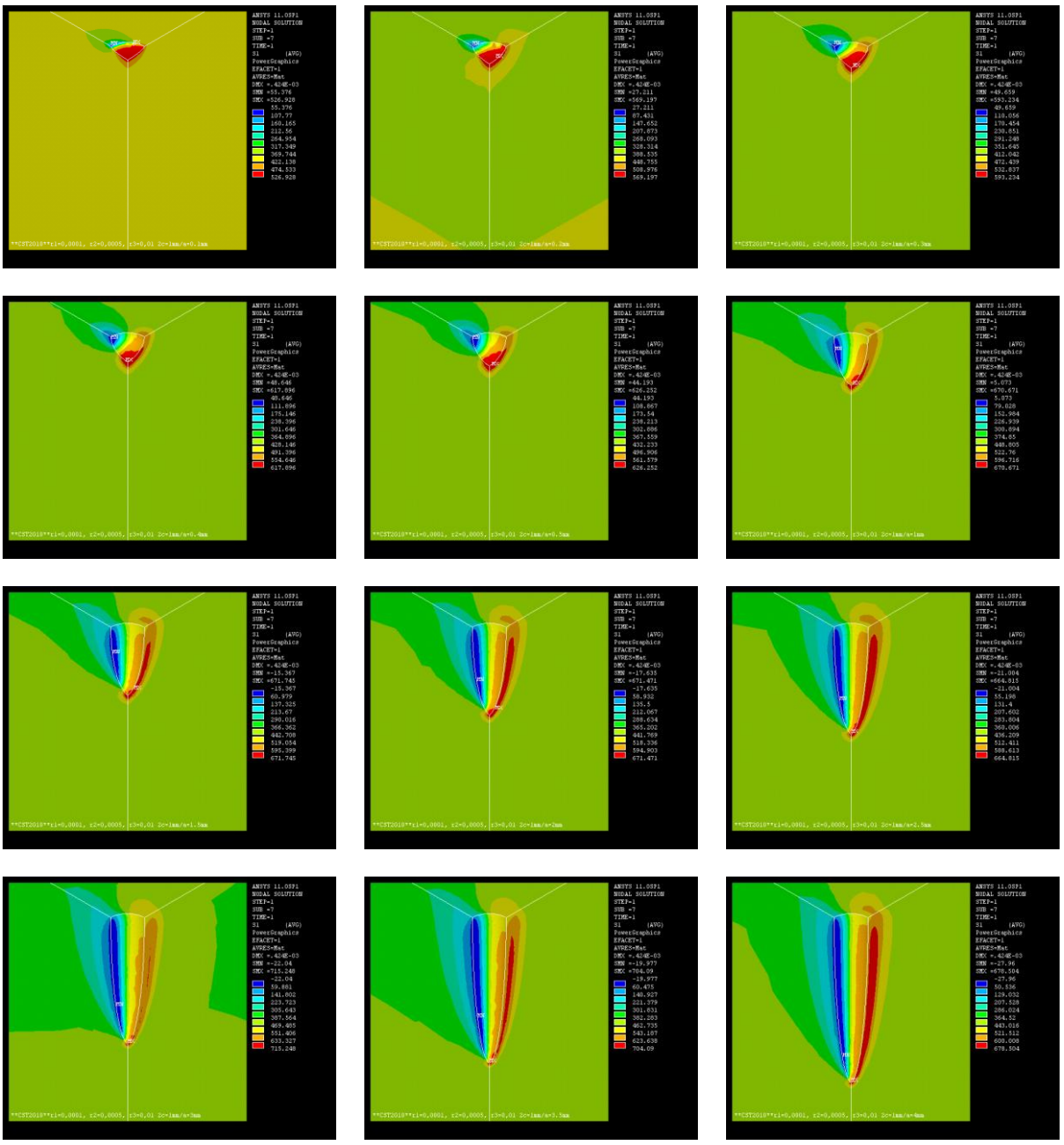

SOURCE: Bertin, 2013

From top to bottom and left to right pits with depths, respectively equal to: 0.1, 0.2, 0.3, 0.4, 0.5, 1.0, 1.5, 2.0, 2.5, 3.0, 3.5 and 4.0 mm.

ATTACHMENTS

ATTACHMENT A – National All Pipeline Systems: All Reported Incident Details: 1993-2012

Complete Table - National All Pipeline Systems: All Reported Incident Details: 1993-2012

Reported Cause of Incident	Number	%	Fatalities	Injuries	Property Damage as Reported	% of Property Damage
Corrosion						
external corrosion	804	7.7%	11	69	345556699	5.7%
internal corrosion	826	7.9%	13	6	266828739	4.4%
unspecified corrosion	290	2.7%	1	11	7632845	0.1%
Sub Total	1920	18.3%	25	86	620018283	10.3%
Excavation damage						
operator/contractor excavation damage	217	2.0%	1	49	39345988	0.6%
third party excavation damage	1666	15.9%	141	447	383676805	6.4%
previous damage due to excavation	14	0.1%	0	4	25387923	0.4%
unspecified excavation damage	51	0.4%	4	5	23975468	0.4%
Sub Total	1948	18.6%	146	505	472386184	7.9%
Incorrect operation						
damage by operator or operator's contractor	12	0.1%	1	1	576561	0.0%
overfill/overflow of tank/vessel/sump	29	0.2%	0	0	29918076	0.5%
incorrect valve position	40	0.3%	0	0	6519940	0.1%
pipeline/equipment overpressured	20	0.1%	0	0	8417286	0.1%
incorrect installation	22	0.2%	0	1	2074511	0.0%
incorrect equipment	2	0.0%	0	0	5823	0.0%
other incorrect operation	40	0.3%	1	18	33724498	0.5%
unspecified incorrect operation	575	5.5%	16	138	64252635	1.0%
Sub Total	740	7.0%	18	158	145489330	2.4%
Material/weld/equipament failure						
construction installation or fabrication-related	72	0.6%	0	0	25873679	0.4%
manufacturing-related	41	0.3%	8	51	404253131	6.7%
environmental cracking-related	35	0.3%	0	3	1073472622	17.9%
body of pipe	75	0.7%	3	18	41862764	0.7%
pipe seam	65	0.6%	2	7	80049672	1.3%
unspecified pipe body or seam	83	0.7%	0	2	80710852	1.3%
butt weld	69	0.6%	0	0	46251507	0.7%
fillet weld	29	0.2%	0	0	21786376	0.3%
unspecified weld	78	0.7%	0	0	18806718	0.3%
fusion joint	2	0.0%	0	1	116855	0.0%
compression fitting	1	0.0%	0	0	43267	0.0%
mechanical fitting	5	0.0%	1	1	1411486	0.0%
joint/fitting/component	204	1.9%	2	7	67396252	1.1%
other pipe/weld/joint failure	2	0.0%	0	2	163020	0.0%
unspecified mat'l/weld failure	140	1.3%	0	0	1972771	0.0%
malfunction of control/relief equipment	329	3.1%	1	5	54772572	0.9%
valve	4	0.0%	0	0	555076	0.0%
pump/compressor-related equipment	132	1.2%	0	1	5374369	0.0%
threaded connection/coupling failure	153	1.4%	0	4	22218454	0.3%
non-threaded connection failure	263	2.5%	0	3	77011717	1.2%
defective or loose tubing/fitting	25	0.2%	0	0	1432896	0.0%
failure of equipment body	23	0.2%	0	0	4638315	0.0%
other equipment failure	78	0.7%	1	2	7785264	0.1%
unspecified equipment failure	756	7.2%	0	0	4796672	0.0%
unspecified mat'l/weld/equip failure	151	1.4%	1	48	27585202	0.4%

Sub Total	2815	26.9%	19	155	2070341509	34.6%

Complete Table - National All Pipeline Systems: All Reported Incident Details: 1993-2012 (cont.)

Reported Cause of Incident	Number	%	Fatalities	Injuries	Property Damage as Reported	% of Property Damage
Natural force damage						
earth movement	196	1.8%	5	44	300196225	5.0%
heavy rains/floods	162	1.5%	0	1	1008688866	16.8%
lightning	63	0.6%	4	2	31304176	0.5%
temperature	122	1.1%	5	32	18863316	0.3%
high winds	58	0.5%	1	0	401671907	6.7%
other natural force damage	12	0.1%	1	2	4580759	0.0%
unspecified natural force damage	101	0.9%	0	2	21952682	0.3%
Sub Total	714	6.8%	16	83	1787257931	29.8%
Other outside force damage						
fire/explosion as primary cause	241	2.3%	10	29	69585487	1.1%
vehicle not engaged in excavation	252	2.4%	20	59	103172217	1.7%
maritime equipment or vessel adrift	1	0.0%	0	0	96700	0.0%
fishing or maritime activity	13	0.1%	0	0	26780047	0.4%
electrical arcing from other equipment/facility	16	0.1%	0	5	50908899	0.8%
previous mechanical damage	25	0.2%	0	1	24340744	0.4%
intentional damage	30	0.2%	4	10	4341379	0.0%
other outside force damage	33	0.3%	0	2	32632872	0.5%
unspecified outside force damage	155	1.4%	7	9	27640669	0.4%
Sub Total	766	7.3%	41	115	339499014	5.6%
All other causes						
miscellaneous cause	1325	12.6%	85	328	438440668	7.3%
unknown cause	160	1.5%	27	59	104631963	1.7%
unspecified	54	0.5%	0	0	422118	0.0%
Sub total	1539	14.7%	112	387	543494749	9.0%
Totals	**10442**	**100.0%**	**377**	**1489**	**5978487000**	**100.0%**

Table extracted from: http://primis.phmsa.dot.gov/comm/reports/safety/AllPSIDet_1993_2012_US.ht